

# UAB

Universitat Autònoma de Barcelona



UNIVERSITAT AUTÒNOMA DE BARCELONA  
ESCOLA D'ENGINYERIA  
DEPARTAMENT D'ENGINYERIA QUÍMICA  
GRUP D'ENGINYERIA CEL·LULAR I BIOPROCESSOS

## **Study and characterisation of human HEK293 cell line as a platform for recombinant protein production**

A dissertation submitted in partial fulfillment of the requirements  
for the degree of Doctor of Philosophy in Biotechnology at  
Universitat Autònoma de Barcelona

**Leticia Liste Calleja**

July 2015

## CHAPTER 4. RESULTS (II): PRODUCTION OF CapPCV2 USING AdV-HEK293 EXPRESSION SYSTEM

### 4.1. INTRODUCTION

Up to date there are three different generations of adenoviral vectors based on the modifications performed on the genome of the natural adenovirus. These modifications have been addressed in pursuit two major objectives: (1) obtaining space within the adenoviral genome in order to insert the gene of interest and (2) avoiding virus replication inside the organism body that might cause any disease. The strategies to obtain the vectors have been directed to eliminate regions of the adenoviral genome and replace them by the desired gene. There are three types of adenoviral vectors depending on the adenoviral genome regions that have been modified (Figure 4.1). The genes in the wild-type adenovirus can be divided in early genes (designated by E) and late genes (designated by L). The latter, encode mostly for proteins that make up components of the viral capsid or are involved in the assembly of the capsid. In the **first generation adenovirus vectors**, the transgene is inserted in place of E1 and/or E3 regions. E1 genes have regulatory functions that allow for transcription and translation of the late genes, so they are indispensable for viral replication. Consequently, E1 region must be provided in trans in the producer cell lines. The E3 region encodes products that counteract host defence mechanisms; these products are not essential for viral replication in vitro, and therefore no complementing cell line is necessary. First-generation adenovirus vectors elicit a significant immune response in vivo, mainly due to the de novo synthesis

of viral proteins. To avoid this problem, **second-generation adenoviral vectors** combining deletion of different early regions (E1/E3 and E2/E4) were generated, increasing the vector cloning capacity up to 14kb<sup>1</sup>. E2 and E4 regions are also necessary for viral replication and they must be also provided in trans by the producer cell line. Nevertheless, trans-complementation during amplification of these vectors could be less efficient in comparison to first generation vectors due to the fact that some E2- and E4-encoded proteins are toxic<sup>2</sup>. A third class of adenovirus vectors is represented by the so-called '**gutted**' or '**helper-dependent**' adenoviruses. These vectors are deleted for all viral genes, keeping only the 5' and 3' inverted terminal repeats (ITRs) and the packaging signal ( $\Psi$ ) from the wild-type adenovirus<sup>3-5</sup>. Such viruses can in theory accommodate multiple transgenes, totalling about 37 kb. In contrast to first- and second-generation adenoviral vectors, viral proteins are not provided in trans by producer cells but instead a adenoviral helper-virus is used for vector amplification. The helper-virus is a first-generation adenoviral vector with a packaging signal flanked by recombinase recognition sites<sup>2</sup>. Complementary cell lines for the production of third generation AdV vectors have been derived from those producing first- and second-generation vectors. Additionally, they constitutively express the recombinase Cre or/and FLP or  $\Phi$ C31<sup>6</sup>.

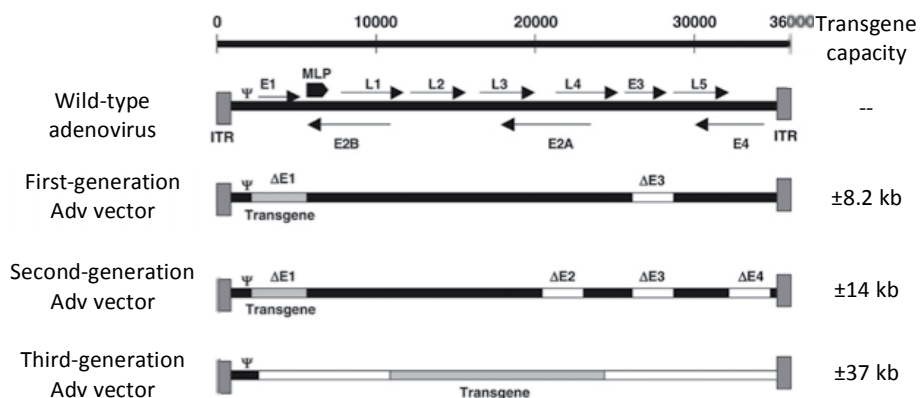


**Figure 4.1.** Different generations of adenoviral vectors. Early transcripts are represented by E1-E4 regions and late transcripts are represented by L1-L5 regions.

In the present work, adenoviruses will be used as an expression system for the production of the protein CapPCV2 (r-CapPCV2), which will be used as vaccine candidate against PCV2 diseases. The recombinant adenovirus vector has been obtained using AdEasy XL Adenoviral vector system (Agilent Technologies). This system is based on the principle of homologous recombination in bacteria and the generated adenoviral vectors are E1/E3 deleted (i.e. first-generation vectors). As *CapPCV2* gene is short (less than 1kb), the capacity of a first-generation vector will be enough to accommodate the foreign DNA. In Figure 4.2, the scheme of the process for the generation of

recombinant vectors is depicted. Briefly, the gene of interest (GOI) is cloned in a shuttle vector (pShuttleCMV), which will be transformed to an *E.coli* strain pre-transformed with a vector backbone containing the adenoviral genome (pAdEasy-1). This feature avoids co-transfection of two plasmids and dramatically decreases background caused by the non-recombinant shuttle plasmid, making it easier to obtain colonies that contain the recombinant adenoviral vector. The plasmid encoding the adenovirus genome and GOI will be transfected to *E.coli* ultracompetent cells (Materials and Methods section 8.1.2.3) in order to replicate the plasmid. Finally, the plasmid will be linearized and transformed to AD-293 cells, which are HEK293-derived cells with improved cell adherence properties.

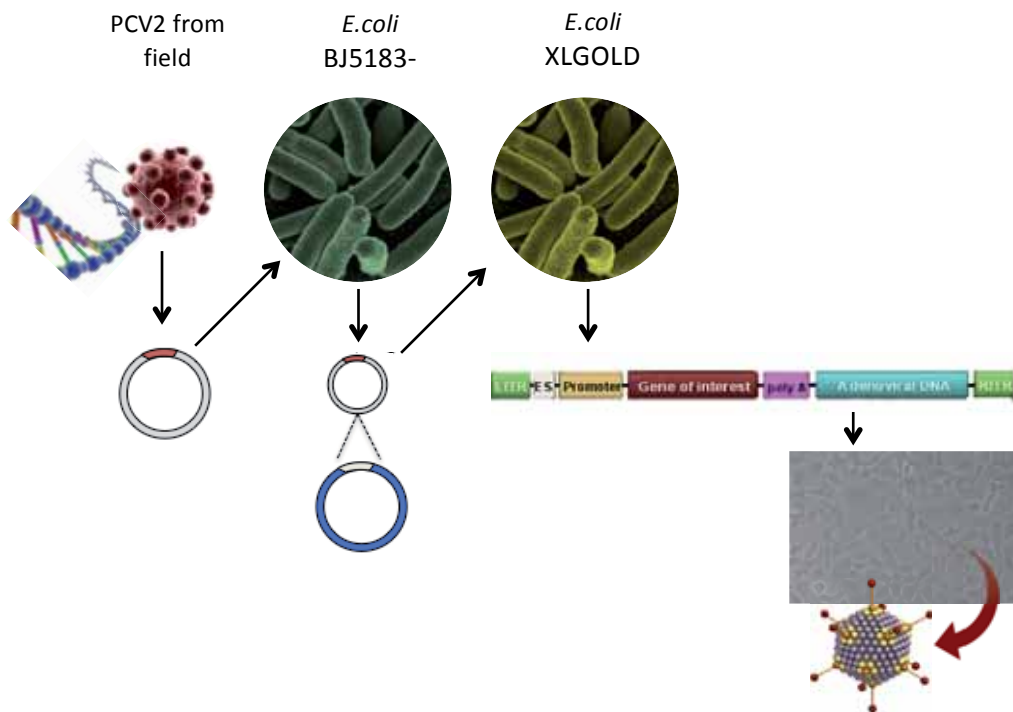


**Figure 4.2.** Process diagram for the obtaining of recombinant adenovirus expressing the protein of interest.

## 4.2. GENERATION OF THE RECOMBINANT AdV ENCODING *CapPCV2*

### 4.2.1. *CapPCV2* OBTENTION AND CHARACTERISATION

The first step for the generation of the recombinant adenovirus in this research project was obtaining the gene encoding for the protein of the capsid of Porcine circovirus serotype 2 (*CapPCV2*). The initial material was the serum from a pig infected by PCV2 virus from field, which its specific strain was unknown. As stated in the Introduction chapter, there are genomic differences among all the range of PCV2 strains and at least 5 different genomes have been identified. Also, due to its high evolutionary rate, PCV2 can adapt quickly to environmental pressures resulting into thousands of PCV2 strains. Therefore, it was mandatory to sequence the viral genome in order to precisely characterise 5'- and 3'-end of *CapPCV2* gene, which was highly important because the cloning of the gene into pShuttle required to add enzymatic restriction sites at the extremes of the gene. Also, it must be assessed the absence of *PmeI*, *PacI*, *EcoRI* and *HindIII* enzymatic restriction sites within *CapPCV2* sequence because these enzymes will be used during the generation of the recombinant adenoviral vector.

First of all, DNA isolation from sera was performed followed by a PCR amplification of *CapPCV2*. The primers used for the amplification (as well as all the primers that will be cited in this chapter) are listed in Materials and Methods chapter (Section 8.6.2). The primer alignment is schematically represented in Figure 4.3 (also, depicted in more detail in Figure 10.2.1 in Appendix 10.2). The expected size of the amplified fragment was 760bp and after agarose gel electrophoresis of the PCR product, this fragment was correctly identified (Figure 4.4) and purified from gel.

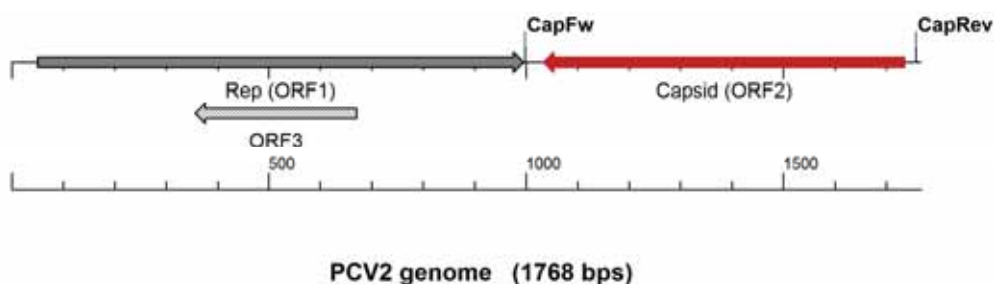


**Figure 4.3.** PCV2 genome scheme. ORFs are depicted as arrows and position of primers used for sera extracted-DNA amplification are indicated

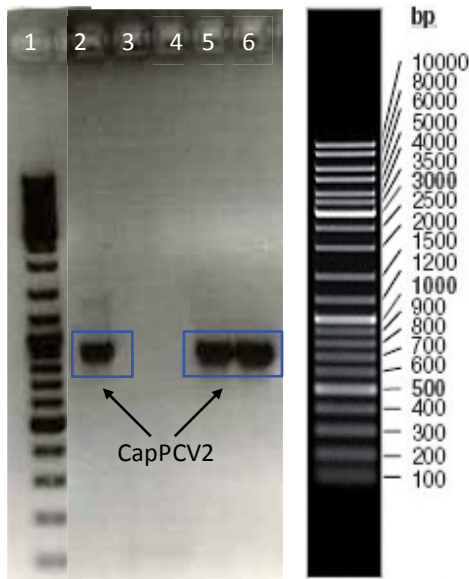


**Figure 4.4.** PCR of DNA isolated from PCV2-infected sera. Dna Ladder: GeneRuler™ 1kb DNA Ladder (Fermentas 0313).

Lane Number	ID sample
1	DNA Ladder
2	Sample (DNA extracted from sera)
3	PCR Neg. Ctrl (H <sub>2</sub> O)
4	DNA Extrac. Neg. Ctrl (H <sub>2</sub> O)
5	PCR Pos. Ctrl (H <sub>2</sub> O)
6	DNA Extrac. Pos. Ctrl (H <sub>2</sub> O)

**Table 4.1.** Identification of samples loaded on the agarose gel presented in Figure 4.4

The

reafter, genomic sequencing was carried out at UAB Genomics Service using a sequentiator based on Sanger methodology (ABI 3130XL). Three primer pairs were designed and used for finely sequence 5'- and 3'-end of

*CapPCV2*, the obtained sequences were bioinformatically analysed and a final consensus sequence was obtained (Figure 10.2.4 in Appendix 10.2). The absence of *PmeI*, *PacI*, *EcoRI* and *HindIII* restriction sites was also confirmed, so the isolated sequence could be directly used for the generation of the recombinant adenovirus without additional modifications. Upon the sequentation of *CapPCV2*, the correct design of the primers that were used to insert the enzymatic sites could be done.

#### 4.2.2. *CapPCV2* CLONATION INTO ADV GENOME BY ADEASY XL TECHNOLOGY.

PCR using ATG and STOP primers (Materials and Methods section 8.6.2) was performed in order to add *KpnI* and *HindIII* restriction sites at 5' and 3' of the gene, respectively. Thereafter, *CapPCV2* was cloned into pShuttleCMV by cohesive-end cloning strategy and transformed into E.coli competent cells. The plasmid generated after *CapPCV2* insertion will be referred to as pShuttleCMV\_ *CapPCV2* (Figure 4.5B). After each transformation presented in this chapter, a minimum of 20 clones were selected to make a master plate and colony PCR characterisation. From the positive clones, enzymatic restriction pattern characterisation of a minimum of 5 clones was performed. Finally, the gene integrated into the final plasmid to be transfected to mammalian cells was sequenced in order to confirm absence of mutations. In this section, only the results showing the characterisation of the selected clones carrying the recombinant vector of interest are presented.

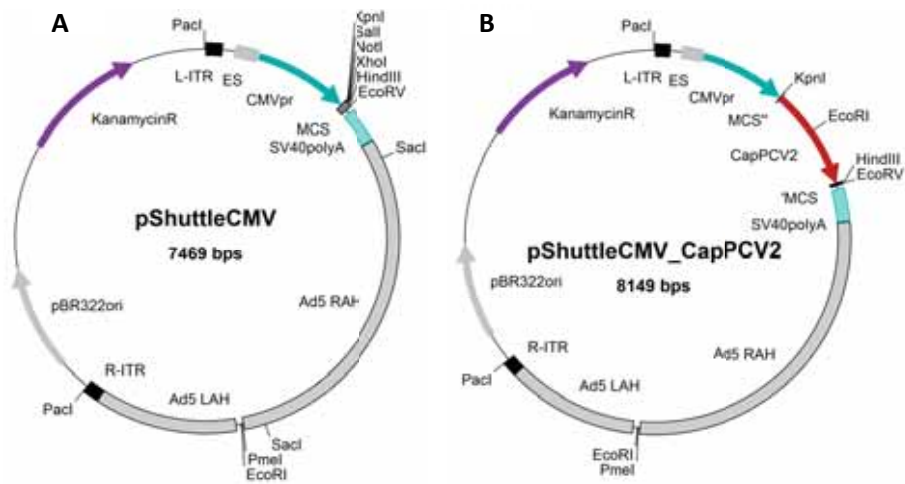


**Figure 4.5.** pShuttleCMV vector map before (A) and after (B) GOI's insertion.

Specifically, the characterisation of the clones obtained after pShuttleCMV\_CapPCV2 transfection was performed by two different PCR using distinct pair of primers (PCR1 and PCR2). Besides, EcoRI was selected for restriction pattern identification. The results obtained corresponding to the final selected clone (onwards Clone6) are shown in Figure 4.6. The fragment expected after PCR1 was about of 700bp whereas a longer fragment of 824 was expected after PCR2. These two bands were clearly observed after colony-PCR (Lane 2 and Lane 3 on gel A depicted on Figure 4.6) while they were absent on the amplification of pShuttleCMV before GOI cloning (Lane 4 on the same gel). Regarding EcoRI digestion, two fragments of 5209 and 2940bp were expected when all the recombinant vector is digested which were clearly observed after restriction (Lane 3 on gel B of Figure 4.6). Digestion of pShuttleCMV without CapPCV2 was also included as negative control and the linearisation of the vector was observed (Lane 2 on the same gel). CapPCV2 in pShuttleCMV\_CapPCV2 vector of the selected clone was sequenced in order to ensure that any mutation had occurred. The obtained sequence was 100% homologous expected one (Figure 10.2.4 in Appendix 10.2).

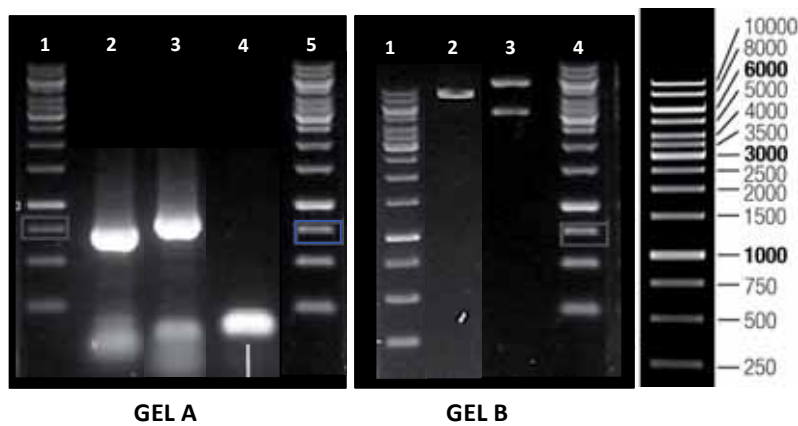


**Figure 4.6.** Characterisation of Clone 6 by colony-PCR (gel A) and enzymatic restriction pattern (gel B). DNA Ladder: GeneRuler™ 1kb DNA Ladder (Fermentas #SM0313).

**Table 4.1.** Identification of samples loaded on the agarose gel presented in Figure 4.6.

GEL A			GEL B		
Lane	ID Sample	Expected size (bp)	Lane	ID Sample	Expected size (bp)
1,5	DNA Ladder	--	1	DNA Ladder	--
2	Clone6_PCR1	722	2	pShuttleCMV_EcoRI digested	7469
3	Clone6_PCR2	824	3	Clone6_EcoRI digested	5209, 2940
4	pShuttleCMV_PCR2	No band	4	DNA Ladder	--

After its characterisation, pShuttleCMV-CapPCV2 was *PmeI*-linearized and transformed into *E.coli* BJ5183-AD-1 electrocompetent cells, which already harbour the vector encoding the adenovirus genome (pAdEasy-1). Within these cells, homologous recombination between the two vectors takes place. As indicated in Figure 4.7, there is a unique recombination zone on the right side of the AdV genome encoded in pAdEasy-1 vector (Ad5 RAH), but there are two possible recombination events on the left side of AdV genome (Ad5 LAH and pBR322ori). It is important to highlight this feature as it will result in two different enzymatic restriction patterns of the recombinant vector, both of them indicating correct homologous recombination. The vector generated after homologous recombination in BJ5183-AD-1 cells will be referred to as pAD1-pSCMV-CapPCV2.



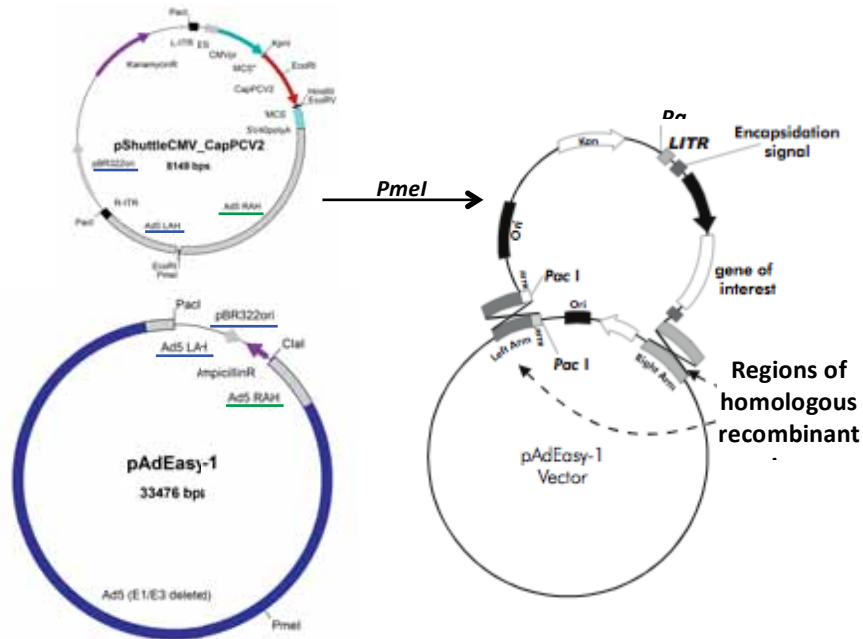


**Figure 4.7.** Scheme representing homologous recombination that takes place in *E.coli* BJ5183-AD-1 after transformation. In green is underlined the unique recombination zone on the right side of both vectors (pShuttleCMV and pAdEasy-1) and in blue are highlighted the two recombination zones on their left side.

After the overnight incubation under selective pressure (kanamycin presence in the culture plates), three populations could be observed on the transformation plates: very large colonies, intermediate-sized and small-sized colonies. The vector after homologous recombination is relatively large ( $\approx 40\text{kb}$ ) and low copy number, so the positive clones after electroporation will slowly grow under the selective pressure of the antibiotic. Consequently, the small and intermediate colonies are the potential recombinants while the large colonies represent background from the shuttle vector. Hence, only the smallest colonies were picked for *E.coli* transformants screening. The results of the characterisation of the new selected clone (Clone EQ) are presented in Figure 4.8, Table 4.4 and Table 4.5. As in previous section, after PCR amplification a band of 722bp (PCR1) and a band of 824bp (PCR2) were expected. These bands were correctly detected, indicating the presence of *CapPCV2* within the vector (Gel A on Figure 4.8). For the enzymatic restriction pattern characterisation, *PacI* restriction was carried out. Two different outcomes were expected depending on the homologous recombination site between the two vectors. Two fragments of  $\approx 30\text{kb}$  and  $3.0\text{kb}$  should be detected if the recombination took place between the left arm homology sites (LAHs) whereas the fragments will be  $\approx 30\text{kb}$  and  $4.5\text{kb}$  in size if recombination occurred between the two replication origin (pBR322 Ori). As shown in gel B of Figure 4.8, the recombination took place between pBR322Oris, as indicated by the presence of the band of approximately  $4.5\text{kb}$ .

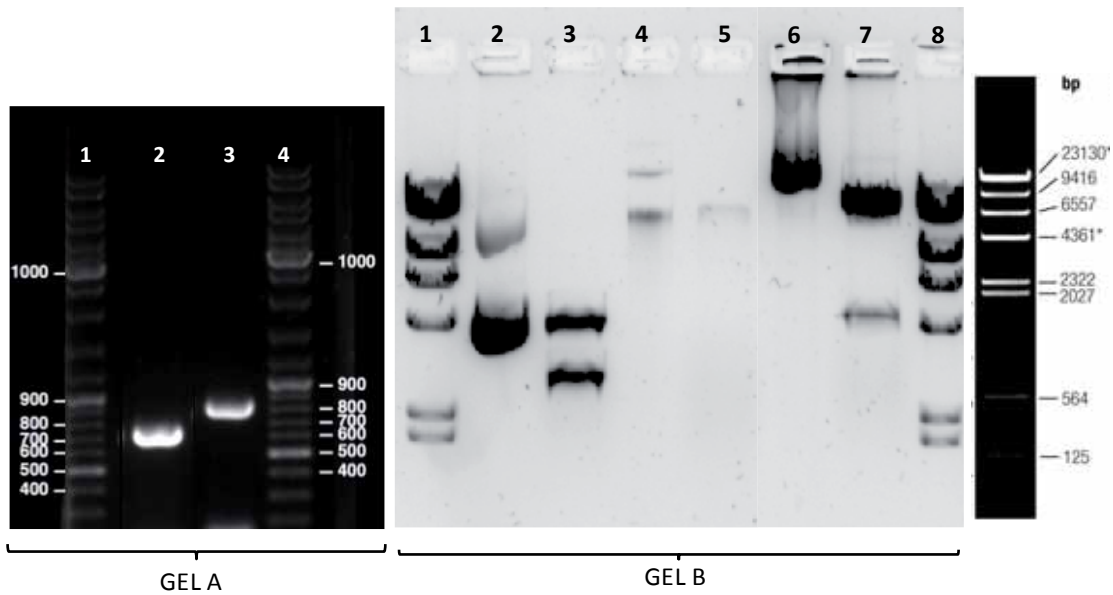


**Figure 4.8.** Results of the characterisation of clone EQ. Gel A: colony-PCR characterisation; Gel B: enzymatic restriction pattern characterisation. DNA Ladder on gel A: GeneRuler™ DNA Ladder Mix (Fermentas #SM0333). DNA Ladder on gel B: Lambda DNA/HindIII Marker (Fermentas #SM0103).

**Table 4.4.** Identification of the samples on gel A in Figure 4.8.

Lane	ID Sample	Expected size (bp)
1	DNA Ladder	--
2	CloneEQ_PCR2	722
3	CloneEQ_PCR1	824
4	DNA Ladder	--

**Table 4.5.** Identification of the samples on GelB in Figure 4.8.

Lane	ID Sample	Expected size (kB)
1	DNA Ladder	--
2	pShuttleCMVundigested	Undefined (relaxed, coiled, supercoiled)
3	pShuttleCMV_Pacl digested	4.5, 2.94
4	pAdEasy-1 undigested	Undefined (relaxed, coiled, supercoiled)
5	pAdEasy-1 Pacl digested	33, 5
6	Clone EQ undigested	Undefined (relaxed, coiled, supercoiled)
7	Clone EQ Pacl digested	30, 4.5
8	DNA Ladder	--

BJ5183-AD-1 *E.coli* strain is proficient in gene *recA* which encodes for RecA protein. This protein plays a central role in homologous recombination and therefore, it was necessary for the generation of the recombinant pAdEasy1-pSCMV-*CapPCV2* vector. Nevertheless, it is not recommended to perform plasmid amplification in *recA+* strains, as the stability of extrachromosomal segments of DNA (i.e. plasmids) is not ensured. For this reason, pAdEasy1-pSCMV-*CapPCV2* was transformed by heat-shock transformation method (Materials and Methods section 8.7.1) into XLGOLD *E.coli* cells order to obtain clones *recA-* in which the amplification of the vector can be stably performed. The selected clone after this transformation was named clone 2.9. The sequentation of *CapPCV2* gene within this clone was carried out and the absence of mutations was confirmed.

#### **4.2.3. TRANSFECTION INTO AD293 CELLS FOR PRIMARY VIRAL STOCK GENERATION AND rAdV-*CapPCV2* DETECTION.**

After ensuring that *CapPCV2* has not undergo any mutation that could affect to the correct expression of the protein, pAD1-pSCMV\_ *CapPCV2* vector was *PacI* linearized and purified in order to transfect AD293 cells for obtaining the primary viral stock. The transfection method used was based on a modified CaPO<sub>4</sub> method and is explained in detail in Material and Methods Section 8.9.4. Five days post transfection cytopathic effect (CPE) was clearly detected and cells were harvested in order to recover intracellular rAdV-*CapPCV2*. The cells that were still attached to the plate at the time of harvest were recovered in cell media by softly detaching them using a cell scrapper. Cells were centrifuged and media was replaced either by viral storage buffer or PBS. Thereafter, cells lysis was carried out by thaw/freeze protocol. This primary virus stock was qualitative analysed for cytopathic effect, *CapPCV2* detection by PCR amplification and r-*CapPCV2* detection by ELISA on a first round infection for virus amplification. 24hours post infection (hpi) of this first viral production round, cells were harvested and separated from media by centrifugation. Extracellular viral fraction (cell media) and intracellular viral fraction (lysed AD-293) were separately analysed. The band expected after PCR2 amplification (≈800bp) was clearly detected in both fractions in all the infected cultures, and it was absent in the uninfected cell culture (negative control) (Figure 4.9). Hence, although any cytopathic effect (CPE) could be detected at that time after infection, we could ensure that the recombinant adenovirus was infective. Besides, *CapPCV2* gene has not been lost during transfection or virus amplification.

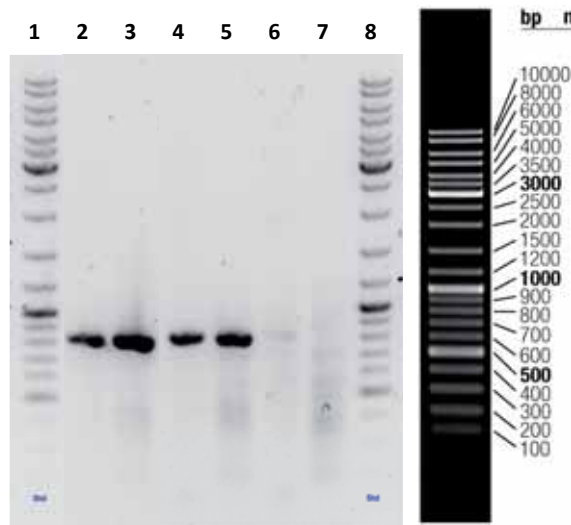


**Figure 4.9.** PCR characterisation of rAdV-*CapPCV2*.

**Table 4.6.** Identification of samples in Figure 2.9.

Lane	ID Sample	Lane	ID Sample
1	DNA Ladder	5	I.F. rAdV- <i>CapPCV2</i> (PBS)
2	E.F. rAdV- <i>CapPCV2</i> (St.B.) <sup>*</sup>	6	E.F. uninfected
3	I.F. rAdV- <i>CapPCV2</i> (St. B.) <sup>*</sup>	7	I.F. uninfected
4	E.F. rAdV- <i>CapPCV2</i> (PBS)	8	DNA Ladder

<sup>\*</sup> E.F.: extracellular fraction (cell media); I.F.: intracellular fraction (AD293 lysate); St.B.: storage buffer.

72hpi, cells started to detach from tissue plate resulting in the formation of plaques in the monolayer. Hence, the generated recombinant adenovirus could correctly replicate and propagate in AD293 cells. The observed CPE was more severe in cells infected with rAdV-*CapPCV2* stored in viral storage buffer in comparison with the recombinant adenovirus stored in PBS (Figure 4.10), meaning that the first buffer was more suitable for virus preservation. Composition of this buffer is detailed in Materials and Methods chapter (section 8.10.1.2). Finally, CapPCV2 protein could be successfully detected by Elisa test (INgezim PCV DAS, Ingenasa) indicating the suitability of the adenovirus vectors constructed. The absorbance detected in the samples infected with rAdV-*CapPCV2* storage buffer doubled the absorbance of samples infected with rAdV-*CapPCV2* PBS (data not shown), which was in good correlation with the observed CPE.

After the successful obtention of rAdV-*CapPCV2*, the study of the infection process in order to obtain the vaccine candidate was addressed and the results are presented in the next sections of this Chapter.

### 4.3. SELECTION OF THE BEST CONDITIONS FOR ADENOVIRUS INFECTION

There are several key parameters that affect the viral infection process and its optimisation is crucial for the bioprocess development. These parameters are related to the environmental conditions, to the ratio between virus and host cells and to temporary actions such as the time of infection and the time of harvesting. These factors are briefly described below.

#### Environmental conditions

The environmental conditions are mainly related to the cell culture media used. Cell media will not only affect to the physiological state of the cell but also can disturb the viral infection process. In Chapter 1 of this doctoral thesis it has been shown that depending on the media and the supplements used, cells can grow better and achieve higher cell densities. This would be directly related to a better physiological cellular state and it would result in cells more suitable to be infected. Nevertheless, media appropriated for cell growth can be not recommended for infection. Some factors such as osmolarity or pH can affect the capacity of the virus to infect the cells. Consequently, cell media and supplements tested in the first chapter will be evaluated for viral infection and production.

#### Multiplicity of Infection

The multiplicity of infection (MOI) is the ratio between the number of infective particle units and the number of cells to be infected. This parameter has a major influence during the initial stages of the infection when cells and virus must get in contact and the virus must be adsorbed. As a general rule, the greater the MOI is, more cells will be infected. Nevertheless, it has been reported that there are no significant differences on infecting cell cultures at  $1 \times 10^6$  cell/mL with MOI=1 or MOI=25<sup>7</sup>. The determination of the optimal MOI value ensures an adequate infection while maximising the production yield.

#### Time of infection

The time of infection (TOI) is a key factor on the specific viral production of the process. Once the viruses have entered the cell, they need to replicate their genome and produce the proteins for the new viral particles at the expense of the host cell's energy. Consequently, it is mandatory to define a

moment in which there is a relative high cell density presenting a good metabolic and physiologic state. Also, at TOI the environmental conditions should be adequate in order to avoid any nutritional limitation or by-product inhibition that can affect the biocatalyzer during the infective cycle. Typically, cells are infected in the middle of the exponential growth phase, in order to ensure correct culture conditions. Nevertheless, the time frame to select optimal TOI could be extended until a point close to the end of cell growth, at which the virus of interest would have enough time to perform a complete viral cycle. In a cell culture, the time of infection is directly related to a specific viable cell concentration. This last parameter is much more used when referring to TOI than the hours of cell culture<sup>7-9</sup>. Therefore, along this chapter TOI will be expressed as cell density at TOI (cell/mL) instead of hours of cell culture.

#### Time of harvest

The time of harvest (TOH) is defined as the post infection time in which the product of interest is withdrawn. In the bioprocess addressed in this Chapter, the products of interest are two: the recombinant adenoviral vector itself (*rAdV-CapPCV2*) and the recombinant protein encoded in that vector (*CapPCV2*). The optimal TOH is when the maximal concentration of product is achieved without affecting its quality.

TOH can be decided depending on if the product of interest is recovered from the intracellular or the extracellular fraction. It is reported that 48hpi the volumetric adenovirus productivity is typically at its maximum, but at that time a small percentage of the virus (usually less than 50% and as low as 10%) has been released from cells<sup>7</sup>. In case that it is desired to recover adenovirus on the extracellular space, it must be taken in mind that the stability of the adenovirus in the media should be assessed. Besides, when the product of interest is the recombinant protein, it must be considered if the protein will be secreted to extracellular space or if it will remain in the cytosol. In the first case, protein stability in cell broth must be considered, as in the case of AdV recovery. In the second case, it must be taken into account that 24hpi, cell viability starts to drop and the intracellular processes related to cell death might affect protein quality. Also, other factors such as catalytic activity, protein aggregation<sup>10,11</sup> or glycosilation pattern should be considered when evaluating the quality of the produced recombinant protein.

The optimum of each of the stated parameters will depend on AdV serotype, transgene, and also the input MOI. Therefore, the optimal values must be studied for each particular bioprocess.

In the current research project, the optimisation of the explained parameters will be studied with

two objective functions: maximisation of adenoviral vector productivity and maximisation of protein productivity. In order to study the infection parameters it is highly valuable to establish a fast, precise, reproducible, low time consuming and cost effective method of titration and protein quantification. The titration of the recombinant adenovirus generated in this project (rAdV-*CapPCV2*) is performed with an immunochemical assay. This type of assays typically present high variability and are time-consuming. Besides, *CapPCV2* quantification is carried out by ELISA technique, which present two major drawbacks: high variability and high cost. For these reasons, the research of the best infection parameters was addressed with a recombinant adenovirus expressing the Green Fluorescence Protein instead of with the generated rAdV-*CapPCV2*. The use of fluorescent proteins improves the detection of infected cells and reduces both the viral titre variability and the titration time<sup>12</sup>. Moreover, GFP quantification techniques such as fluorimetry or flux cytometry are more reproducible and cost-effective in comparison to ELISA test. The set-up of the protocols for rAdV-GFP and rAdV-*CapPCV2* are detailed in Appendix 10.3.

In the following sections, the study of the best infection conditions are presented. It should be mentioned that as small differences on the experiments onset would led to significant differences on their outcome, a simple diagram of the experimental design with a brief description of it will be done along the next sections of this chapter.

#### **4.3.1. EVALUATION OF CELL MEDIA AND SUPPLEMENTS EFFECT ON ADV INFECTION AND ADV PRODUCTION.**

Cell media evaluated in Chapter 1 for cell growth were evaluated again but in terms of their suitability for adenovirus production. Two parameters were studied: the influence of media on the efficacy of infection and the effect on adenovirus production. On one hand, we wanted to evaluate whether the physicochemical media conditions and cell state at the selected TOI were suitable to enable a good entrance of the virus to the cell. On the other hand, we wanted to asses whether cell media could supply the necessary resources during the whole infective cycle in order to get a good viral production. The evaluation of the infection parameters will be performed based on the infective viral progenie measurements. In these preliminary experiments, TOI was established at the middle of the growth phase in order to ensure an appropriate cell state for AdV infection. MOI was set at 1, a middle value to avoid massive cell damage in a single-round infection process. Finally, TOH was selected on basis to the most reported in literature and it was set at 48hpi. In Figure 4.11, an scheme of the experimental approach for cell media evaluation is presented. Cells were adapted to grow in the corresponding media before the experiment onset. At least three passages checking

correct duplication time and viability were performed. At the beginning of the experiment, complete media replacement was performed for results reproducibility concerns. As the studied variables were efficiency of infection and AdV production, a unique cell culture for each media was carried out in order to avoid cell growth differences before infection. At TOI, the mother cell culture was split into three cultures to be infected and one uninfected culture for correct cell growth assessment. 20hpi a sterile sample was taken to determine the percentage of infected cells by flow cytometry (i.e. percentage of positive GFP cells) and GFP intensity. At TOH (48hpi) cells were harvested and supernatant was separated from cells in order to quantify extracellular viral fraction separately from intracellular viral fraction.

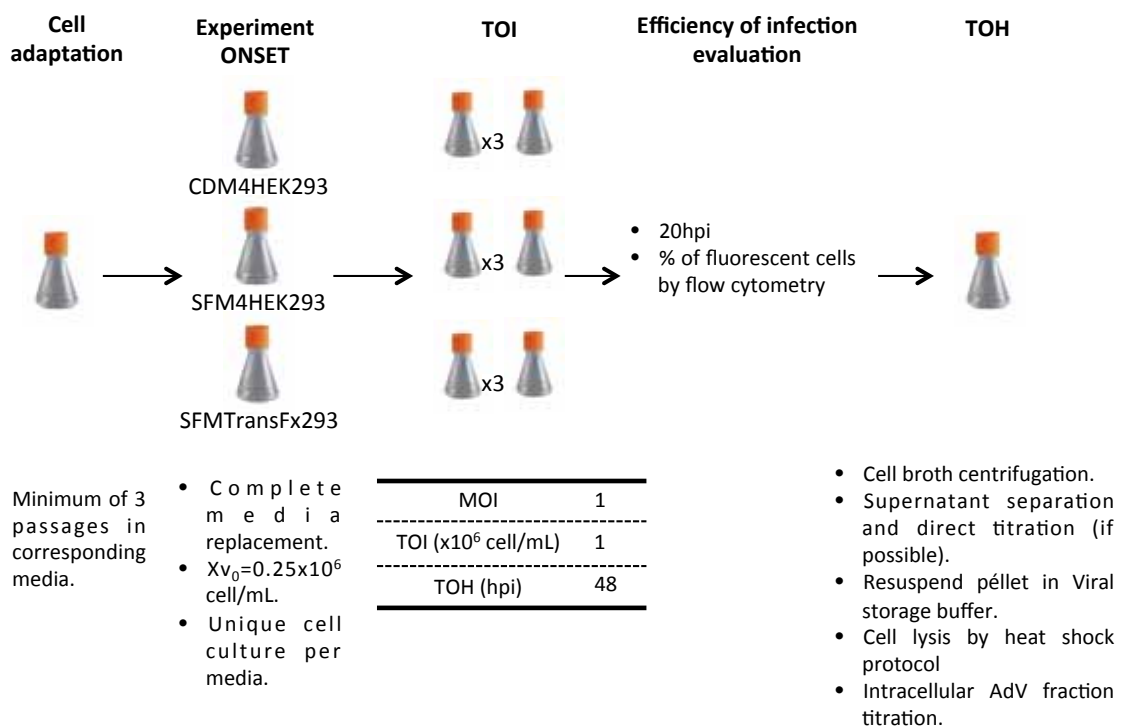


**Figure 4.11.** Scheme of the experiment for cell media selection for AdV infection and production.

The results of the infection of HEK293 cultures in each media are presented in Figure 4.12. In regard the efficiency of infection (Figure 4.12A), it can be noticed that there were not significant differences among the three media. Moreover, the percentages of infection for all media were in good correlation with the percentage predicted by Poisson distribution for an effective infection (Eq.4.1)<sup>13</sup> which at MOI=1 is 63%, indicating that there was no negative effect of the media on infection efficiency.



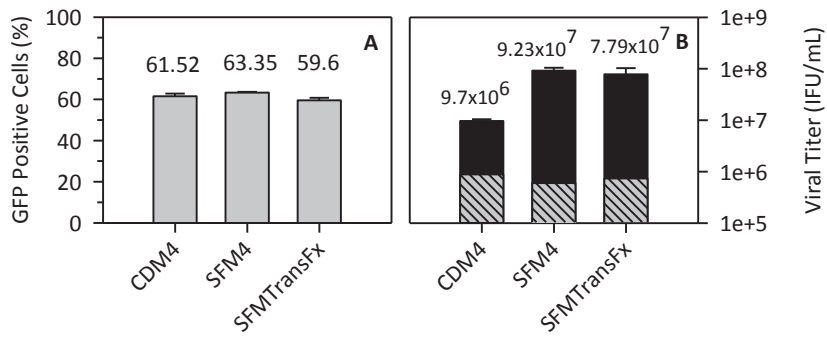


**Figure 4.12.** A) Efficiency of infection of the three commercial media tested. Percentages of cells expressing the gene reporter (GFP) are given as the average of three replicates ( $n=3$ ). Error bars represent standard deviation of one measure of each replicate. B) Viral titer obtained from the infection of HEK293 cultured in the three commercial media tested. Grey dashed part of the bar represents the inoculated virus ( $IFU_0$ ) and total height of the bar represents the final titer calculated at TOH ( $IFU_f$ ). Hence, black part corresponds to the net adenovirus production.  $IFU_f$  is calculated as the sum from extracellular and intracellular fraction. Error bars indicate the standard deviation of the titers obtained. Specific values of averages and standard deviation are specified on the top of each bar.

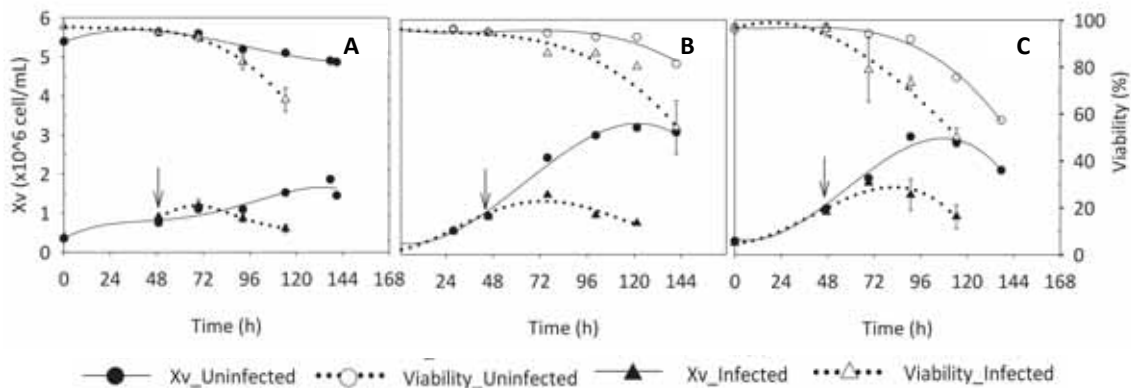


**Figure 4.13.** Cell growth and viability profiles of infected and uninfected cell cultures in each media. A) HyQ CDM4HEK293 B) HyQ SFM4HEK293 C) HyQ SFMTransFx-293

$$P(k) = \frac{(e^{-m} \cdot m^k)}{k!} \quad (\text{Eq. 4.1})$$

Where:

$P(k)$  = probability than any cell is infected with  $K$  particles

$m$ =MOI

$k$ =number of viral particles in a given cell

between HyQ SFM4HEK293 and HyQ SFMTransFx-293 cell media ( $(9.230 \pm 1.27) \times 10^7$  and  $(7.58 \pm 2.49) \times 10^7$  Infective particle units/mL (IPU/mL) respectively), whereas the use of HyQ CDM4HEK293 resulted in one log-unit decrease of the final titre ( $(9.70 \pm 0.78) \times 10^6$ ). These results can be explained through the analysis of cell growth evolution depicted in Figure 4.13. After infection, cell culture grew for 24h although the growth rate decreased in comparison to uninfected cell culture, regardless the cell media used. Thereafter, viability dropped continuously until TOH. This is in good correlation with virus cell cycle: DNA replication occurs approximately between 10-24hpi and virus assembly and DNA packaging happens around 20-48hpi<sup>7</sup>. The energy spent for viral DNA replication is the cause of growth rate decrease after infection, while no CPE is observed until the onset of virus maturation. In case of HyQ SFM4HEK293 and HyQ SFMTransFx-293 cell media, the uninfected cultures grew 72 additional hours from TOI in infected cultures, indicating that media could still provide enough energy to cells and this energy would be redirected from cell growth duplication to adenovirus production in infected cell cultures. In contrast, a drastic drop on growth rate was estimated in the uninfected culture in HyQ CDM4 media, although viability drop was softer in comparison to the infected cultures in this media. This observation made us conclude that the lower specific production in HyQ CDM4 media was due to some nutritional limitation that was also affecting the cell growth in the uninfected culture.

As AdV specific production was not significantly different between HyQ SFM4HEK293 and HyQ SFMTransFx-293 and cell media and culture strategies study (Chapter 1) were mainly performed in HyQ SFMTransFx-293, it was decided to study the effect of nutritional supplements on AdV infection and production using that media as basal media. The experimental design was the same as described in Figure 4.11 but instead of different cell media, different nutritional supplementations were studied. Specifically, the conditions tested were: 5%FBS, 10% CB5 (80g/L) and 5%FBS +10%CB5 (80g/L) addition.

In Figure 4.14A it can be observed that the expected percentage of infection (around 63%) was reached in all conditions, although the addition of FBS slightly increased this percentage up to  $68.00 \pm 0.4\%$  in comparison to the  $58.25 \pm 0.07\%$  obtained when FBS was deprived. The positive effect of FBS became more evident when focusing on the viral titre obtained. As presented on the right bar chart of the same figure, the maximal viral production was achieved when FBS was added solely to HyQ SFMTransFx-293 ( $4.12 \cdot 10^8$  IPU/mL). This viral titre represents an increment of 5.5 times the viral titre obtained in cell cultures without supplementation. Differently, the addition of CB5 had no significant effect in comparison to cell medium without supplementations. Contrarily to the evaluation of the causes of low AdV production on the prior presented culture media study, the

reduction of AdV volumetric production when CB5 was added could not be related to a possible nutrient limitation of media. As shown in Figure 4.15, uninfected cell cultures progressed as expected. This is, that in the worst AdV production scenario (HyQ SFMTransFx-293 10%CB5 supplemented) cells grew exponentially until 114h of cell culture, which represents 72 additional hours of exponential growth upon TOI in the infected cell cultures. The fact that uninfected cells could grow exponentially for this additional time, rule out the possibility of nutrient limitation.

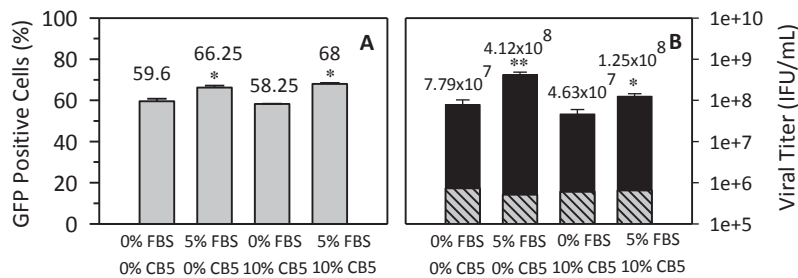


**Figure 4.14.** A) Efficiency of infection of HyQ SFMTransFx-293 without supplementation and supplemented with one or both supplements (FBS and CB5). B) Viral titer obtained from the infection of HEK293 cultured in the same conditions as panel A. Grey dashed part of the bar represents the inoculated virus (IFU<sub>0</sub>) and total height of the bar represents the final titer calculated at TOH ([IFU]<sub>f</sub>). Hence, black part corresponds to the net adenovirus production. Specific values of averages for each parameter and condition are presented on the top of each bar.

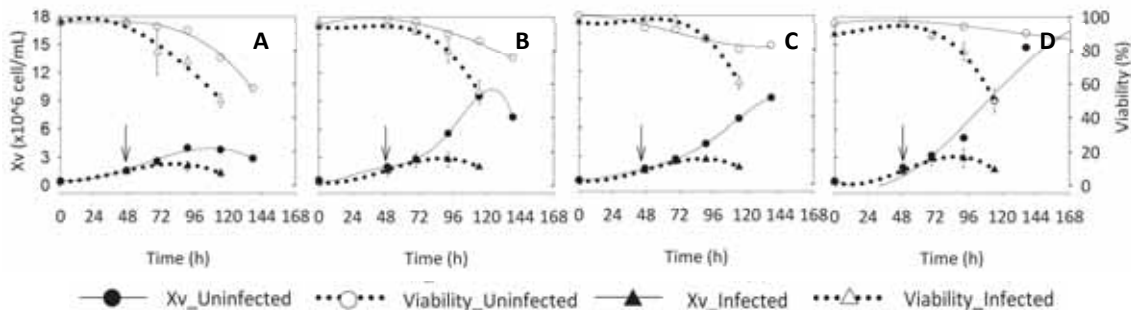


**Figure 4.15.** Cell growth of infected cultures in contrast to uninfected cultures in HyQ SFMTransFx-293 with different supplementation. A) 0%FBS 0% CB5 B) 5%FBS 0% CB5 C) 0%FBS 10% CB5 D) 5%FBS 10% CB5.

Besides, the reduction on final AdV production under this condition could not be only related to the depletion of FBS. When FBS was added in combination with CB5, viral production was almost doubled with respect the basal medium, but the viral titre did not reach the value obtained on FBS sole supplementation condition. Therefore, it can be assessed that although CB5 does not interfere on the infection process it does negatively affect to the production of adenovirus. Nevertheless, the beneficial effect of this nutritional supplement on cell growth has widely been shown in Chapter 1. Therefore, since further cell culture strategies development using CB5 would be studied in order to

increase even more the cell densities already achieved, it was decided to study infection parameters with the addition of this supplement to media. Increasing the biocatalyzer concentration (i.e. HEK293) would compensate the decrease on process productivity that CB5 would cause due to the slight reduction on AdV production.

#### **4.3.2. MOI, TOI AND TOH SELECTION.**

The infection parameters MOI, TOI and TOH previously described are closely related one to each other. For instance, the highest the MOI would be, the lowest the TOH, as the infection would develop faster and also no reinfection would occur. In order to study the interrelated effect of the three parameters, a fractional factorial experiment with three variables studied at different levels was carried out. The experiment was design in order to accomplish a double final objective: (1) maximise protein production and (2) maximise adenovirus production. The selected experimental space was decided on basis the following premises:

##### TOI

This parameter directly depends on cell growth of the cell strain to be infected in the selected cell media using a determined cell culture strategy. Based on the studies presented in Chapter 1, working in batch mode with HyQ SFMTransFx media 5%FBS and 10%CB5 (80g/L) supplemented, the maximal cell density for infection could be extended until approximately  $13 \times 10^6$  cell/mL (i.e. approximately 48 hours before reaching  $X_{v_{max}}$ ) (Fig.4.16). Nevertheless, in order to ensure proper cell condition, it was decided to reduce the experimental TOI range to the half of the maximal cell density that can be achieved. Hence, two TOIs were selected in this first optimisation approach:  $1 \times 10^6$  cell/mL as it is the most reported value in literature and  $5 \times 10^6$  cell/mL as a value close to the end of  $\mu_{max}$  phase.

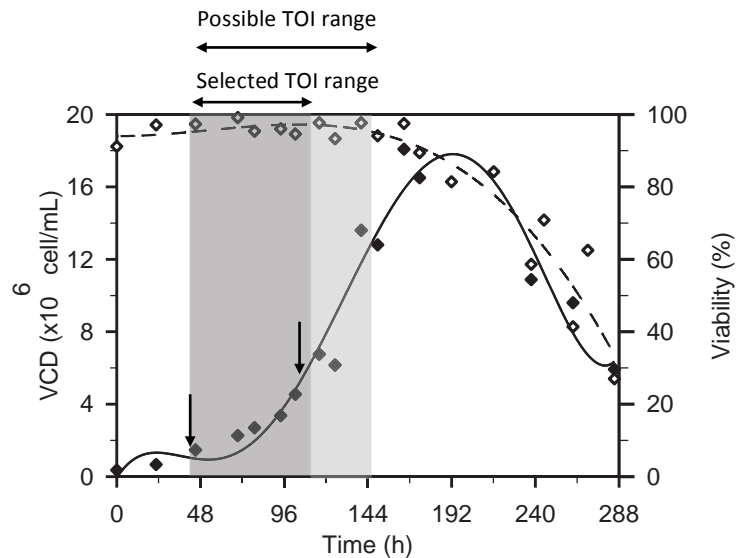


**Figure 4.16.** Reference cell culture of HEK293 growing in SFMTransF<sub>x</sub>-293 media 5%FBS and 10%CB5 (80g/L) supplemented. The time frame where TOI could be studied is light-grey shadowed and the final selected TOI range is dark-grey shadowed.. Arrows indicate the final selected TOIs.

### MOI

Based on previous studies performed within our research group an intermediate MOI=5 was selected. From this value, equidistant values (+1 and -1) were determined at MOI=7.25 and MOI=2.75. A value of MOI<1 was also included in the study in order to get information about how a non-single round infection performs. Consequently, the equidistant point from 2.75 (MOI=0.5) was selected.

### TOH

Due to the limitation of GFP detection in cell media (see Appendix 10.3) and also because *Cap*-PCV2 cloned into the adenoviral vector does not have any tag for purification purposes, it was decided to recover the protein of interest in the intracellular fraction.

After the preliminary studies presented in Appendix 10.3, the range within 32-48hpi was studied for protein production. In regards AdV production, it must be pointed out that only the infective fraction of AdV production will be considered for production and productivity evaluation. Therefore, the experimental TOH range was delayed in comparison to the one studied for protein production to ensure proper virus maturation. Two TOHs were selected for AdV production optimisation: 48hpi and 56hpi.

**Table 4.7.** Factorial design for GFP production maximisation. Each condition is performed in triplicate.

Parameter	Level ID	Real Value
TOI (X10 <sup>6</sup> cell/mL)	+	5
	-	1
MOI	+	7.25
	0	5
	-	2.75
	--	0.5
TOH (hpi)	++	48
	+	45
	0	41
	-	38
	--	35
	---	32

The study of best infection parameters will be presented in two separated sections. First, maximisation of protein production will be discussed and secondly, AdV production maximisation will be exposed.

#### 4.3.2.1. SELECTION OF BEST INFECTION PARAMETERS FOR PROTEIN PRODUCTION MAXIMISATION.

The response variable measured in order to evaluate protein production was intracellular fluorescence intensity and cell density. The evaluation of the results will be done on basis of specific production ( $Y_{GFP/x}$ ), specific production rate ( $q_{pGFP}$ ), volumetric production ( $Vp_{GFP}$ ) and volumetric productivity ( $Qp_{GFP}$ ). The calculation of these parameters is specified and argued below:

$$\text{Specific production } (Y_{GFP/x}) = \frac{[GFP]}{TCD} \quad (\text{Eq. 4.2})$$

Where:

[GFP] is the GFP concentration of the sample

TCD is total cell density

Total cell density was considered to be more appropriate than viable cell density due to the fact that dead cell population could be as fluorescent as living cell population (see Appendix 10.3). Nevertheless, it must be pointed out that that the sample preparation process could cause cell lysis to membrane-damaged cells (i.e. cells considered dead by the Trypan-blue viability assessment methodology used) resulting in GFP release to media. This fraction of GFP would not be considered

as only the intracellular fluorescence is measured and this would result in some underestimation of GFP production.

$$\text{Specific production rate } (q_{pGFP}): \frac{\Delta[GFP]}{\Delta ICT} \quad (\text{Eq. 4.3})$$

Only data from the period in which GFP could be expressed was considered for calculation of Integral total cell concentration (i.e. 32hpi onwards). This was decided in order to avoid  $q_{pGFP}$  underestimation due to the early period of viral cycle ( $\approx 12$ h) when virus entrance, uncoating and DNA replication take place but there is not GFP protein production.

$$\text{Volumetric production } (P_{GFP}) = [GFP]_{\max} \quad (\text{Eq. 4.4})$$

Where:

$[GFP]_{\max}$  is the maximal GFP concentration measured

$$\text{Volumetric productivity } (Qp_{GFP}) = \frac{[GFP]_{\max}}{T_{[GFP]_{\max}}} \quad (\text{Eq. 4.5})$$

Where:

$T_{[GFP]_{\max}}$  is the time to  $[GFP]_{\max}$

Two different  $Qp_{GFP}$  ( $Qp_{1GFP}$  and  $Qp_{2GFP}$ ) are evaluated. For  $Qp_1$  calculation, only the time from the infection until  $[GFP]_{\max}$  is considered, whereas for  $Qp_2$  the time from the beginning of the bioprocess until infection is also taken into account.

The experiment was performed as depicted in Figure 4.17. All the cultures to be infected derived from a unique cell culture in order to avoid variability on cell growth before infection. A unique viral dilution was performed and different volumes from this dilution were inoculated to cell culture in order to obtain the desired MOI. This strategy was decided to avoid dilution errors and hence, reduce intra-experimental variability. At the selected TOH, an aliquot from cell broth was sterile removed and fluorescence quantification was performed by fluorimetry.

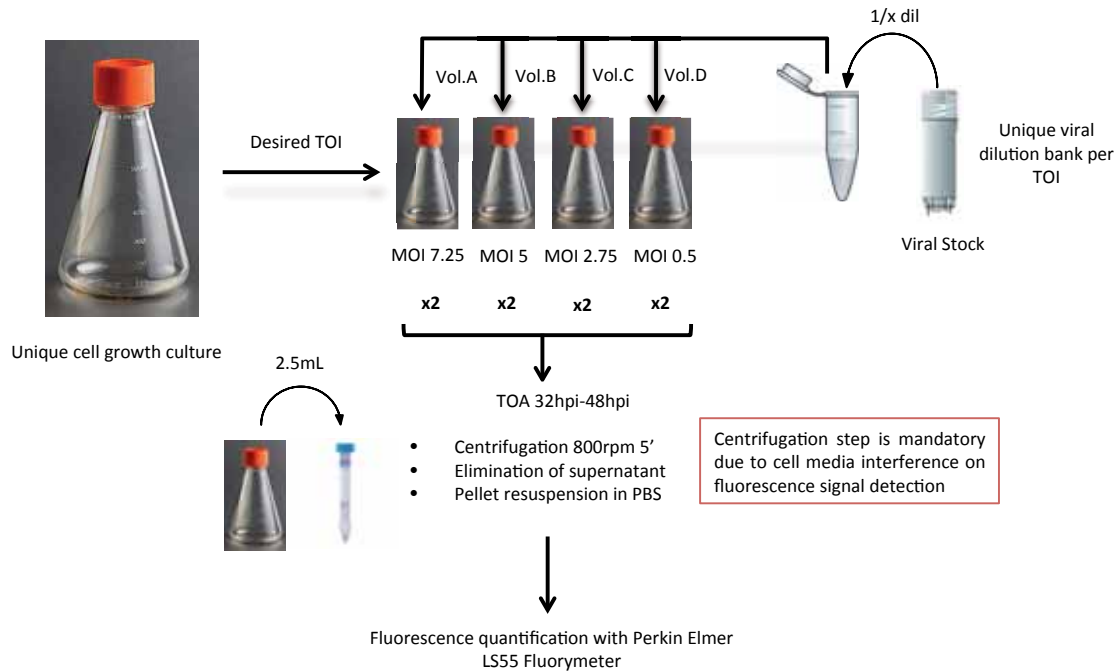


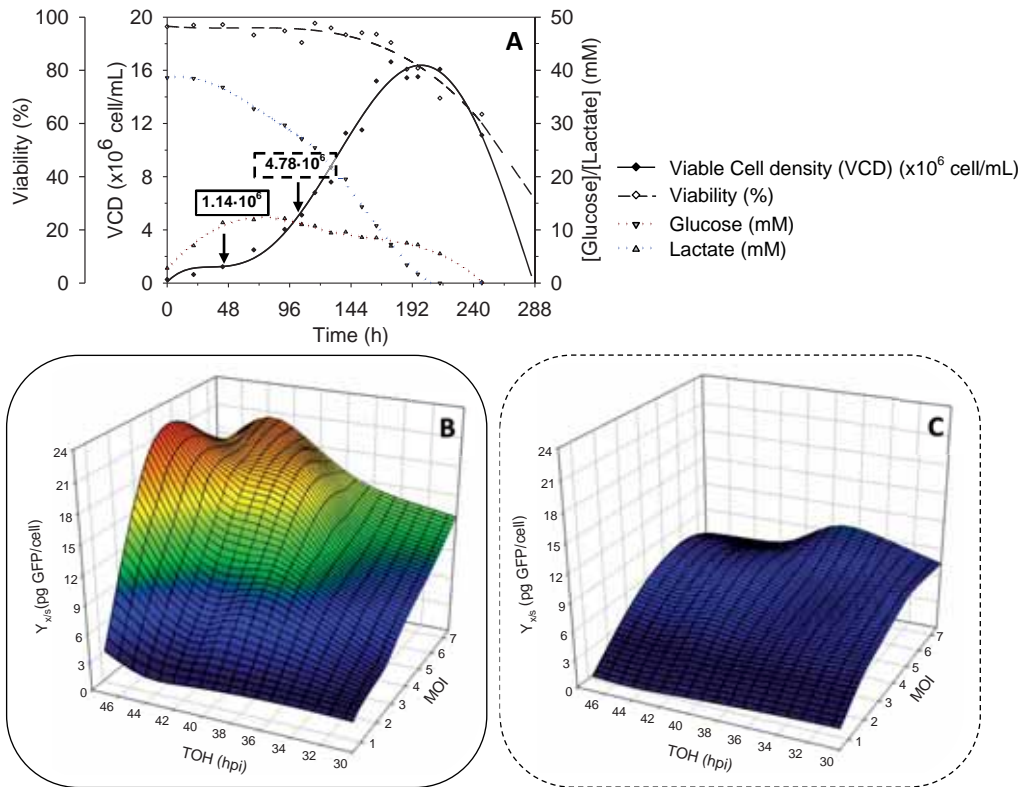
**Figure 4.17.** Scheme of the experiment for the selection of the best infection parameters for protein production maximisation.

The first important point to be addressed on the discussion of the experiment's outcome is the noteworthy decrement on specific production ( $Y_{GFP/x}$ ) observed when cells were infected at the higher TOI. In Figure 4.18B and Figure 4.18C the surface response curve of  $Y_{GFP/x}$  as function of MOI and TOH at the two evaluated TOIs are presented. The maximal value for specific production was encountered at intermediate MOIs and at the highest harvesting time evaluated when cells were infected at  $TOI=1 \times 10^6$  cell/mL. Under that conditions,  $Y_{GFP/x}$  was reduced almost three times at  $TOI=5 \times 10^6$  cell/mL in comparison to  $TOI=1 \times 10^6$  cell/mL. This fact indicates that although cells were still exponentially growing (control cell culture, Figure 4.18A), the environmental conditions or the physiological cell state were not appropriate for adenovirus infection and replication, thus reducing final protein concentration.



If we focus on maximal  $Y_{GFP/X}$  at  $TOI=1 \times 10^6$  cell/mL, no significant differences could be detected among MOIs 7.25, 5 and 2.75. Hence, the latter should be the preferred one for GFP production in order to increase process profitability. Infecting cells at  $MOI > 5$  would increase the requirements for a virus seed inventory (hence, process cost) without increasing protein production.

**Figure 4.18.** (A) Control of cell growth culture (B) Evaluation of  $Y_{GFP/X}$  at different MOI and TOH when infection



of HEK293 was performed at  $TOI=1 \times 10^6$  cell/mL or at (C)  $TOI=5 \times 10^6$  cell/mL

Concerning specific production it is also worth to mention the prompt achievement of maximal  $Y_{GFP/X}$  at  $MOI=7.25$  when cells were infected at the higher TOI in regard infection at the same MOI but at the lower TOI. This could be explained on basis to the sudden drop on viability and aberrant cell morphology (although not complete cell lysis) that was observed at  $MOI=7.25$  and  $TOI=5 \times 10^6$  cell/mL from early stages after infection, which was not detected when cells were infected at the same MOI but  $TOI=1 \times 10^6$  cell/mL. The highest the CPE is, the more GFP will be released to the extracellular space, resulting in a drop of GFP concentration as only the intracellular fraction is measured. Also, inadequate physiological cell state might lead to intracellular protein instability and consequently, drop on fluorescence emission. The greater drop on GFP quantification in comparison to the drop on total cell count will result in a reduction of the ratio  $[GFP]/TCD$ , hence specific production.

In regards  $q_{pGFP}$  evaluation at  $TOI=1 \times 10^6$  cell/mL, no significant differences can be detected between MOI 7.25 and MOI 5 but a substantial increment was estimated for infection at MOI 2.75 (Table 4.9, red square), confirming the suitability of HEK293 infection at this MOI.

**Table 4.9.** Comparison of GFP production parameters at different infection conditions. Maximal values for each parameter are underlined. Groups of data are highlighted in coloured squares to better follow the discussion. Arrows indicated the direction at which values should be compared for better understanding of the text.

	MOI	$q_{pGFP}$ ( $\mu\text{g}_{GFP}/\text{cell}\cdot\text{d}^{-1}$ )	$P_{GFP}$ ( $\mu\text{g}_{GFP}/\text{mL}$ )	$Qp_{1GFP}$ ( $\mu\text{g}_{GFP}/\text{mL}\cdot\text{d}^{-1}$ )	$Qp_{2GFP}$ ( $\mu\text{g}_{GFP}/\text{mL}\cdot\text{d}^{-1}$ )
TOI= $1 \times 10^6$	7.25	16.22±1.19	25.38±0.96	14.92±0.56	6.70±0.25
	5	17.44±1.19	29.79±0.07	16.21±0.10	7.58±0.03
	2.75	<b><u>27.79±2.52</u></b>	39.67±4.72	20.32±2.41	<b><u>9.81±1.17</u></b>
	0.5	6.28±1.20	10.72±0.63	5.48±0.32	2.65±0.16
TOI= $5 \times 10^6$	7.25	ND	46.42±0.82	<b><u>34.81±0.61</u></b>	7.13±0.13
	5	ND	<b><u>46.45±3.22</u></b>	27.19±1.88	6.74±0.47
	2.75	1.99±0.90	40.76±1.68	23.86±0.99	5.92±0.24
	0.5	0.72±0.08	13.61±0.82	6.95±0.42	1.91±0.11

\* It could only be calculated until T=41hpi. Afterwards, a significative productivity drop was detected.

With respect to volumetric production ( $P_{GFP}$ ), the greatest GFP concentrations were achieved when infections were performed at the highest TOI and high MOIs (Table 4.9, blue square). Nevertheless, the increment on maximal [GFP] was not proportional to the increment of cell density. In the case of a direct relation between cells to be infected and GFP production, a five-fold increment on volumetric production should be expected when infecting at  $TOI=5 \times 10^6$  cell/mL instead of  $TOI=1 \times 10^6$  cell/mL. However, only 1.5 to 2-fold-increment was achieved. Once again, the increment on MOI was not related to a higher  $P_{GFP}$ , neither at  $TOI=1 \times 10^6$  cell/mL nor at  $TOI=5 \times 10^6$  cell/mL. In fact, at the lower TOI tested, the infection MOI=2.75 resulted in higher volumetric production which is consistent with the higher specific production calculated at that MOI. Finally, focusing on  $Qp_{GFP}$ , higher values were achieved at  $TOI=5 \times 10^6$  cell/mL when only the time from infection is considered ( $Qp_{1GFP}$ , Table 4.9, orange square). Among the MOIs tested at this cell density of infection, 7.25 resulted in the highest estimated  $Qp_{GFP}$ . However, the  $Qp_{GFP}$  increment was not proportional to the increase of MOI. Besides, if the time needed to reach cell density of infection is considered ( $Qp_{2GFP}$ , Table 2.9, green square),  $TOI=1 \times 10^6$  cell/mL, MOI= 2.75 and TOH = 48hpi should the conditions selected based on the volumetric productivity of the process. Nevertheless, it is important to bear in

mind that this decision would directly depend on the design of the process. On the one here presented, infected cells derived from the same inoculum. Hence, three additional days were needed to reach cell density for the higher TOI. This could be avoided by implementing an inoculum train where cells would be maintained at  $5 \times 10^6$  cell/mL. Consequently, only time after infection would affect to  $Qp_{GFP}$  and thus, the highest cell density for infection should be considered, as it would result in higher volumetric productivity of the process.

Taking into account all these data, two different scenarios can be distinguished. When the infection is performed at low TOI, the best results for protein production are achieved working at intermediate MOIs (i.e. MOI=2.75). This would be related to an optimal condition of cell culture, enabling a good entrance of the virus to the cell and the cell efficiently producing the recombinant protein at the maximum rate. Infection at TOI= $1 \times 10^6$  cell/mL and MOI>2.75 may result in a massive block of intracellular mechanisms and hence, reduction of specific protein productivity ( $q_{pGFP}$ ). On the other hand, at TOI= $5 \times 10^6$  cell/mL the infection seems to be more inefficient, as in this scenario the greater values for volumetric productivity are achieved at higher MOIs (i.e. MOI=5 or MOI=7.25). The more viruses, the more chances that the event virus-attach-cell occurs. If this first step of the infection is inefficient, more events are needed to result in the same number of final viruses entering the cell. Moreover, intracellular cell condition at high TOI might be worst for protein production, as  $q_p$  is reduced for all the MOIs tested in comparison to these parameter at low TOI. It is interesting to point out that between TOI= $1 \times 10^6$  cell/mL and TOI= $5 \times 10^6$  cell/mL a lactate shift from production and secretion to consumption is noticed (Figure 4.18A). This metabolic change of the cells coincides with the end of the exponential growth rate and might also be related to the lower protein production when infecting at the higher TOI. Nevertheless, further studies of the relation between metabolic shift and protein production should be carried out to validate this hypothesis.

#### 4.3.2.2. SELECTION OF BEST INFECTION PARAMETERS FOR rAdV PRODUCTION.

As previously stated, the response variable measured for the evaluation of the AdV production was the infective particles produced by HEK293 and harvested at the end of the bioprocess. The evaluation of the results will be done on basis the specific production ( $Y_{Adv/x}$ ), the infective particle ratio (IPU<sub>R</sub>), the volumetric production ( $P_{Adv}$ ) and volumetric productivity ( $Qp_{Adv}$ ). Some modifications on the calculation of  $Y_{Adv/x}$ ,  $P_{Adv}$  and  $Qp_{Adv}$  had to be done in order to determine their value more accurately and reduce variability on the results.

$$\text{Specific production } (Y_{Adv/x}) = \frac{[Adv]_{TOH}}{VCD_{TOI}} \quad (\text{Eq. 4.6})$$

Where:

$[Adv]_{TOH}$  is the Adenovirus concentration at the time of harvest (TOH) calculated after sample titration.

$VCD_{TOI}$  is viable cell density calculated at the time of infection (TOI).

In some of the studied conditions, cells were severely damaged at TOH and the vast majority of cells presented aberrant morphology that hindered cell count and viability determination. This mostly happened at the latest TOH (56hpi) and at higher MOIs. The possible error on cell count could significantly affect the results and consequently, the obtained conclusions. Besides, at the highest TOH and  $MOI > 1$  cell lysis due to adenovirus infection has already started. Differently to GFP quantification, extracellular fraction of adenovirus was also considered. Hence, if cell density at TOH is used for  $Y_{Adv/x}$  determination, an overestimation of this value would be made. To avoid both cases, it was decided to use viable cell density at time of infection to work out  $Y_{Adv/x}$ .

$$\text{Infective particle ratio } (IPU_R) = \frac{[IPU]_f}{[IPU]_o} \quad (\text{Eq. 4.7})$$

Where:

$[IFU]_f$  is the concentration of infective particle units at TOH.

$[IFU]_o$  is the concentration of infective particle units at TOI.

$$\text{Volumetric production } (Vp_{Adv}) = [Adv]_{TOH} \quad (\text{Eq.4.8})$$

Where:

$[Adv]_{TOH}$  is Infective particle units concentration at the indicated time of harvest (i.e. 48 or 56hpi).

For Adv production evaluation, only two TOH were selected instead of performing a complete kinetic study of Adv production. Therefore, it was decided to analyse the results at both TOH instead of selecting the one at which  $[Adv]$  was maximal.

$$\text{Volumetric productivity } (Qp_{Adv}) = \frac{[Adv]_{TOH}}{TOH} \quad (\text{Eq. 4.9})$$

The experiment was carried out as depicted in Figure 4.19. As it was performed in the experiments for GFP production maximisation previously presented, all cultures of this experimental set derived from a single cell culture in order to avoid variability on cell growth before infection. Also, a single viral dilution was performed and different volumes from this dilution were inoculated to cell culture depending on the MOI desired. At the selected TOH, an aliquot from cell broth was sterile removed and cell lysis was performed by heat shock protocol. In order to avoid intra-assay variability, the sample removed at TOH=48hpi was stored at  $-80^{\circ}\text{C}$  until the sample of TOH=56hpi was taken. The titration of both samples was then performed in a single assay.

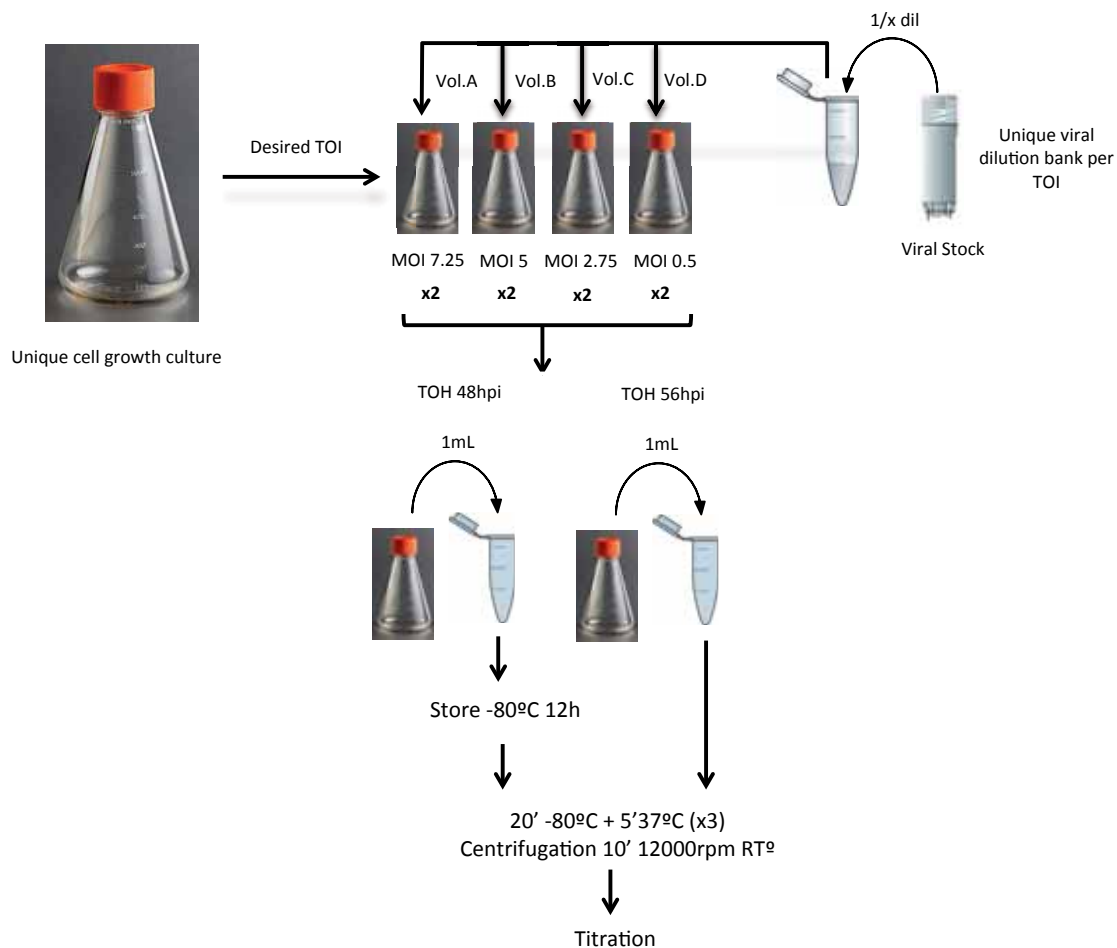
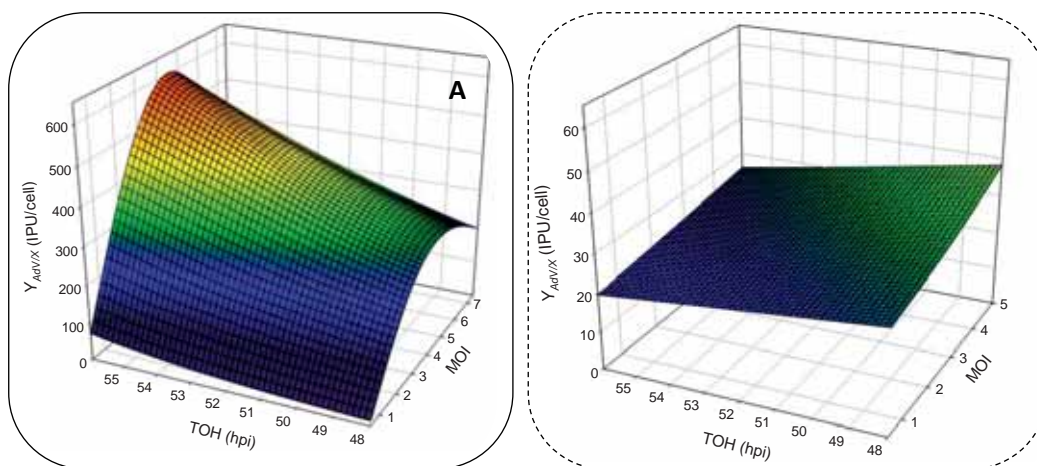


**Figure 4.19.** Scheme of the experiment for the selection of the best infection parameters for AdV production maximisation.

As it can be observed in the charts of Figure 4.20, the infection at  $\text{TOI}=5 \times 10^6$  cell/mL resulted in a significant drop of  $Y_{AdV/X}$  in comparison to infection at  $\text{TOI}=1 \times 10^6$  cell/mL, which correlates well with the results presented in the prior section. However, the influence of TOI on the reduction of specific

production was greater in Adenovirus than in GFP production. The most important fall occurred at MOI 2.75 TOH=56hpi when  $Y_{Adv/X}$  was reduced more than 20 times at  $TOI=5 \times 10^6$  cell/mL in comparison to  $TOI=1 \times 10^6$  cell/mL. The lowest drop on specific Adv production was observed at MOI=0.5 TOH=56hpi and it was approximately 5-fold reduction which was still higher than the highest drop calculated for GFP production (i.e. 3-fold drop at high TOI in regard low TOI). It can be hypothesised that the production of a monomeric protein would require less energy and would occur before in viral cycle than the production of all the capsid proteins and their assembly for the production of new viral particles. Even if the Adv could be produced, the final assembly might be incomplete resulting in non-infective Adv. Consequently, if the environmental conditions or the physiological cell state at  $TOI=5 \times 10^6$  cell/mL have a detrimental effect on GFP production, this effect will be far more evident for a more complex process in terms of time and energy (i.e. Adenovirus production).

The parabolic shape of the tridimensional representation of specific production as function of MOI and TOH when infection was performed at  $TOI=1 \times 10^6$  cell/mL (Figure 4.20A) indicates that the best condition for Adv production is an intermediate MOI ( $3 < MOI < 5$ ) and a TOH=58hpi. Although the results suggest that longer times of harvest should be tested in order to clearly define a  $Y_{Adv/X}$  maximal point, this was not performed on basis of the constraints of the studied bioprocess (i.e. recombinant protein must be recovered in the intracellular fraction for easier downstream process). Besides, the flat shape of the  $TOI=5 \times 10^6$  cell/mL implies that any significant differences are found in  $Y_{Adv/X}$  among the selected infection conditions.



**B**

**Figure 4.20.** Evaluation of  $Y_{Adv/X}$  at different MOI and TOH when infection of HEK293 was performed at (A)  $TOI=1 \times 10^6$  cell/mL or (B)  $TOI=5 \times 10^6$  cell/mL. y-axis had to be re-scaled (x10 in chart A) for correct visualization purposes

The second parameter evaluated was the infective particle unit ratio ( $IPU_R$ ). The results offer additional data to determine the already discussed drop on adenovirus production when increasing TOI.  $IPU_R$  values for all the MOIs tested at different TOIs and TOHs are compiled in the Table 4.10 and the representation of the results for each TOI tested is presented in Figure 4.21. The first point to be addressed is that at  $TOI=1 \times 10^6$  cell/mL there is a direct relation between  $IPU_R$  and TOH regardless the MOI (black arrows, Figure 4.21, left panel). On the contrary, at  $TOI=5 \times 10^6$  cell/mL an inverse relation between  $IPU_R$  and TOH was noticed (black arrows, Figure 4.21, right panel). This could indicate that media conditions at upper TOI affect virus stability, so the longer the virus remains in the extracellular space would lower the infective capacity of the virus. It is also interesting to comment that at low TOI and  $MOI > 1$ ,  $IPU_R$  and MOI are inversely related. This is, that despite the TOH,  $IPU_R$  increased as MOI decreased until  $MOI < 1$  (blue arrows in Figure 4.21, left panel). In contrast, at  $TOI=5 \times 10^6$  cell/mL the inverse relation between MOI and  $IPU_R$  was maintained even for  $MOI < 1$ . This fact indicates that the viral load does also affect viral cycle progression at higher TOI. Increasing MOI resulted in a higher probability that more than one virus enter the cell leading to a more aggressive infection. This means that more virus trying to replicate within the same cell might cause more severe CPE and eventually cell machinery may be blocked resulting in less viral production. The hypothesis is, that the better the physiological state of the cell is, the better the cells progress after infection at higher MOI. This would fit with the obtained results: at low TOI, the physiological cell state would enable the correct infection cycle progress at MOI 2.75 resulting in a more effective adenovirus production and  $IPU_{R(MOI\ 2.75)} > IPU_{R(MOI\ 0.5)}$ . Conversely, at  $TOI=5 \times 10^6$  cell/mL the cell state wouldn't somehow resist to an infection at the same MOI leading to an inversion of  $IPU_R$  relation ( $IPU_{R(MOI\ 2.75)} < IPU_{R(MOI\ 0.5)}$ ).

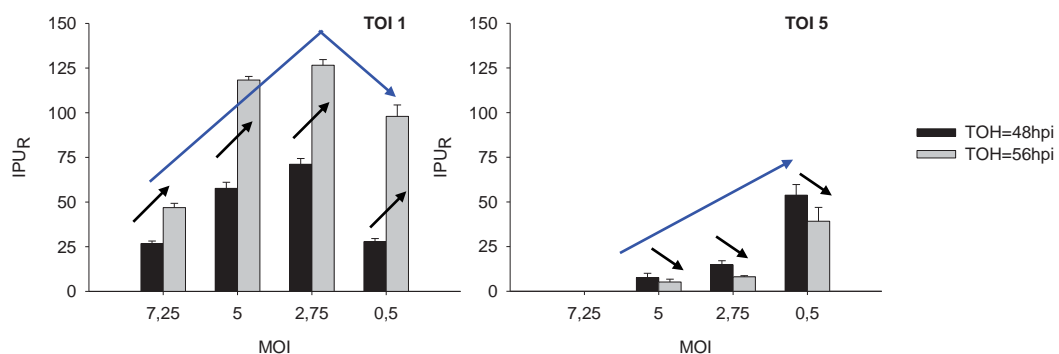


**Figure 4.22.**  $IPU_R$  calculated for each MOI and TOI at the two different TOHs evaluated. Left panel:  $TOI=1 \times 10^6$  cell/mL; Right panel:  $TOI=5 \times 10^6$  cell/mL.

**Table 4.10.** IPU<sub>R</sub> at the different evaluated conditions.

MOI	TOI= 1x10 <sup>6</sup> cell/mL		TOI= 5x10 <sup>6</sup> cell/mL	
	48hpi	56hpi	48hpi	56hpi
	7.25	26.73±1.46	46.86±2.39	nd
5	57.62±3.42	118.26±2.07	7.63±2.43	5.19±1.55
2.75	71.15±3.23	126.57±3.17	14.80±2.30	8.07±0.62
0.5	27.80±1.78	97.96±6.35	53.78±5.94	39.19±7.75

Finally, focusing on the effect of TOH on IPU<sub>R</sub>, different tendencies depending on TOI can be observed. At low TOI, IPU<sub>R</sub> increases along with TOH, whereas at TOI=5x10<sup>6</sup> cell/mL a decrement of IPU<sub>R</sub> was detected at higher TOH.

Regarding volumetric production evaluation, completely different outcomes were obtained depending on the TOI. In Figure 4.22 and Table 4.11 AdV volumetric productions of the different conditions tested are presented. On one hand, at TOI=1x10<sup>6</sup> cell/mL the AdV final titre lowered along with the decrement on MOI as it was expected, but with the exception of MOI=7.25. The lower  $P_{AdV}$  at MOI=7.25 in comparison to MOI=5 or 2.75, might be related to the sharper drop on viability of cell culture. The mechanisms triggered inside of dying cells can affect the replication capacity of the adenovirus. Besides, AdV release to media might occur earlier in infected cultures at higher MOIs. If this was the case for MOI=7.25, the environmental conditions of the extracellular space might also affect adenovirus stability and infective capacity resulting in the observed drop of the final titre. On the other hand, at TOI=5x10<sup>6</sup> cell/mL  $P_{AdV}$  did not significantly differ regardless the studied MOI. This means, that at this cell density, efficiency of adenovirus production is much lower and the final titre will be the same in cultures infected with different viral inoculum.

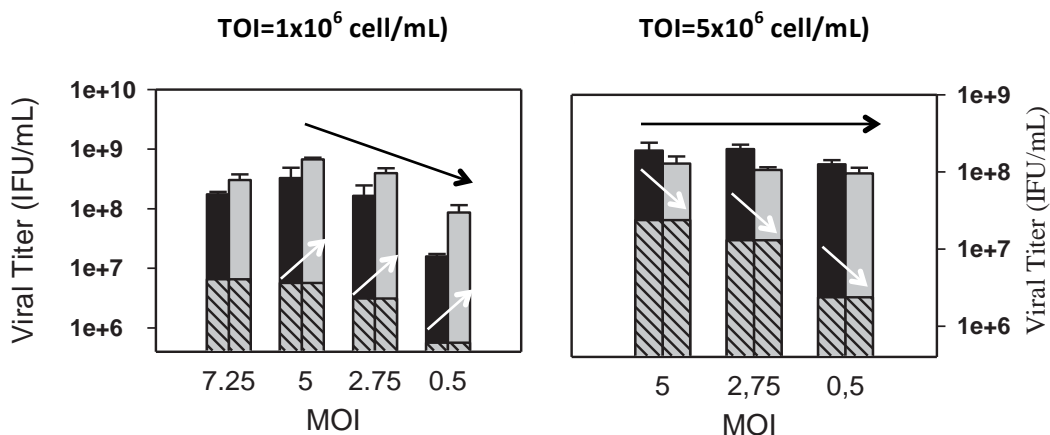


**Figure 4.22.** Volumetric production of rAdV at different MOI, TOI and TOH. Left Panel: TOI 1x10<sup>6</sup> cell/mL. Right panel: TOI=5X10<sup>6</sup> cell/mL. Plain black bars: TOH=48hpi; Plain grey bars: TOH=56hpi; Patterned grey bars: [IFU]<sub>0</sub>. The overall height of the bar represents [IFU]<sub>t</sub>, meaning that the plain part of the bar represents the net adenovirus production. White arrows indicate the tendency on adenovirus production depending on TOH for a



given MOI. Black arrows indicate the tendency on Adenovirus production depending on MOI regardless the TOH.

The second important observation on the evaluation of  $P_{Adv}$  is that at  $TOI=1 \times 10^6$  cell/mL the final AdV titer increased along with TOH despite the studied MOI (Table 4.11, blue square). Nevertheless, the magnitude of the increment was higher as MOI was reduced. As previously discussed, these differences on the magnitude of increment could be related either to a faster viral infection process at higher MOI (resulting into prompter viral release and possible adenovirus inactivation in cell broth) or to a more aggressive infection as MOI increases (resulting in massive cell damage and impossibility of finishing cell cycle). Conversely, final AdV titre decreased along with TOH at  $TOI=5 \times 10^6$  cell/mL, even at the lowest MOI studied. This probably means that although cells can still grow exponentially, the environmental conditions at this cell density are not suitable for finishing the whole viral cycle and produce infective adenovirus. Finally, it is worth to mention, that differently to what has been encountered for GFP volumetric production,  $P_{Adv}$  is lower at  $TOI=5 \times 10^6$  cell/mL than at  $TOI=1 \times 10^6$  cell/mL (Table 4.11, orange square) which supports the idea that infecting at higher TOI was less efficient for AdV production than in recombinant protein production.

**Table 4.11.** Comparison of AdV production parameters at different infection conditions. Maximal values for each parameter are underlined.

	MOI	$P_{Adv}$ (48hpi) ( $\times 10^7$ IFU/mL)	$P_{Adv}$ (56hpi) ( $\times 10^7$ IFU/mL)	$Qp_{1Adv}$ ( $\times 10^7$ IFU/mL·d <sup>-1</sup> )	$Qp_{2Adv}$ ( $\times 10^7$ IFU/mL·d <sup>-1</sup> )
TOI= $1 \times 10^6$	7.25	17.44±2.71	30.58±9.34	13.10±0.67	6.44±0.33
	5	<u>32.69±1.32</u>	<u>67.09±7.75</u>	↓ <u>28.75±0.50</u>	<u>14.13±0.25</u>
	2.75	15.10±2.40	39.54±4.04	16.95±4.25	8.32±2.09
	0.5	1.58±0.22	8.11±1.26	3.47±1.55	1.71±0.76
TOI= $5 \times 10^6$	7.25	nd	nd	nd	nd
	5	18.05±3.16	12.28±1.24	9.03±2.87	2.58±0.82
	2.75	19.29±2.07	10.52±0.73	9.64±1.50	2.76±0.43
	0.5	12.73±1.92	9.28±1.64	6.37±0.70	1.82±0.20

\* $Qp_1$  and  $Qp_2$  here presented have been calculated at TOH=56hpi for  $TOI=1 \times 10^6$  cell/mL and at TOH=48hpi for  $TOI=5 \times 10^6$  cell/mL

Finally, the evaluation of the calculated volumetric productivities led us to conclude that for production of adenovirus the infection at  $TOI=1 \times 10^6$  cell/mL is preferred. Contrarily to what was observed for GFP production,  $Qp$  was higher at low TOI, whether considering time after infection ( $Qp_1$ ) or time from cell culture seeding ( $Qp_2$ ) (Table 4.11, green square). This is also in good

correlation with the higher drop on ADV volumetric production at  $\text{TOI}=5 \times 10^6$  cell/mL in comparison to the drop on GFP volumetric production.

Taking into account all the data presented so far and the analysis performed, it was determined that regardless the product to recover (i.e. recombinant adenovirus or recombinant protein) the time of infection should be set at  $1 \times 10^6$  cell/mL and the selected MOI should be 2.75 on basis to  $q_{pGFP}$  and  $\text{IPU}_R$ . On the contrary, different TOH should be selected depending on the product to recover. For protein production maximisation, the best TOH at the stated TOI and MOI, was 48hpi as the vaccine candidate (i.e. r-CappCV2) must be intracellular recovered. Focusing on adenovirus vector maximisation, TOH=56hpi should be selected for  $\text{TOI} = 1 \times 10^6$  cell/mL and  $\text{MOI}=2.75$ . Nevertheless, since r-CapPCV2 is actually the vaccine candidate, TOH was finally selected as the preferred one for the studied bioprocess.

### 4.3.3. EFFECT OF MEDIA REPLACEMENT ON PROTEIN AND ADENOVIRUS PRODUCTION

The evaluation and discussion of the drop on  $q_p$  and  $Q_p$  when increasing TOI regardless the product of interest (GFP or Adv) led to the idea that environmental conditions could be affecting cell productivity. In Chapter 1 it has already been discussed that in between the two TOIs tested on the evaluation of infection parameters ( $1 \times 10^6$  and  $5 \times 10^6$  cell/mL), a drop on specific growth rate was noticed, together with a shift on lactate metabolism. Besides, when studying the effect of cell media replacement on cell growth (Chapter 3, Section 3.3.2) it was assessed how the media replacement resulted in an elongation of exponential growth phase. Taking all this into account, it was decided to perform media replacement at the time of infection, and evaluate the effect of the replacement on the efficiency of infection, GFP production and Adv production. Two different TOIs were selected, one as pre-shift TOI (TOI= $1 \times 10^6$  cell/mL) and the other as post-shift TOI (TOI= $8 \times 10^6$  cell/mL). Based on the results obtained in section 4.3.2.2, the infections were performed only at MOI=2.75. The time of harvest for protein production evaluation was set between 36 and 48hpi and a unique TOH (48hpi) was selected for adenovirus production evaluation.

The first studied parameter was the influence of media replacement (onwards MR) on the efficiency of infection. In order to do so, the fluorescence of the infected cultures was analysed by flow cytometry at 24hpi. At that point, almost 100% of cells were infected (i.e. were fluorescent). Interestingly, two populations could be distinguished regardless the TOI and MR performance: a high-fluorescent population and a low-fluorescent population (Figure 4.23). Even more interesting was the fact that the percentage of cells within the “high-fluorescent” population and the fluorescence mean of this population were higher in cell cultures in which MR was performed in comparison to the cultures where MR was not carried out. This could be related to a better physiological cell state and more energy available for adenovirus replication and GFP production. So, it can be concluded that MR improves infection efficiency.

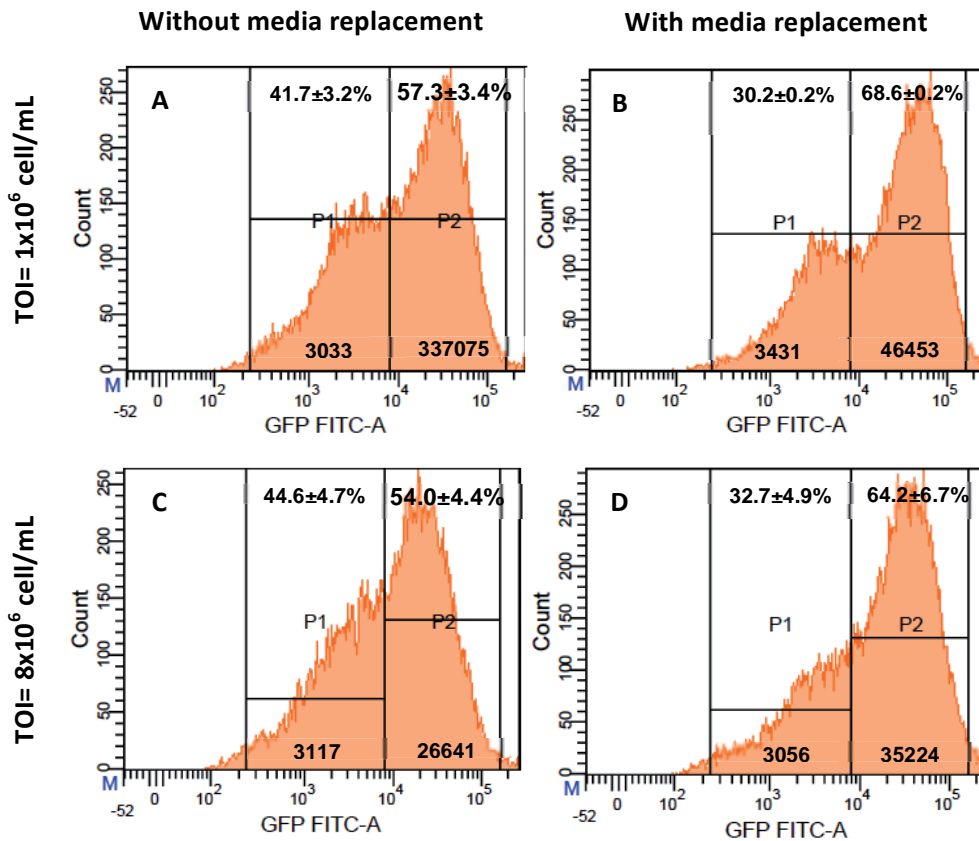


**Figure 4.23.** Flow cytometer histograms of infected HEK293 cell cultures with rAdV-GFP at 24hpi. (A) Infection at TOI=1x10<sup>6</sup> cell/mL without media replacement; (B) Infection at TOI=1x10<sup>6</sup> cell/mL with media replacement (C) Infection at TOI=8x10<sup>6</sup> cell/mL without media replacement; (D) Infection at TOI=1x10<sup>6</sup> cell/mL with media replacement (D).

GFP production and kinetics are in good correlation with the results of infection efficiency. In Figure 4.24 progression of intra- and extracellular fluorescence for cultures infected at low TOI with and without MR (Figure 4.24B and Figure 4.24A respectively) and high TOI with and without MR (Figure 4.24D and Figure 4.24C respectively) are depicted. At TOI=1x10<sup>6</sup> cell/mL MR slightly increased total GFP produced whereas the positive effect of MR was much more remarkable at TOI=8x10<sup>6</sup> cell/mL resulting in a three-fold increment on intracellular fluorescence in regard infection without MR. It is also noteworthy to mention the differences on GFP kinetics depending on the replacement of media. At TOI=1x10<sup>6</sup> cell/mL with MR, a pronounced exponential profile of the extracellular GFP was detected in comparison to a lower protein release to media at the same TOI but without MR. This fact, together with the sharper drop on viability of infected cultures when MR was carried out, might indicate a faster progression of viral cycle, and prompter release of the produced protein to media. When cells were infected at TOI=8x10<sup>6</sup> cell/mL and MR was performed, again a steep exponential profile of GFP release to the extracellular space was observed. This release might also be related to a proper physiological state of the cells, resulting in a more efficient viral replication. At the same TOI but without MR, a sudden release to intracellular GFP to media was also noticed from t=41hpi.

Nevertheless, the low overall GFP production might indicate a bad cell condition for adenovirus replication resulting in severe cell damage after infection and consequent GFP release to the media. This is totally different to the proposed hypothesis for fluorescence kinetics at low TOI with MR, which might be related to an efficient and fast adenovirus replication.

Production and productivity values are compiled in Table 4.12. Due to the quicker GFP release to media than it was expected,  $Y_{GFP/X}$  values have only been calculated for TOH in which intracellular GFP was maximal, which for almost all the cultures correspond to the first sample (i.e. TOH=38hpi).  $V\rho_{GFP}$  and  $Qp_{GFP}$  have been calculated as detailed in section 4.3.2.1.

**Table 4.12.** Comparison of GFP production parameters in cell cultures infected at MOI 2.75, at low TOI ( $1 \times 10^6$  cell/mL) or high TOI ( $8 \times 10^6$  cell/mL) with or without media replacement at TOI. Groups of data are highlighted in coloured squares to better follow the discussion.

		$Y_{GFP/X}$	$V\rho_{GFP}$	$Qp_{1GFP}$	$Qp_{2GFP}$
		(pgGFP/cell)	( $\mu$ gGFP/mL)	( $\mu$ gGFP/(mL · d))	( $\mu$ gGFP/(mL · d))
TOI	$1 \times 10^6$	20.42 $\pm$ 4.21	51.66 $\pm$ 1.05	30.43 $\pm$ 0.62	15.41 $\pm$ 0.31
	w MR	21.92 $\pm$ 3.54	62.16 $\pm$ 8.80	39.61 $\pm$ 5.61	20.50 $\pm$ 2.90
TOI	$8 \times 10^6$	20.45 $\pm$ 0.71	50.05 $\pm$ 0.87	31.89 $\pm$ 0.54	7.68 $\pm$ 0.13
	w MR	52.56 $\pm$ 1.52	149.23 $\pm$ 1.34	95.09 $\pm$ 0.85	24.61 $\pm$ 0.22

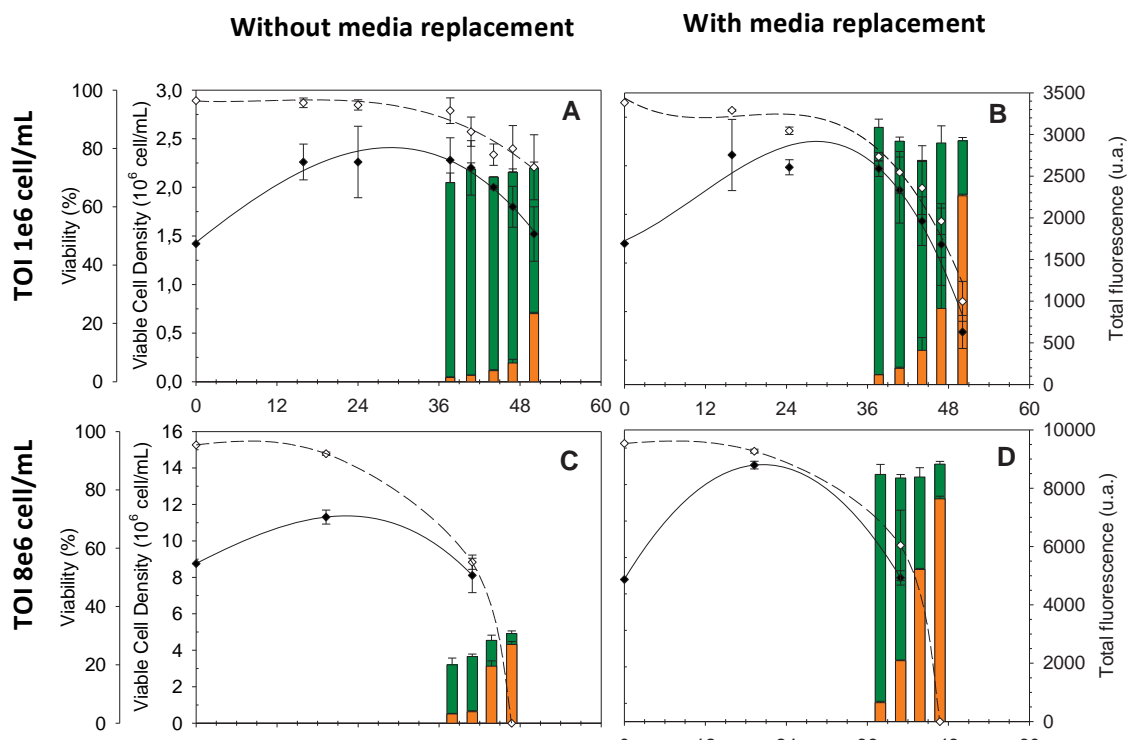


**Figure 4.24.** Evaluation of the effect of media replacement at TOI on GFP production. (A) TOI= $1 \times 10^6$  cell/mL without media replacement (B) TOI= $1 \times 10^6$  cell/mL with media replacement (C) TOI= $8 \times 10^6$  cell/mL without media replacement (D) TOI= $8 \times 10^6$  cell/mL with media replacement. Vertical bars height represent the sum 11

Concerning specific production, the positive effect on MR was much more remarkable at  $\text{TOI}=8 \times 10^6$  cell/mL as it could be inferred from the results presented in Figure 4.24.  $Y_{\text{GFP}/X}$  was comparable at  $\text{TOI}=1 \times 10^6$  cell/mL regardless media replacement performance. In contrast,  $Y_{\text{GFP}/X}$  was 2-fold incremented at  $\text{TOI}=8 \times 10^6$  cell/mL when MR was carried out (Table 4.12, blue square). In terms of volumetric productivity of the process, maximal values were obtained at  $\text{TOI}=8 \times 10^6$  cell/mL when MR was carried out ( $Q_{p_{1\text{GFP}}}=95.09 \pm 0.85 \mu\text{gGFP}/(\text{mL} \cdot \text{d})$ ; Table 4.12). Nevertheless, we encountered once again that the increment on  $Q_p$  was not proportional to the increment of TOI (Table 4.12, orange square). Consequently, if both the time pre and post infection are considered for volumetric productivity estimation ( $Q_{p_2}$ ), values became comparable between the TOIs tested when MR was performed ( $20.50 \pm 2.90$  and  $24.61 \pm 0.22 \mu\text{gGFP}/(\text{mL} \cdot \text{d})$  at low and high TOI, respectively) (Table 4.12, green squares).

The effect of media replacement on Adv production was also assessed and the results are presented in Figure 4.25. As it was expected after the evaluation of GFP evolution, the majority of the adenovirus (>70%) were in the supernatant at  $\text{TOH}=48\text{hpi}$ , except for the infections performed at  $\text{TOI}=1 \times 10^6$  cell/mL without media replacement, in which cell damage due to adenoviral lysis was not significantly noticed at that TOH. The positive effect of MR was clearly evident at  $\text{TOI}=8 \times 10^6$  cell/mL where a 2-fold increment on final titre (and hence, on  $\text{IFU}_R$  and  $Y_{\text{Adv}/X}$  (Table 4.13)) was achieved in comparison to the situation in which no MR was performed. On the contrary, MR at  $\text{TOI}=1 \times 10^6$  cell/mL had not a significant effect on adenovirus production. The slight reduction on volumetric production ( $P_{\text{Adv}}$ , Table 4.11) is more related to experimental approach variability rather than a real drop on Adv production. Focusing on volumetric productivities, a positive effect was also encountered for media replacement at  $\text{TOI}=8 \times 10^6$  cell/mL. Nevertheless, the positive effect of MR on  $Q_p$  was not proportional to cell density at TOI, resulting in a reduction of  $Y_{\text{Adv}/X}$  and  $Q_p$  at high TOI in comparison to low TOI.

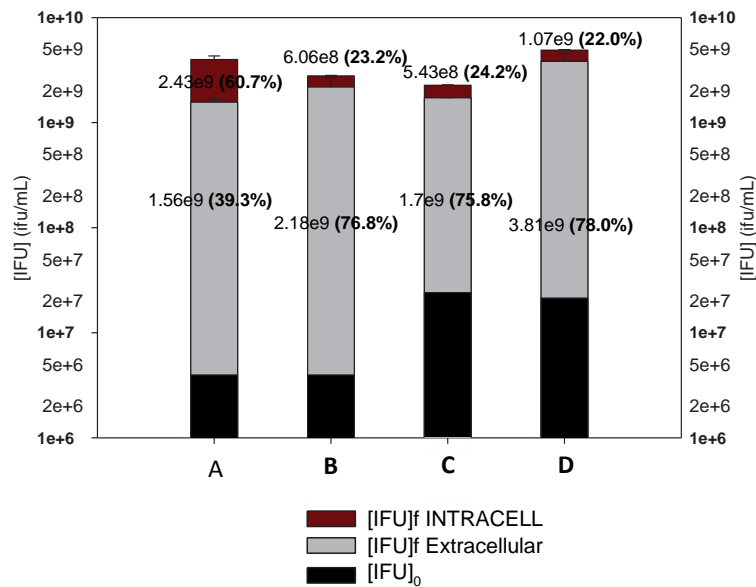


**Figure 4.25.** Effect of media replacement on adenovirus production. (A) TOI= $1 \times 10^6$  cell/mL without media replacement (B) TOI= $1 \times 10^6$  cell/mL with media replacement (C) TOI= $8 \times 10^6$  cell/mL without media replacement (D) TOI= $8 \times 10^6$  cell/mL with media replacement. Numbers represent viral titre for the corresponding fraction and which percentage from the total produced virus does it represent. Black part of the bar represents the viral inoculum and it is overlapped to the viral production after infection. Total bar height represents the sum of intracellular and extracellular virus at TOH=48hpi. Hence, red part of the bar represents IFU in the intracellular space and grey part of the bar represent IFU in the supernatant. Net viral production (i.e.  $IFU_t - IFU_0$ ) should be calculated from the end of black part of the bar till the top of the bar.

**Table 4.13.** Comparison of rAdV-GFP production parameters in cell cultures infected at MOI 2.75, with or without media replacement at TOI.

		$P_{Adv}$	$Y_{Adv/X}$	$IFU_R$	$Qp_{1Adv}$	$Qp_{2Adv}$
		( $\times 10^8$ Adv/mL)	(Adv/cell)		( $\times 10^8$ Adv / (mL · d))	( $\times 10^8$ Adv / (mL · d))
TOI $1 \times 10^6$	w/o MR	39.90±1.96	2771	1006	19.95±0.98	10.92±0.53
	w MR	27.892±5.77	1923	700	13.95±2.98	8.05±1.67
TOI $8 \times 10^6$	w/o MR	22.41±1.03	256	93	11.21±0.52	3.23±0.15
	w MR	48.84±0.53	628	228	24.42±0.26	7.53±0.08

In order to evaluate if the metabolic shift from lactate production to lactate consumption could be the cause behind the lower productivity when infecting at high TOI, the concentration of this metabolite was measured along cell culture. As it is depicted in Figure 4.26A and 2.26C, in cell cultures where media replacement was not performed, lactate was produced and secreted to media until reaching a concentration around 12-13mM at around 96h of cell culture. At that point, the concomitant consumption of glucose and lactate was triggered until the end of cell culture, as it has been previously mentioned in this work. When media replacement was made at TOI= $1 \times 10^6$  cell/mL

(Figure 4.26B), the metabolic shift had not been triggered yet. After the replacement of media, lactate was fast produced until reaching a concentration of approximately 13mM at 24hpi. At that point, the lactate switch from production to consumption occurred, coinciding with the metabolic shift on cell cultures where MR was not performed. Conversely, at  $\text{TOI} = 8 \times 10^6$  cell/mL the metabolic shift happened approximately 36 hours before infection. While in cell cultures without media replacement lactate continued to be consumed until the end of cell culture, media exchange could revert the metabolic change and lactate started to be produced once again after media replacement for 24 hours. These observations led us to hypothesise that the drop on recombinant protein or adenovirus is related to this metabolic shift and/or to the conditions triggering the shift. When cells are infected before the shift has occurred, cells are equally productive regardless media replacement. On the contrary, once cells have changed their metabolism, they cannot longer maintain the specific productivity. By reverting the metabolic shift cells return to the initial metabolic state and this might be related to the a partial recovery of  $q_p$ . However, further research should be carried out in order to evaluate this hypothesis.

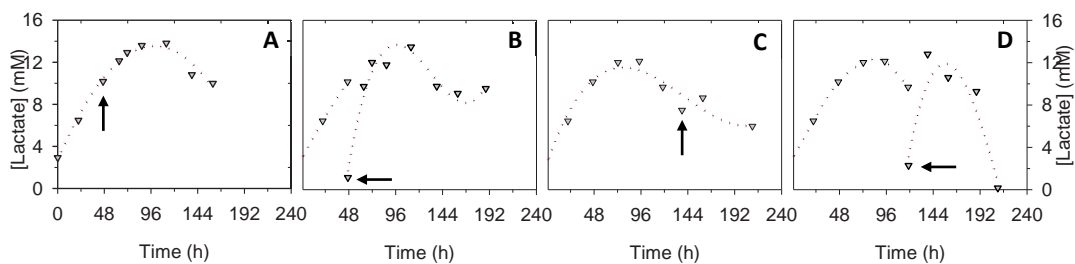


**Figure 4.26.** Extracellular lactate evolution along cell culture. (A)  $\text{TOI} = 1 \times 10^6$  cell/mL w/o MR (B)  $\text{TOI} = 1 \times 10^6$  cell/mL with MR (C)  $\text{TOI} = 8 \times 10^6$  cell/mL w/o MR (D)  $\text{TOI} = 1 \times 10^6$  cell/mL with MR. Arrows indicate the time of infection.



#### 4.4. EVALUATION OF r-CapPCV2 AND rAdV-CapPCV2 PRODUCTION.

After the complete analysis of infection parameters presented in previous sections, the infection parameters selected for obtaining the vaccine candidate were: MOI=2.75, TOI= $1 \times 10^6$  cell/mL, TOH=48hpi without media replacement at TOI. We then performed the infection of HEK293 suspension cells with rAdV-CapPCV2 in these conditions. The infection of the cells with rAdV-GFP was carried out in parallel in order to compare the results avoiding possible interassay variability.

The efficiency of infection could not be assessed as it has been done in previous sections due to the lack of a reporter gene within rAdV-CapPCV2. However, the viability progression of all cell cultures was similar and therefore, a similar efficiency of infection was assumed regardless the strain of the adenovirus used. Surprisingly, it was found out that CapPCV2 specific production ( $Y_{CapPCV2/X}$ ) drastically dropped in comparison to GFP. Whereas  $Y_{p/X} = 11.96 \pm 0.87$  pg/cell was estimated for GFP, this value was reduced to  $2.57 \pm 0.25$  fg/cell for CapPCV2.

This unexpected result led us to evaluate protein production upon AdV infection in a different HEK293 cell line. The selected one was AD-293 cell line, which is the one used for the complementation of the recombinant adenovirus generated in this project (rAdV-CapPCV2). It was known in advance that the infection of adherent cells and suspension cells might perform differently. Therefore, we cannot compare the results of suspension cell line infection (HEK293) with the obtained after adherent cell line infection (AD-293). Instead, we will compare the outcomes of infection with the two AdV vectors (rAdV-CapPCV2 and rAdV-GFP) of AD-293. The most important difference between infection of HEK293 cells and AD-293 cells would probably be the increment on probability that a particular viral particle would attach to a cell in suspension cell culture (i.e. HEK293) due to the continuous shaking of media. Hence, the infection parameters previously selected, could not be the best for infection of adherent cells. However, as a starting point for protein production evaluation, MOI TOI and TOH parameters were kept at the same values than in infection of suspension cells. Besides, to ensure a good infection of adherent cells an additional MOI as high as 27.5 was tested (10-fold increment of the reference value). The results are evaluated on basis of protein and adenovirus specific production ( $Y_{CapPCV2/X}$  and  $Y_{Adv/X}$ , respectively) and volumetric productivity of the process ( $Qp$ ). It must be clarified that as AD293 cells are adherent, the experiments regarding their infection had to be designed quite different from those in suspension cultures. The major implication of these differences is that  $Y_{CapPCV2/X}$ ,  $Y_{Adv/X}$  and  $Qp$  had to be

calculated differently than specified in previous sections of this chapter. Below is briefly specified how these parameters were calculated:

$$\text{Specific production } (Y_{P/X}) = \frac{P_{TOH}}{\text{Cells}_{TOI}} \quad (\text{Eq. 4.10})$$

Where:

P is the product of interest (i.e. GFP, CapPCV2, rAdV-GFP, rAdV-CapPCV2)

$P_{TOH}$  is the product quantity at TOH

$\text{Cells}_{TOI}$  is the total number of viable cells at the time of infection

$$\text{Volumetric productivity } (Q_{pp}) = \frac{[P]_{TOH}/FC}{T_{\text{seeding to TOI}} + TOH} \quad (\text{Eq. 4.11})$$

Where:

P is the product of interest (i.e. GFP, CapPCV2, rAdV- GFP, rAdV-CapPCV2)

FC is the concentration factor of the sample\*

$T_{\text{seeding to TOI}}$  is the time needed for the cells to adhere to plate after t-flask inoculation

\*For FC in  $Q_{pp}$  calculation, the cell media volume that was needed for cell inoculation was taken into account. It is important to highlight that this volume can be modified and consequently, FC and  $Q_{pp}$  values would differ from the ones here calculated. In the bioprocess studied in this section, cell media volume was 2mL/well in a 6 well-plate. This was made on basis of (1) covering all well surface (2) preventing massive evaporation of media during the infection process (3) provide cells with enough nutrients.

In Table 4.14 and 4.15 the values of the calculated production parameters are presented. The most important fact is the great difference on specific production ( $10^3$ -fold difference) depending on the protein expressed (Table 4.14). This drop on specific protein production is comparable to the one found out when infecting suspension cells. We then wanted to assess whether the drop on  $Y_{p/x}$  was related to a lower capacity of infection or replication of the viral vector itself. However, cytopathic effect was similar for all infected cell cultures. Therefore, although it was not quantitatively assessed, it can be assumed a similar capacity for infection of both adenoviruses (rAdV-GFP and rAdV-CapPCV2). Moreover, based on  $Y_{AdV/x}$  and infective particle ratio ( $IFU_R$ ) values (Table 4.15) it can be said that rAdV-GFP could complete more efficiently the viral cycle, resulting in higher AdV specific production,  $IFU_R$  and recombinant protein production in comparison to rAdV-CapPCV2. Nevertheless,

differences on adenovirus production between the two viral vectors studied were not as severe as those encountered for protein production. Altogether led us to think that the low CapPCV2 production was more related to the viral protein itself rather than to an inefficient viral vector or bioprocess conditions. In other words, the expression system based on HEK293 and adenovirus was encountered to be not suitable for r-CapPCV2 production.

**Table 4.14.** Comparison of protein (GFP and CapPCV2) production parameters in adherent cell cultures infected at low MOI (2.75) and high MOI (27.5)

	MOI	$Y_{p/x}$ (pg/cell)	$Qp$ ( $\mu\text{g}/(\text{mL}\cdot\text{d})$ )
GFP	2.75	44.421 $\pm$ 0.786	9.95 $\pm$ 0.08
	27.5	52.073 $\pm$ 1.283	11.66 $\pm$ 0.21
CapPCV2	2.75	(41.291 $\pm$ 0.002)e-3	(9.25 $\pm$ 0.60)e-3
	27.5	(53.031 $\pm$ 0.005)e-3	(11.88 $\pm$ 1.97)e-3

**Table 4.15.** Comparison of viral vector (rAdV-GFP and rAdV-CapPCV2) production parameters in adherent cell cultures.

	MOI	$Y_{p/x}$ ( $\times 10^3$ AdV/cell)	IFU <sub>f</sub> /IFU <sub>0</sub>	$Qp$ ( $\times 10^8/\text{mL}\cdot\text{d}$ )
rAdV-GFP	2.75	5.90 $\pm$ 1.63	350 $\pm$ 1.00	13.2 $\pm$ 3.79
rAdV-CapPCV2	2.75	1.41 $\pm$ 0.82	128 $\pm$ 0.75	3.15 $\pm$ 0.23

\*Only intracellular viral fraction has been considered which at TOH was around 98% of the total virus (i.e. intracellular and extracellular viral fraction)

## 4.5. CONCLUSIONS

In this chapter a bioprocess for the production of r-CapPCV2 has been studied. This bioprocess is based on the infection of HEK293 cells with a recombinant adenovirus encoding *CapPCV2* (rAdV-*CapPCV2*). First of all, the generation of rAdV-*CapPCV2* was addressed and it was successfully achieved. Thereafter the study of the infection parameters was carried out in order to maximise the production of the two different products of interest: the recombinant protein which will be used as the vaccine candidate and the adenoviral vector itself, as it will be needed in each batch of the production process in order to obtain CapPCV2 protein. The infection parameters studied were cell media, multiplicity of infection (MOI), time of infection (TOI) and time of harvest (TOH). After the thorough analysis of the results, the selected parameters for increasing protein and AdV production were the ones presented in Table 4.16.

**4.16.** Selected parameters for infection

Cell media	TOI	MOI	TOH
HyQ SFMTransFx-293+4mM glutaMAX+ 5%FBS+10%CB5 (80g/L)	$1 \times 10^6$ cell/mL	2.75	48 hpi

Besides, two main conclusions should be pointed out. On one hand, the infection at MOI higher than 2.75 would not result in a proportional increment on process productivity neither for recombinant protein nor for adenovirus vector. Hence, this MOI (or similar) should be selected in order to increase process profitability. On the other hand, infecting at  $TOI > 1 \times 10^6$  cell/mL dramatically affects specific production and therefore, productivity of the process. After some preliminary observations on HEK293 metabolism, we have hypothesised that the metabolic shift from lactate production to lactate and glucose concomitant consumption, could be somehow related to this drop on recombinant protein and AdV production. In the experiments presented so far, the lactate metabolic shift was always observed shortly after cell density reaches  $1 \times 10^6$  cell/mL. This shift can be reverted after media exchange and specific production of the process is partially recovered, enabling the infection at higher cell densities and incrementing volumetric productivity of the process. This fact would open the door to study different infection strategies to take profit of the potential of the biocatalyzer (i.e. HEK293), which can grow until cell densities as high as  $26 \times 10^6$  cell/mL. Nevertheless,

this study has not been faced in this work due to the low specific production obtained for the protein of interest (r-CapPCV2). The low production was related to the protein itself rather than to the bioprocess definition or the viral vector, and hence, it would be unfeasible to design a cost-effective bioprocess. Therefore, in pursuit of outperforming CapPCV2 productivity, two approaches will be addressed on the next chapter of this research work. On one hand, the possibility of improving protein production by codon optimization of the sequence will be studied. On the other, the obtaining of stable cell lines expressing the protein of interest will be tackled.

## 4.6. REFERENCES

1. Zhang, J. in *Manual of Industrial Microbiology and Biotechnology* (ed. H, B. R.) 57–178 (2010).
2. Lang, R. in *Biosimilars and follow-on biologics: world market* (ed. Low, G.) (Visiongain, 2012).
3. Grossvenor, S. A New Era in Cell Culture Media Development. *BioPharm Int.* 20–23 (2015).
4. Keenan, J., Pearson, D. & Clynes, M. The role of recombinant proteins in the development of serum-free media. *Cytotechnology* **50**, 49–56 (2006).
5. Chu, L. & Robinson, D. K. Industrial choices for protein production by large-scale cell culture. *Curr. Opin. Biotechnol.* **12**, 180–187 (2001).
6. Grillberger, L., Kreil, T. R., Nasr, S. & Reiter, M. Emerging trends in plasma-free manufacturing of recombinant protein therapeutics expressed in mammalian cells. *Biotechnol. J.* **4**, 186–201 (2009).
7. Altaras, N. E. *et al.* Production and Formulation of Adenovirus Vectors. *Adv. Biochem. Engin. Biotechnol.* **99**, 193–260 (2005).
8. Lecina, M., Tintó, A., Gálvez, J., Gòdia, F. & Cairó, J. J. Continuous perfusion culture of encapsulated hybridoma cells. *J. Chem. Technol. Biotechnol.* **86**, 1555–1564 (2011).
9. Fenge, C. & Lüllau, E. in *Cell Culture Technology For Pharmaceutical And Cell-Based Therapies* (eds. Ozturk, S. S. & Hu, W.-S.) 185–190 (CRC Press, 2005).
10. Whitford, W. G. Fed-Batch Mammalian Cell Culture in Bioproduction.
11. Yamané, T. & Shimizu, S. Fed-batch Techniques in Microbial Processes. *Adv. Biochem Eng/Biotechnol* **30**, 147–194 (1984).
12. Hoskisson, P. A. & Hobbs, G. Continuous culture – making a comeback? 3153–3159 (2005).
13. Aunins, J. G. Large-scale mammalian cell culture Hu and John G Aunins. 148–153
14. Voisard, D., Meuwly, F., Ruffieux, P., Baer, G. & Kadouri, A. Potential of Cell Retention Techniques for Large-Scale High-Density Perfusion Culture of Suspended Mammalian Cells. (2003).
15. Klöckner, W. & Büchs, J. Advances in shaking technologies. *Trends Biotechnol.* **30**, 307–314 (2012).
16. Zhang, H., Wang, W., Quan, C. & Fan, S. Engineering Considerations for Process Development in Mammalian Cell Cultivation. 103–112 (2010).
17. Zhou, W. & Hu, W.-S. On-line characterization of a hybridoma cell culture process. *Biotechnol. Bioeng.* **44**, 170–177 (1994).

18. Galvez, J. Desenvolupament i anàlisi d'un bioprocés per a l'obtenció de vectors adenovirals. (Universitat Autònoma de Barcelona, 2010).
19. Altamirano, C., Paredes, C., Illanes, A., Cairó, J. J. & Gòdia, F. Strategies for fed-batch cultivation of t-PA producing CHO cells: substitution of glucose and glutamine and rational design of culture medium. *J. Biotechnol.* **110**, 171–179 (2004).
20. Gagnon, M. *et al.* High-end pH-controlled delivery of glucose effectively suppresses lactate accumulation in CHO fed-batch cultures. *Biotechnol. Bioeng.* **108**, 1328–1337 (2011).
21. Vallée, C., Durocher, Y. & Henry, O. Exploiting the metabolism of PYC expressing HEK293 cells in fed-batch cultures. *J. Biotechnol.* **169**, 63–70 (2014).
22. Petiot, E. *et al.* Metabolic and Kinetic analyses of influenza production in perfusion HEK293 cell culture. *BMC Biotechnol.* **11**, 84 (2011).

## CHAPTER 5. RESULTS (III): GENERATION OF STABLE CELL LINES CapPCV2 PRODUCERS

### 5.1. INTRODUCTION

During the past two decades, big efforts have been directed to the development of stable cell lines for recombinant protein production. The improvements on the technologies for the obtention of stable cell lines have highly reduced the time required for of cell line development and have increased the yield of manufacturing processes<sup>1,2</sup>. There is a huge number of methods for the generation of cell lines stably expressing the protein of interest, although they can be divided into three main groups:

1. **Random integration** of the gene of interest within the genome of the host using integrative plasmids.
2. **Semi-directed integration** of the gene of interest within the genome of the host using retroviral or lentiviral vectors. These viruses naturally remain integrated in host's genome (latent viral cycle phase) and this feature is used to introduce the gene of interest.
3. **Site-directed integration** of the gene of interest by means of different tools and technologies that rely on the recognition of specific genetic sequences within the genome host (homologous recombination).

As stated in the introduction, two different approaches will be explored for the generation of stable cell lines in this work based on two different strategies. On one hand, the illegitimate (or random)



integration has been selected because its advantages in front of the other two approaches. First of all, the illegitimate integration does not require the generation of recombinant retroviral and lentiviral vectors, neither the study of the parameters for optimal infection in order to get the desired results, which can be quite tedious and time consuming. Moreover, illegitimate integration event occurs more often in comparison to site-directed integration and also multiple copies of the gene can be integrated in the genome of the host cell<sup>3</sup>, resulting into relative high producer cell lines. However, this strategy has three major drawbacks for the development of a bioprocess. First, random integration and amplification creates heterogeneous pools, making the selection of high producers a time-consuming and laborious process<sup>4</sup>. Second, the long-term expression stability of the foreign DNA cannot be assured and it has been an extensive issue of study<sup>3</sup>. Third, due to the randomly integration of DNA, the outcome of the initial transfection might not be reproducible and hence, the bioprocess characterisation must be assessed for each cell line to be established. In order to avoid these downsides of the strategy, the site-directed integration of our gene of interest has also been addressed for stable cell line generation. There are different natural proteins that have been engineered in order to enhance the effectiveness of site-directed insertion. Among them, site specific recombinases (SSRs)<sup>5-8</sup>, zinc finger nucleases (ZFNs), Transcription activator-like effector nucleases (TALENs), the CRISPR/Cas System and engineered meganucleases<sup>5,9-11</sup>, are the most commonly used. As stated in the Introduction, the insertion using SSRs by Recombinase mediated cassette exchange (RMCE) technology has been selected. This technology has been applied to cell lines that have already been characterised as unique-site for RMCE master cell lines. Therefore, the derived positive clones should have only one copy of the gene of interest, which might result in less productive cell lines in comparison to the illegitimate integration. Nevertheless, this second strategy would result in a more consistent and stable expression of the protein, which is highly important for the implementation of a bioprocess. Moreover, this strategy allows to significantly reduce the time for stable cell line obtaining (from 2 to 4 weeks)<sup>12</sup>. This is remarkably important if we focus on the economic perspective of the process development and optimization. Once the cell culture process has been optimized for a given cell line, the gene can be rapidly changed in the master cell line, resulting in a new cell line expressing a different product of interest. Hence, the established bioprocess is more flexible in regards the final product.

## 5.2. GENERATION OF STABLE CELL CapPCV2 PRODUCERS LINES BY ILLIGITIMATE DNA INTEGRATION

### 5.2.1. OBTENTION AND CHARACTERISATION OF PLASMIDS FOR TRANSFECTION

The correct expression of a given protein upon illegitimate DNA integration depends on a myriad of factors<sup>13</sup>. These factors might be related to (a) the features of the vector (e.g. vector size, promoter, gene sequence) (b) the integration into host's genome (e.g. site of integration, modifications after integration, number of integrated copies) (c) the posttranslational processing (e.g. correct folding, protein aggregation and solubility) and even related to (d) cell culture (e.g. temperature, nutrient availability, cell culture mode). Hence, it is highly recommended to perform transient transfections previous to the final transfection for stable cell line generation in order to select some features directly related to the plasmid vector which might influence protein expression. Among these features we wanted to characterise the influence on the level of protein expression of the following:

- The genetic sequence of the gene to be expressed.
- The promoter of the gene of interest.
- The addition of a secretion signal in order to ease downstream processes.
- The addition of a "tag" sequence for purification purposes.

In order to evaluate these vector features, four plasmids were generated and transiently transfected to HEK293-3F6 cell line for the assessment of CapPCV2 protein production levels. In Table 5.1 the main features of the vectors obtained are compiled. First of all, codon optimisation for the expression in mammalian cell lines of *CapPCV2* sequence was performed. This was mainly decided on basis to the results presented and discussed in Chapter 4, which shown very low r-CapPCV2 production although the viral vector encoding the gene was properly produced. The effectiveness of codon optimisation has already been reported for other proteins and therefore we wanted to study this approach for r-CapPCV2 production improvement<sup>14,15</sup>. Besides, in order to ease downstream of the bioprocess, it was decided to change from the intracellular expression of the protein (as it was evaluated on Chapter 4) to its extracellular expression. In this direction, the secretion signal sequence from Interleukyn-2 (SSIL-2) was added o the optimised sequence of CapPCV2 (onwards *CapPCV2op*). The whole *SSIL2-CapPCV2op* was chemically synthesised and cloned into the pIRESpuro3 plasmid vector. The generated vector will be named pIRESpuro3-SSIL2-*CapPCV2op* (Table 5.1). As a control of codon optimisation strategy, the native sequence of the protein was also

cloned into the same backbone vector (i.e. pIRESpuro3) and the generated plasmid will be named pIRESpuro3-*CapPCV2* (Table 5.1).

For the evaluation of promoters influence on protein expression, two different ones were selected. On one hand, we chose the Citomegalovirus promoter (CMV) as it is a strong promoter widely used on the expression of recombinant proteins in mammalian cell lines. This promoter was present in the pIRESpuro3 vector. On the other hand, we chose the  $\beta$ -actin chicken promoter as it has been reported to perform better than CMV in some mammalian cell lines<sup>16</sup>. This promoter was present in the pOPING backbone vector, which also encoded for the secretion signal of the receptor protein-tyrosine phosphatase (RPTPmu) (Table 5.1). This feature, along with the SSIL2 cloned upstream of *CapPCV2op* in pIRESpuro3 vector, made possible the comparison of two different secretion signals in terms of protein secretion.

Finally, the suitability of cloning a “tag” sequence was evaluated using the pOPING vector. This vector encodes for a 6-histidine tag downstream of the gene of interest. By deleting the STOP codon on *CapPCV2* and with the correct cloning strategy explained later in this chapter, the sequence of the gene was fused in frame with the 6-His tag. The vector encoding for this construct will be named pOPING-*CapPCV2HisTag* (Table 5.1). The expression of *CapPCV2* linked to the tag will be compared to the expression of the same protein in the same vector but with any tag for purification (i.e. pOPING-*CapPCV2*).

The procedure for obtaining the plasmids for preliminary transient expression of *CapPCV2* protein as well as the characterization of the final plasmid vectors is explained below.

**Table 5.1.** Main features of the plasmid vectors generated for transient transfection.

Id Plasmid	pIRESpuro3-SSIL2- <i>CapPCV2op</i>	pIRESpuro3- <i>CapPCV2</i>	pOPING- <i>CapPCV2</i>	pOPING- <i>CapPCV2HisTag</i>
Plasmid Backbone	pIRESpuro3	pIRESpuro3	pOPING	pOPING
GOI Inserted*	<i>SS-IL2 - CapPCV2op</i>	<i>CapPCV2</i>	<i>CapPCV2</i>	<i>CapPCV2 STOP codon deleted</i>
Promoter	CMV	CMV	$\beta$ -actin chicken	$\beta$ -actin chicken
Expected expression	Extracellular (SS-IL2)	Intracellular	Extracellular (RPTPmu)	Extracellular (RPTPmu)
Purification tag? (y/n)	N	N	Y	N
GOI size (bp)	790	702	702	702
Insertion site	NheI-BamHI	NheI-AgeI	Age-I-PmeI	AgeI-PmeI

\*GOI: gene of interest

*CapPCV2op*: genetic sequence optimised for mammalian cell expression

*CapPCV2*: natural sequence of the gene (i.e. non optimised for mammalian cell expression)

### 5.2.1.1. pIRESpuro3-SSIL2-CapPCV2 AND pIRESpuro3-SSIL2-CapPCV2op

The generation of *pIRESpuro3\_CapPCV2* vector was carried out through a site-directed ligation strategy of the *CapPCV2*. The details of the methodology concerning each step of the clonation process are specified in Materials and Methods chapter (section 8.10.2). Briefly, the plasmid vector pShuttle-CMV-*CapPCV2* (clone6. See chapter 4 section 4.2.2) was KpnI-HindIII digested in order to obtain *CapPCV2* gene. The insertion of the new restriction sites in 5'- and 3'-endings of *CapPCV2* (NheI and AgeI, respectively) was performed by PCR with the corresponding primers. Finally, pIRESpuro3 and PCR product (i.e. NheI-*CapPCV2*-AgeI) were NheI+AgeI restricted, followed by t4-ligation and heat-shock transformation into *E.coli* Dh5 $\alpha$ .

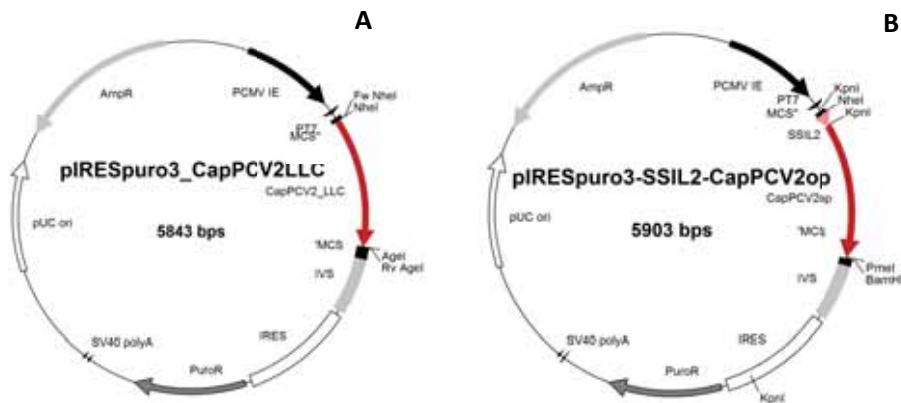


**Figure 5.1.** pIRESpuro3 with GOI cloned into it. (A) GOI is *CapPCV2* (B) GOI is *SSIL2-CapPCV2op*. Main features and identification of primers for PCR characterisation of *E.coli* transformants are depicted. The enzymes used for GOI insertion are also represented. The backbone plasmid map (pIRESpuro3) with MCS completely specified can be found in Materials and Methods (section 8.5.1.3.)

*SSIL2-CapPCV2op* construct was chemically de novo and the codon optimisation of the gene was performed for the improvement of protein expression in mammalian cells using OptimumGene<sup>TM</sup> algorithm (Genescript, proprietary gene optimization technology). Two KpnI restriction sites flanking the secretion signal were added on the design of the gene synthesis in order to easily replace the secretion signal, if desired. Also, PmeI was added downstream of *CapPCV2op* in order to be able to conveniently excise the optimised sequence in case that it is desired to clone it in another expression vector. PmeI restriction will result in a blunt-end gene and hence, compatible with any expression vector despite their restriction site availability. The whole sequence KpnI-*SSIL2*-KpnI-*CapPCV2op*-PmeI was cloned into pIRESpuro3 through a site-directed strategy within NheI-BamHI enzymatic restriction sites.

As in Chapter 4, the characterisation of the vector was carried out by colony PCR (20 clones), enzymatic restriction pattern (10 clones) and gene sequencing (2 clones). The results of colony PCR

for the final selected clones are presented in Figure 5.2A and Table 5.2 and enzymatic restriction pattern is shown in Figure 5.2B and table 5.3. *E.coli* clone containing pIRESpuro3-CapPCV2 will be named clone A1 and the *E.coli* clone holding pIRESpuro3-SSIL2-CapPCV2op will be referred to as clone F5.

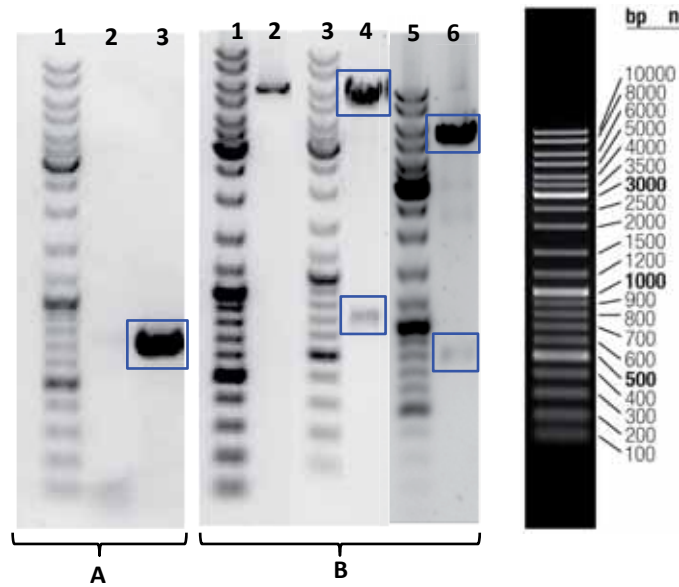


**Figure 5.2.** (A) PCR characterisation of selected *E.coli* Clone A1 (B) Enzymatic digestion pattern characterisation of selected *E.coli* clone A1 and of selected *E.coli* Clone F5. Digestion with NheI and AgeI was performed. DNA Ladder: GeneRuler™ DNA Ladder Mix (Fermentas 0333).

**Table 5.2.** Identification of samples Gel A of Figure 5.2.

Lane	ID sample	Expected Size(bp)
1	DNA Ladder	--
2	pIRESpuro3	--
3	Clone A1	722

**Table 5.3.** Identification of samples on Gel B of Figure 5.2.

Lane	ID sample	Expected Size (bp)
1	DNA Ladder	--
2	pIRESpuro3 NheI AgeI rest.	5121;50
3	DNA Ladder	--
4	Clone A1 NheI AgeI rest.	5121;709
5	DNA Ladder	--
6	Clone F5 NheI AgeI rest.	5121;782

### 5.2.1.2. pOPING-CapPCV2 AND pOPING-CapPCV2HisTag

Both plasmids were obtained through a site-directed ligation strategy of *CapPCV2*. *AgeI* and *PmeI* enzymatic restriction sites were added 3' and 5' of GOI (respectively) in order to clone it into the backbone vector (Figure 5.3) and guarantee the proper cleavage of the secretion signal peptide. The unique difference between the generated plasmids derived from pOPING, is that in pOPING-*CapPCV2HisTag* the STOP codon of *CapPCV2* has been deleted by PCR amplification in order to maintain the His-Tag present in the backbone vector, and obtain the His-tag fused to r-*CapPCV2*.

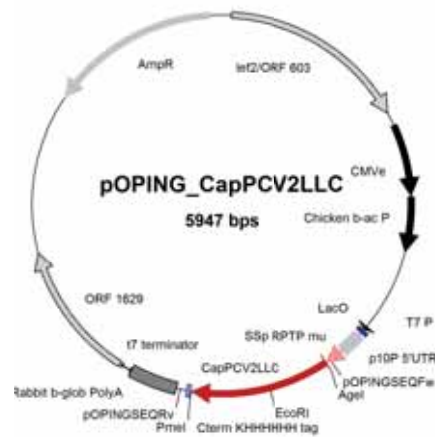


**Figure 5.3.** pOPING vector with GOI cloned into it. Main features and identification of primers used for PCR characterisation of *E.coli* transformants are depicted. *AgeI* and *PmeI* sites –the enzymes used for GOI insertion- are also represented. pOPING-*CapPCV2HisTag* vector has the same sequence except that the STOP codon from *CapPCV2* has been deleted.

The characterisation by colony PCR and enzymatic restriction pattern of the selected clone harbouring each expression vector is presented (Figure 5.4 and Table 5.4). The selected *E.coli* clone harbouring pOPING-*CapPCV2* will be named Clone D1 and the clone containing pOPING-*CapPCV2HisTag* will be referred to as Clone E9. Also, the obtained vectors were sequenced in order to confirm that any mutation was introduced into *CapPCV2*, that the deletion of STOP codon was correctly performed and that *CapPCV2* was in frame with His-tag sequence. All the sequences presented 100% homology with the theoretical sequence.

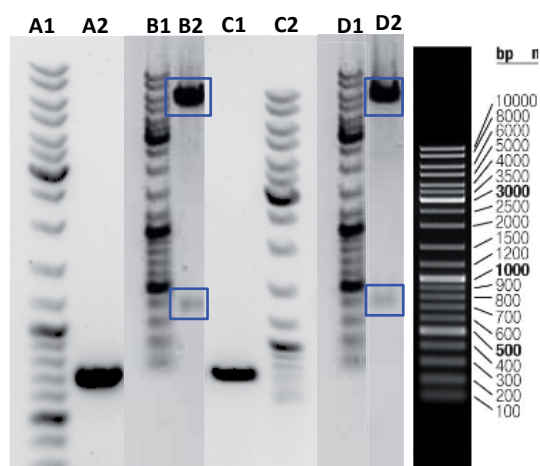


**Figure 5.4.** PCR characterization and Enzymatic digestion pattern characterisation of selected *E.coli* Clone D1 and of selected *E.coli* Clone E9. Plasmid digestion with EcoRI and PmeI was performed. DNA Ladder: GeneRuler™ DNA Ladder Mix (Fermentas 0333).

**Table 5.4.** Identification of the samples loaded in agarose gels presented in Figure 5.4.

Lane	ID sample	Expected Size (bp)
A1	DNA Ladder	--
A2	PCR1 Clone D1	722
B1	DNA Ladder	--
B2	Clone D1 EcoRI PmeI rest.	5554;393
C1	DNA Ladder	--
C2	PCR1 Clone E9	722
D1	DNA Ladder	--
D2	Clone E1 EcoRI PmeI rest.	5554;389

### 5.2.2. TRANSIENT TRANSFECTION FOR BEST EXPRESSION VECTOR SELECTION.

Once the expression vectors were generated and characterised, transient expression of these plasmids in HEK293-F6 cell line was performed in order to evaluate the influence on protein expression or secretion of the selected parameters previously stated (i.e. gene sequence optimisation, promoter, secretion signal sequence and His-tag addition C-term of the protein). PEI-DNA transfection was carried out in shake flask cultures with complete complete media replacement at the time of transfection. The complete transfection protocol is detailed at Material and Methods chapter (section 8.9.1). A positive control for transfection (a plasmid encoding for GFP protein) was included.

Good efficiency of transfection (>60%) was assessed for all cases. Also, in all transfected cultures cell growth stopped after transfection and viability dropped from 90% at time of transfection until approximately 50% after 72hours post transfection (hpt) (data not shown). At that point, cells were harvested and separated from media by centrifugation. Extracellular and intracellular CapPCV2 was quantified (results are presented in Figure 5.5).

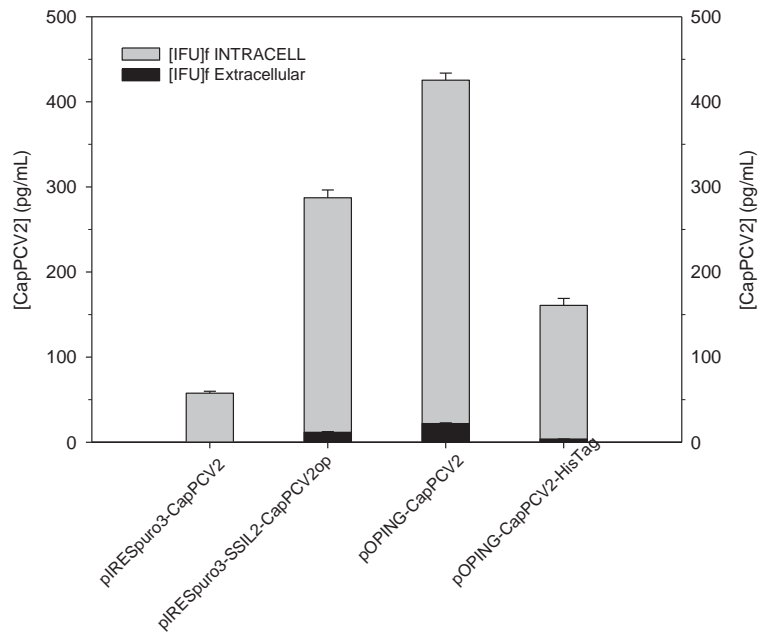


**Figure 5.5.** CapPCV2 production after transient transfection of HEK293 cells with the expression vectors presented in Section 5.2.1. Intracellular and extracellular [CapPCV2] were determined and are depicted as stacked bars. Hence, the total height of the bar represents total protein concentration.

The transfection that resulted in the poorest CapPCV2 production was the one performed with pIRESpuro3-*CapPCV2* for which only  $57.69 \pm 2.17$  pg/mL were obtained after cell lysis. Noteworthy, after codon optimisation the production of the protein of interest was increased almost 5 times. Nevertheless, the secretion of the protein was not successful and only 4% of the total protein detected was found in the supernatant. In regards the effect of the promoter on the expression of the protein of interest, it was found out that the  $\beta$ -actin chicken promoter with the enhancer from CMV (promoter within pOPING vectors) improved protein expression. Specifically, total protein after transfection with pOPING-*CapPCV2* was 1.5-fold higher than the concentration measured after transfection with pIRESpuro3-*SSIL2-CapPCV2op* (Figure 5.5) Interestingly, the secretion of the protein did neither succeed with pOPING-derived expression vectors, although the secretion signal was different from the one in pIRESpuro3-*SSIL2-CapPCV2op*. In particular, for the transfection with pOPING-*CapPCV2* the extracellular fraction was only 5% of the total protein whereas for transfection with pOPING-*CapPCV2HisTag* the percentage of extracellular protein was only about 2%. This could be related to an incorrect folding of the secretion signal peptide due to the *CapPCV2* sequence cloning. Nevertheless, instability or degradation of CapPCV2 protein on the supernatant cannot be ruled out and further experiments should be performed in order to unravel the reasons of the lack of extracellular protein. Finally, the addition of the His-tag to the protein drastically reduced the protein detected at the time of harvest. Total protein concentration detected after pOPING-*CapPCV2HisTag* transfection was less than the half of the concentration detected with transfection



with pOPING-CapPCV2, indicating that the “tag” addition negatively affected some step from gene transcription to protein translation. Hence, this expression vector was discarded for further experiments. The impossibility of cloning a His-tag to the protein, along with the unsuccessful secretion of the protein to the media will directly affect the downstream procedure.

On basis to these results, the best option for protein production maximisation would be the expression of the codon optimised sequence of CapPCV2 under the control of the  $\beta$ -actin chicken promoter. Also, in order to be able to select the positive clones for the generation of a stable cell line, a selectable marker should be present in the final expression vector. Hence, the optimal strategy defined was the replacement of CMV promoter of pIRESpuro3\_SSIL2-CapPCV2op by the  $\beta$ -actin chicken promoter+CMV enhancer of pOPING vector. Nevertheless, due to timing concerns this could not be accomplished and the expression vector pIRESpuro3\_SSIL2-CapPCV2op was used for stable cell line generation as also good results were obtained after the transient expression of this vector.

### 5.2.3. PUROMYCIN KILL CURVE EVALUATION.

The selected plasmid for the generation of CapPCV2 producer cell line, pIRESpuro3\_SSIL2-CapPCV2op, encodes for the puromycin resistance gene. Hence, the selection of the positive clones after transfection was performed by the addition of puromycin to cell culture media. One of the most critical steps for stable cell line generation is the determination of the minimum amount of antibiotic required to completely eliminate non-transduced cells. This is accomplished by performing a kill curve to determine the optimal antibiotic concentration needed to select the transduced cells. A kill curve is a dose-response experiment where the cells are subjected to increasing amounts of antibiotic to determine the minimum antibiotic concentration needed to kill all the cells over the course of 2 to 7 days.

Based on the literature, a broad range of puromycin concentration (i.e. 5-1  $\mu\text{g}/\text{mL}$ , 0.5 stepwise) was selected at first, but any difference could be detected among cell cultures with [puromycin] $\geq 2.0$   $\mu\text{g}/\text{mL}$ . At those concentrations, no cell growth was detected and viability drastically dropped after 24h of cell culture. Hence, a narrower range was tested within the range 0-1.5  $\mu\text{g}/\text{mL}$  in order to tune the final puromycin concentration for HEK293-CapPCV2 positive clones selection. Also, two initial cell densities (“low” and “high”) were evaluated in order to assess if puromycin concentration should be different depending on the cell density of the experiment. “Low” cell density was set at  $X_v = 0.3 \times 10^6$  cell/mL, as this is the one at which all cell cultures for cell growth characterisation are

performed. “High” cell density was fixed at  $X_v=1 \times 10^6$  cell/mL because this is the cell density at which transfection is performed.

As depicted in Figure 5.6, cells could not grow at antibiotic concentrations higher than 1  $\mu\text{g/mL}$ , regardless the inocula cell density. When puromycin was added at 0.75  $\mu\text{g/mL}$ , cell growth was also completely inhibited at the lower cell density tested, whereas cell growth was impaired but not totally suppressed on cell cultures seeded at  $X_{v0}=1 \times 10^6$  cell/mL. The obtained kill curves (Figure 5.6B and Figure 5.6D) showed that a suitable protocol for selection of transfected cells would be working at [puromycin]= 1.0  $\mu\text{g/mL}$  and perform cell passage (1:10 dilution) 96h post transfection. At that time, the population of transfected cells should be ten times higher than the untransfected cells and viability of untransfected population would have dropped to 50%. After two-three cell passages almost all cells present in cell culture might carry the plasmid encoding for puromycine resistance gene and hence, *CapPCV2*.

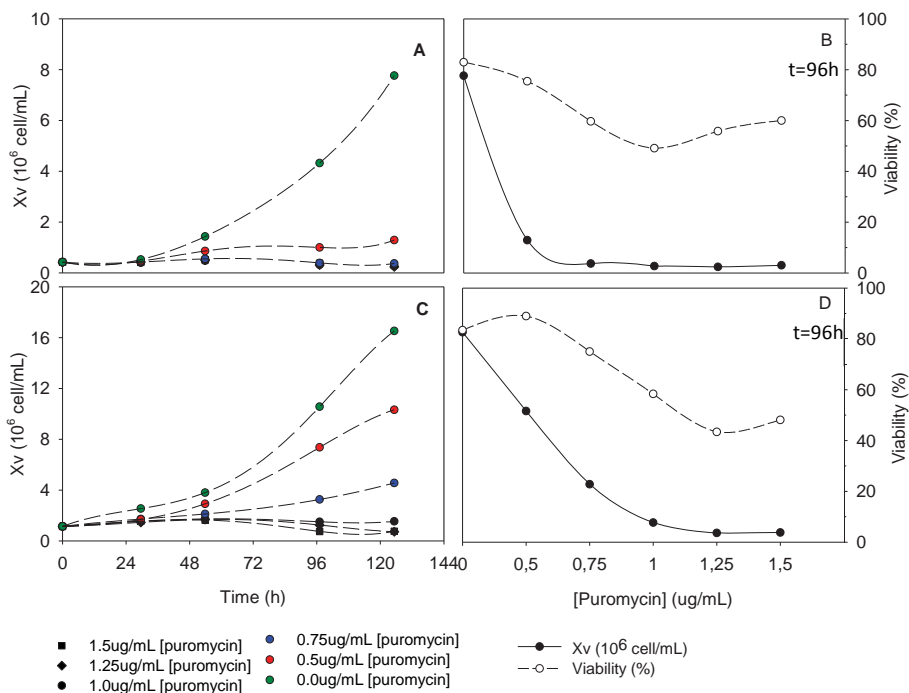


**Figure 5.6.** Cell growth profiles of HEK293 cell cultures with different  $[\text{puromycin}]_0$  at (A)  $X_{v0}=0.3 \times 10^6$  cell/mL and (C)  $X_{v0}=1 \times 10^6$  cell/mL. Kill curves at 96h of cell culture of HEK293 cultures at (B)  $X_{v0}=0.3 \times 10^6$  cell/mL and (D)  $X_{v0}=1 \times 10^6$  cell/mL

#### 5.2.4. STABLE TRANSFECTION INTO HEK293. CHARACTERISATION OF HEK293-CapPCV2 CELL LINE.

After the evaluation of transient transfection results, pIRESpuro3-SSIL2-CapPCV2op expression vector was transfected into HEK293-3F6 cells for the generation of CapPCV2-HEK293 cell line. PEI-DNA transfection with pIRESpuro3-SSIL2-CapPCV2op was performed in shake flask. Media containing the plasmid DNA was completely replaced 24hpt and puromycin was then added to cell culture media in order to select the positive cell population. After three cell passages, the surviving clones were diluted to lower cell densities in media containing increasing puromycin concentrations (up to 3 µg/mL) in order to select the subpopulation with higher number of integrated plasmids. After two weeks, a pool of cells at the highest concentration was selected (onwards HEK293-F5) and cell growth and CapPCV2 protein production was assessed. Cell growth profile of cultures with selective pressure by means of puromycin addition was comparable to the one observed when puromycin was absent (Figure 5.7) and cell growth rate values were also similar (Table 5.5).

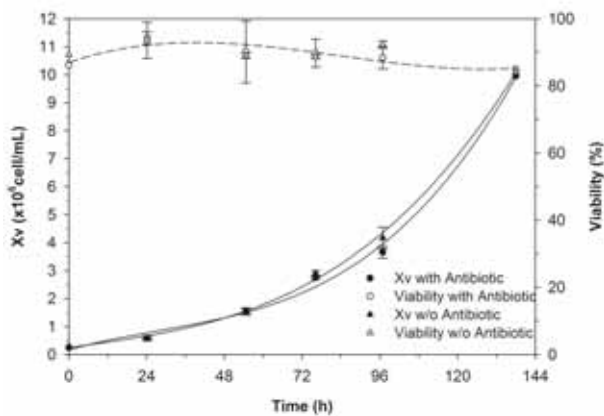


**Figure 5.7.** Cell growth and viability profiles of HEK293-F5 in presence or absence of puromycin.

**Table 5.5.** Specific growth rates of HEK293-F5 clones in presence and absence of puromycin.

	$\mu_{\max}$ ( $\times 10^{-2} \text{h}^{-1}$ )
HEK293-F5 [puro]=1µg/mL	2.84±0.01
HEK293-F5 [puro]=0µg/mL	2.84±0.07
Parental cell (ref. culture)	2.72±0.07

Regarding CapPCV2 production, a specific production ( $Y_{p/x}$ ) of  $0.107 \pm 0.018$  pg/cell was calculated, which corresponds to a specific productivity ( $q_p$ ) of  $0.081 \pm 0.002$  pcd.  $Y_{p/x}$  and  $q_p$  are calculated as specified in Eq.5.1 and Eq.5.2., respectively.

$$Y_{p/x} = \frac{[\text{CapPCV2}]_{\text{TOH}}}{\text{TCD}_{\text{TOH}}} \quad \text{Eq.5.1.}$$

Where:

$[\text{CapPCV2}]_{\text{TOH}}$  is the intracellular protein measured at TOH

$\text{TCD}_{\text{TOH}}$  is the total cell density at TOH

Total cell density was considered for the calculation of  $Y_{p/x}$  on basis that the CapPCV2 produced by cells considered as dead at time of harvest, would be released to media when cell lysis was performed. Hence, if we just consider the viable population,  $Y_{p/x}$  could be overestimated. Nevertheless, it must be kept in mind that once the mechanisms controlling cell death have been triggered, the integrity of the protein of interest cannot be assured and this might result in an underestimation of  $Y_{\text{CapPCV2}/x}$  value.

$$q_p = \frac{[\text{CapPCV2}]_{\text{TOH}}}{\text{ICT}} \quad \text{Eq.5.2.}$$

### 5.3. GENERATION OF STABLE CELL LINES EXPRESSING CapPCV2 BY RMCE.

Four different master cell lines pre-characterised as single integration site were used for the generation of CapPCV2 stable cell lines by site-directed integration. For a better comprehension of the experimental work, the results will be presented in two subsections (5.3.1 and 5.3.2). The first section comprises the results concerning 293 derived cell lines and the second will be focused on the results obtained with 293T derived cell lines. The differential characteristics between the two cell lines are specified in Materials and Methods (section 8.1.1.2).

### 5.3.1. GENERATION OF 293 CELL LINE-DERIVED CapPCV2 PRODUCERS.

#### 5.3.1.1. PARENTAL CELL LINE DESCRIPTION

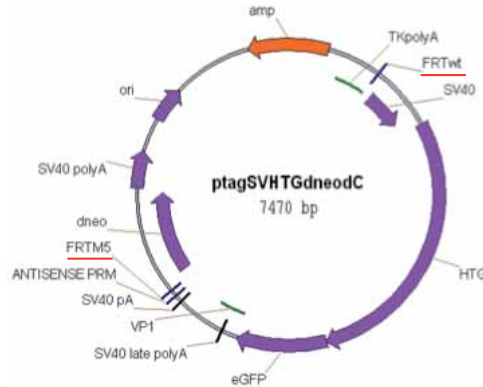


**Figure 5.8** Tagging vector used for the generation of 293 master cell lines.

Three master cells derived from 293 cell line were selected to undergo RMCE (onwards MZ3, MZ9 and MZ10, named generically MZs). These cell lines were kindly provided by Dr R. Schucht (Helmholtz Zentrum für Infektionforschung –HZI– Braunschweig, Germany) and they were already tagged with ptagSVHTGdneodC (Figure 5.8) by electroporation, characterised as single integration site-cells and selected for protein expression above a certain threshold. The reason to perform RMCE in more than one master cell is that they probably differ on the site of integration of the tagging vector in the genome. Hence, the expression of the gene of interest (GOI) may be different depending on epigenetic mechanisms of the integration site region and the possible modification of these mechanisms upon the integration of the foreign gene.

**Table 5.6.** Main features of the tagging vector presented in Figure 5.8

Promoter	Gene exchanged after RCME	Antibiotic for selection
SV40	HTG in frame with eGFP	Neomicyn Ganciclovir

Although the bases of RMCE technology were explained in the Introduction chapter, it is important to mention some characteristics of the tagging vector in order to properly understand the obtention and characterisation of 293 MZs derived clones (section 5.3.1.3). The genetic sequence between FRTwt and FRTM5 (features red underlined in Figure 5.8) will be exchanged by the GOI after homologous recombination has occurred. As specified in Table 5.6, three genes are encoded within this sequence: (1) the enhanced green fluorescence protein reporter gene, (2) the hygromycin phosphotransferase gene fused in-frame with (3) the herpes simplex virus type 1 thymidine kinase gene. The resulting fusion gene (HTG in Figure 5.8) confers hygromycin B resistance for dominant positive selection and ganciclovir sensitivity for negative selection<sup>17</sup>. In this work, the negative selection will be used for the screening of positive clones. The principle of ganciclovir selection is depicted in Figure 5.9. Unlike human thymidine kinase, HSV-thymidine kinase is able to phosphorylate ganciclovir to form ganciclovir-monophosphate, which is then phosphorylated to ganciclovir-diphosphate followed by ganciclovir-triphosphate. Ganciclovir-triphosphate is then incorporated into the DNA, which causes inhibition of DNA synthesis and subsequently leads to apoptosis<sup>18</sup>. Hence, those cells that undergo RMCE will survive if ganciclovir is added to cell media, as they will lack HTG gene.

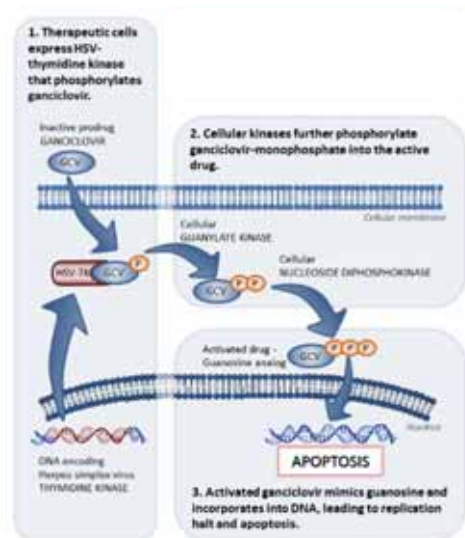


**Figure 5.9.** The HSV-Thymidine Kinase/Ganciclovir principle.

Moreover, in order to assess correct cassette exchange, a second selection method for positive clones was used. The selection method consists on a truncated antibiotic resistance marker present in the tagging vector (and hence, in the genome of the cell) that becomes complemented by the recombination event. Specifically, the neomycin resistance gene (*neo*) from Tn5 with the start codon deleted (*dneo* or  $\Delta neo$ ) is encoded in the tagging vector (Figure 5.8). This gene encodes for an aminoglycoside 3'-phosphotransferase that confers resistance to geneticin. Only those cells in which

the exact homologous recombination between FRT regions has taken place can restore the deleted ATG codon which is present in the targeting vector. Therefore, in this work a positive-negative selection method is applied in order to select positive clones after RMCE.

### 5.3.1.2. OBTENTION AND CHARACTERISATION OF THE TARGETING VECTORS.

Three vectors (Figure 5.10) were selected to generate the final targeting vector set with the gene of *CapPCV2*, which were used to generate the stable cell lines. The original vectors were also kindly provided by Dr R. Schucht and the most important difference among them is that they differ on the promoter controlling the expression of the gene of interest (main features of the vectors are specified in Table 5.7).

**Table 5.7.** Characteristics of interest of original targeting vectors.

ID Vector	Promoter	Promoter origin	GOI Inserted
pTAR-SBC	Simian Vacuolating virus 40 (SV40)	Viral	None
pTAR-EF1 $\alpha$ -GCGR	Human elongation factor-1-alpha (EF1 $\alpha$ )	Human	Glucagon receptor (GCGR)
pTAR-CMV-GCGRnew1	Cytomegalovirus (CMV)	Viral	Glucagon receptor (GCGR)

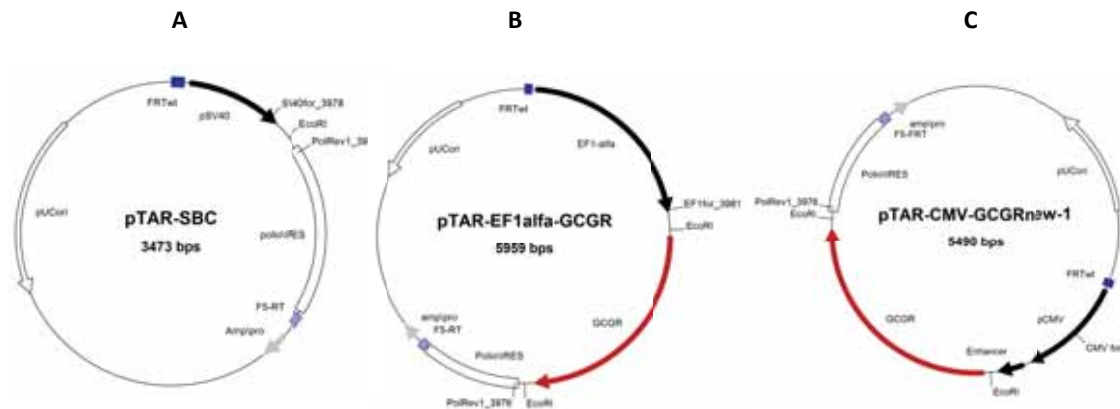


**Figure 5.10.** Original targeting vectors (A) pTAR-SBC (B) pTAR-EF1 $\alpha$ -GCGR (C) pTAR-CMV-GCGRnew1. Main features of the vectors, *EcoRI* sites (the enzyme used for GOI insertion) and primers used for sequentiation are depicted.

According to the results of the preliminary transient transfection experiments previously presented, it was decided to clone the optimised sequence of the gene encoding for *CapPCV2* (*CapPCV2op*) instead of the original sequence obtained from viral DNA extraction. Besides, the inclusion of the secretion signal sequence of Interleukin-2 (SSIL2) was considered for the evaluation of the secretion of the protein in these new cell lines.

The construct *SSIL2-CapPCV2op* was excised from *pIRESpuro3-SSIL2-CapPCV2op* (Figure 5.1B) by the digestion of the vector with *PmeI* and *EcoRV*, resulting in a 5' and 3' blunt-end cassette. Besides, the three original targeting vectors were restricted with *EcoRI*, filled-in with Klenow fragment and dephosphorilated with Calf Intestine Phosphorilase (CIP) to obtain blunt end-vectors ready to ligate with blunt-end *SSIL2-CapPCV2op*. The expected vectors after the ligation of *SSIL2-CapPCV2op* with the original target vectors are specified in the Table 5.8 and the characterisation of the obtained vectors is presented below. As in previous sections, a minimum of 20 colonies was picked for characterization by colony PCR. From the positive ones, a minimum of 10 clones were analysed by enzymatic restriction pattern to ensure correct direction of *SSIL2-CapPCV2op*. Finally, two clones were sequenced to guarantee that any mutation within the GOI has occurred. Only the results of the final selected clones are presented.

**Table 5.8.** Identification of new Targeting vectors after GOI insertion

ID Vector	Original targeting vector	Promoter
pTAR-1	pTAR-SBC	SV40
pTAR-2	pTAR-EF1 $\alpha$ -GCGR	EF1 $\alpha$
pTAR-3	pTAR-CMV-GCGRnew1	CMV



### 5.3.1.2.1. pTAR-1

In the Figure 5.11 an scheme of pTAR-1 is presented with the primers used for colony PCR annotated. The restriction sites of NheI (which was used for enzymatic pattern characterisation) are also depicted. A band of 963bp was expected after PCR amplification, and it was correctly obtained in the clone selected, as it is shown in Figure 5.12a. The expected restriction pattern after incorrect and correct *SSIL2-CapPCV2op* insertion is presented in Figure 5.12b and the correct outcome of the restriction of the selected clone is presented in Figure 5.12c.

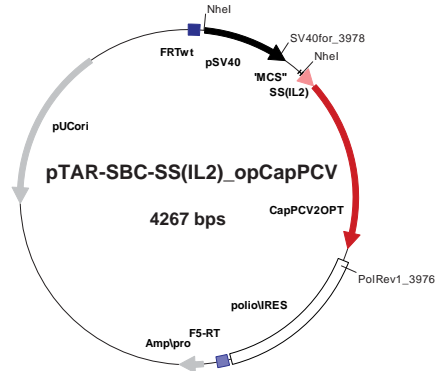


**Figure 5.11.** Scheme of pTAR-1. Main features, primers for PCR-characterisation and sequencing and restriction sites of the enzyme used for enzymatic restriction pattern (NheI) are depicted.

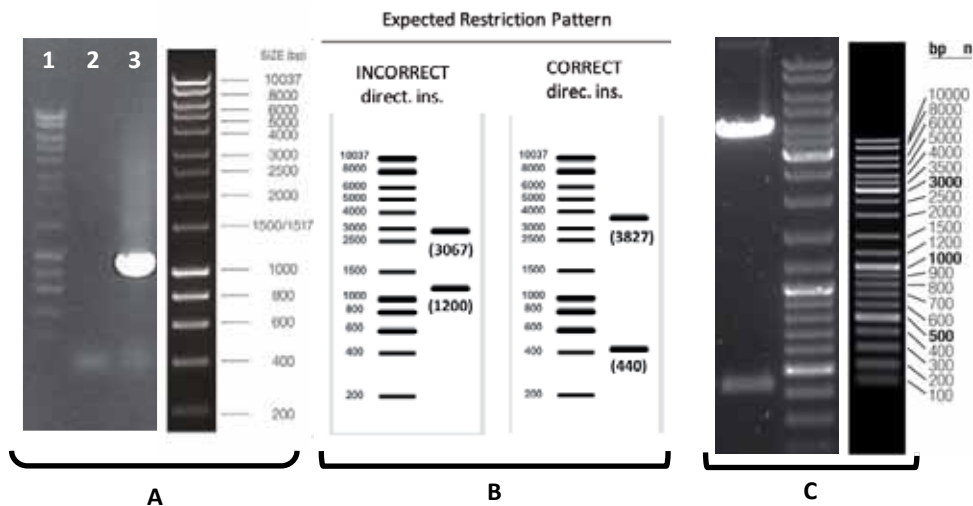


**Figure 5.12.** pTAR-1 characterization (A) Colony PCR results. First lane: DNA Ladder, HyperLadder™ 1kb (Bioline); Second Lane: negative ctrl (H<sub>2</sub>O); third lane: *E.coli* selected clone. (B) Expected restriction pattern. (C) Enzymatic restriction pattern results. First Lane: *E.coli* selected clone; Second Lane: DNA Ladder, HyperLadder™ 1kb (Bioline).

### 5.3.1.2.2. pTAR-2

The scheme of pTAR-2 is depicted in Figure 5.13. The primers used for colony PCR, HindIII and NheI restriction sites (which were used for enzymatic pattern characterisation) are shown. A band of 992bp was expected after PCR amplification, and it was correctly obtained in the clone selected, as it is shown in Figure 5.14a. The expected restriction pattern after incorrect and correct *SSIL2-CapPCV2op* insertion is presented in Figure 5.14b and the correct outcome of the restriction of the selected clone is presented in Figure 5.14c.

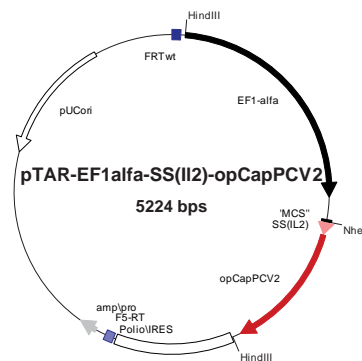


**Figure 5.13.** Scheme of pTAR-1. Main features, primers for PCR-characterisation and sequencing and restriction sites of the enzymes used for enzymatic restriction pattern (NheI and HindIII) are depicted.

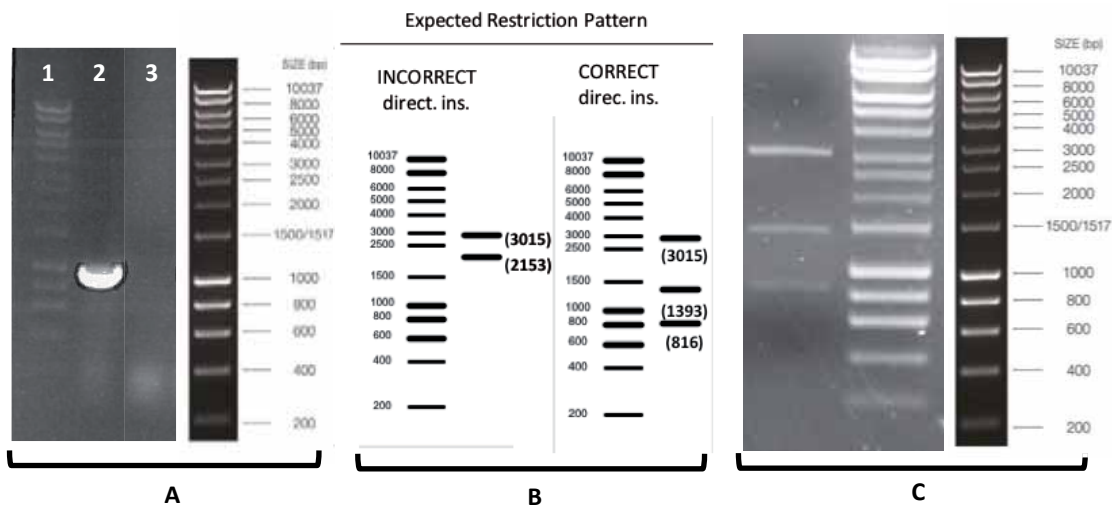


**Figure 5.14.** pTAR-2 characterisation (A) Colony PCR results. First lane: DNA Ladder, HyperLadder™ 1kb (Bioline); Second Lane: *E.coli* selected clone; third lane: negative ctrl (H<sub>2</sub>O). (B) Expected restriction pattern. (C) Enzymatic restriction pattern results. First Lane: *E.coli* selected clone; Second Lane: DNA Ladder, HyperLadder™ 1kb (Bioline).

### 5.3.1.2.3. pTAR-3

In Figure 5.15 the scheme of pTAR-3 with the primers used for colony PCR and *NheI* restriction sites are depicted. A band of 1450bp was expected after PCR amplification, and it was correctly obtained in the clone selected, as it is shown in Figure 5.16a. The expected restriction pattern after incorrect and correct *SSIL2-CapPCV2op* insertion is presented in Figure 5.16b and the correct outcome of the restriction of the selected clone is presented in Figure 5.16c.

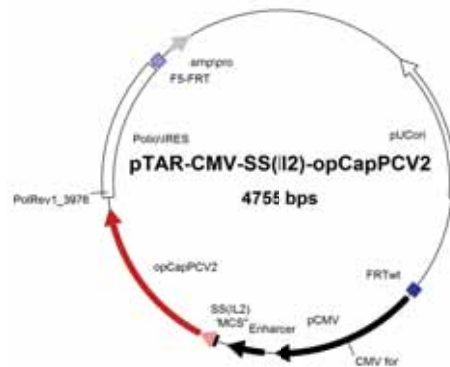


**Figure 5.15.** Scheme of pTAR-1. Main features, primers for PCR-characterisation and sequencing and restriction sites of the enzyme used for enzymatic restriction pattern (*NheI*) are depicted.

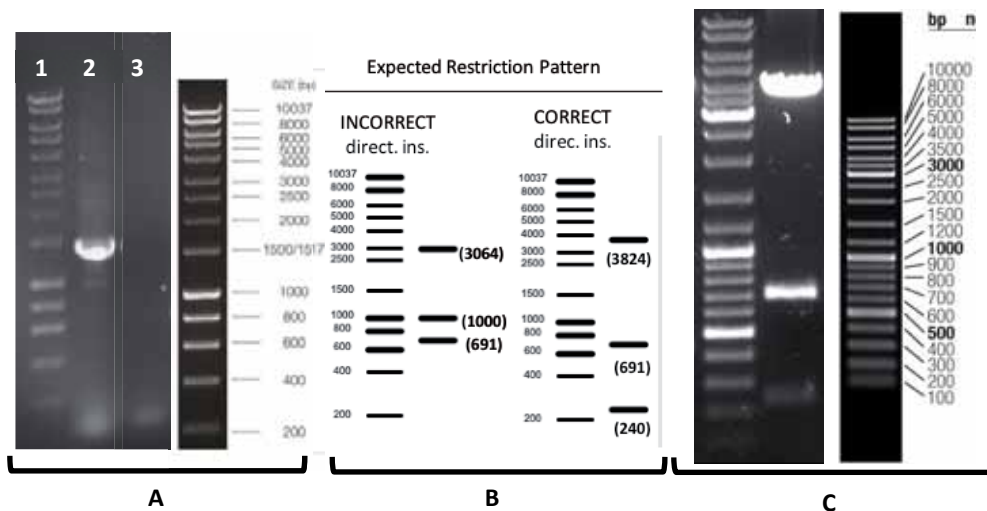


**Figure 5.16.** pTAR-3 characterization (A) Colony PCR results. First lane: DNA Ladder, HyperLadder™ 1kb (Bioline); Second Lane: *E.coli* selected clone; third lane: negative ctrl (H<sub>2</sub>O). (B) Expected restriction pattern. (C) Enzymatic restriction pattern results. First Lane: DNA Ladder, HyperLadder™ 1kb (Bioline); Second Lane: *E.coli* selected clone.

### 5.3.1.3. GENERATION AND CHARACTERISATION OF CapPCV2-293MZ3, CapPCV2-293MZ9 AND CapPCV2-293MZ10

#### 5.3.1.3.1. Generation

The three targeting vectors were transfected into the three HEK293 master cell lines. Hence, nine different cell lines should be obtained each one differing on the promoter controlling the expression of *CapPCV2* and the site of integration of the gene within the cell's genome.

In Figure 5.17 a scheme of the procedure for the generation of CapPCV2-stable cell lines is presented. Briefly, cells were harvested at 70-80% of confluence and they were set in the electroporation cuvette at a cell density of  $10^4$  cell/ $\mu$ L. The vector encoding for the Flipase (pFLip) and the targeting vector encoding for GOI (in this case, pTAR1, pTAR2 or pTAR3) were also added into the cuvette. Then, the cotransfection of the two plasmids was performed by electroporation (methodology described at Materials & Methods, section 8.9.2). Immediately after the electroporation, cells were plated in a cell culture dish in fresh media without selective pressure. Two days post transfection (dpt), geneticin was added to cell media in order to select those cells in which correct RMCE had taken place. On the next day (i.e. 3dpt) ganciclovir was also added in order to increase selective pressure for the positive RMCE clones. Colonies were identified under microscope observation and they were manually picked up and seeded into 96 well plate for further scaling up.

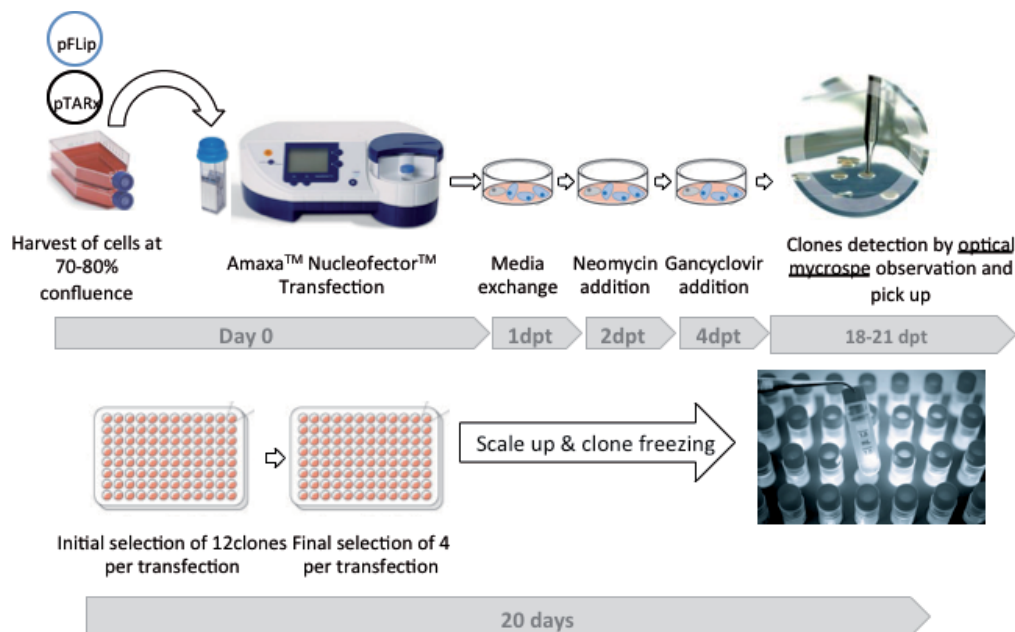


**Figure 5.17.** Scheme of the protocol for obtaining CapPCV2 producer clones derived from 293 cell line after RMCE. Upper panel: transfection and selection of clones. Lower panel: scaling up and cell bank obtention.

### 5.3.1.3.2. Characterisation

Before the results presentation of the clones characterisation and in order to easily go through the next sections, the identification of the 293-MZs derived selected clones is summarized in the Table 5.9.

**Table 5.9.** Identification of 293-MZs derived clones

	pTAR-1 (pSV40)	pTAR-2 (pEF1 $\alpha$ )	pTAR-3 (pCMV)
MZ3	1, 2, 3, 4b	5, 6, 7, 7b, 8	9
MZ9	13b, 14, 15	17, 17b, 18, 19, 20	21, 22b, 23b, 24
MZ10	25, 26, 27	29, 30, 31, 32	33, 34

#### 5.3.1.3.2.1. Characterisation of 293 clones by GFP expression profile

The GFP reporter gene is present on the tagging vectors used for 293 master cells generation (Figure 5.8). Hence, the lost of GFP expression is expected after RCME for the clones derived from 293 master cells. The fluorescence profiles of the parental cell lines and the lack of GFP expression of the clones derived from MZ3, MZ9 and MZ10 are presented on Appendix 10.4. The obtained results indicate that all the selected clones have reverted their positive GFP phenotype, indicating the lost of the gene after RMCE. The residual fluorescence detected (less than 5% of the living cells population for the majority of the clones and at a very low intensity) is more related to be background signal due to the low value of fluorescence intensity set for GFP-negative population selection.

#### 5.3.1.3.2.2. Characterisation of 293 clones by PCR

PCR characterization of the selected clones was done using the primers indicated in Table 3.10. The primer Polio1for hybridises with the Internal Ribosome Entry Site (IRES) present on the targeting vectors (Figure 5.11, 5.13 and 5.15) whereas NeoRev hybridises with the 3' region of  *$\Delta$ neo* gene (ATG deleted) present on the tagging vector (Figure 5.8). After correct RMCE, neo gene remains in the cell genome and the IRES element of the targeting vector is inserted 5' of this gene to restore the deleted ATG. Hence, the use of this pair of primers enables to characterie positive clones regardless

the gene of interest cloned. Before PCR, the genome of each selected clone was isolated (Materials and Methods section 8.10.2.5) and the concentration of DNA was adjusted to 100ng/ $\mu$ L. After PCR, a fragment of 1000bp is expected on those clones that have undergone RMCE.

**Table 5.10.** Primers used for RCME characterization

ID Primer	Primer Sequence (5'-3')	Expected PCR Fragment size (bp)
Polio1for	CGTCAAGAAGGCGATAGAAGGC	1000
NeoRev	CCATGGGACGCTAGTTGTGAA	

The results of PCR characterisation of the clones derived from each cell line are presented in Figure 5.18, Figure 5.19 and Figure 5.20 (clones derived from MZ3, MZ9 and MZ10, respectively). The identification of the samples is specified in Table 5.11, table 5.12 and table 5.13. It can be noticed that for the majority of the clones RMCE was confirmed, but for the 7b, 21, 24, 27, 33 and 34 clones any band amplification could be detected after PCR (i.e. they were false-positive clones). Other authors have reported the growth of false-positive clones under negative selection and it has been related to the inactivation of HSV-tk by events like partial deletions<sup>19,20</sup>. Rise of false-positive clones under positive G418 selection has also been reported although the causes behind the cell's insensitiveness to the antibiotic are not clear<sup>21,22</sup>. The main implication of the fact that the specified selected clones were false positive was that any positive clone derived from the master cell MZ10 with *CapPCV2* expression under CMV promoter control could be selected. Hence, the evaluation of the influence of integration site under CMV promoter could only be done by comparison of MZ3- and MZ9-derived clones.

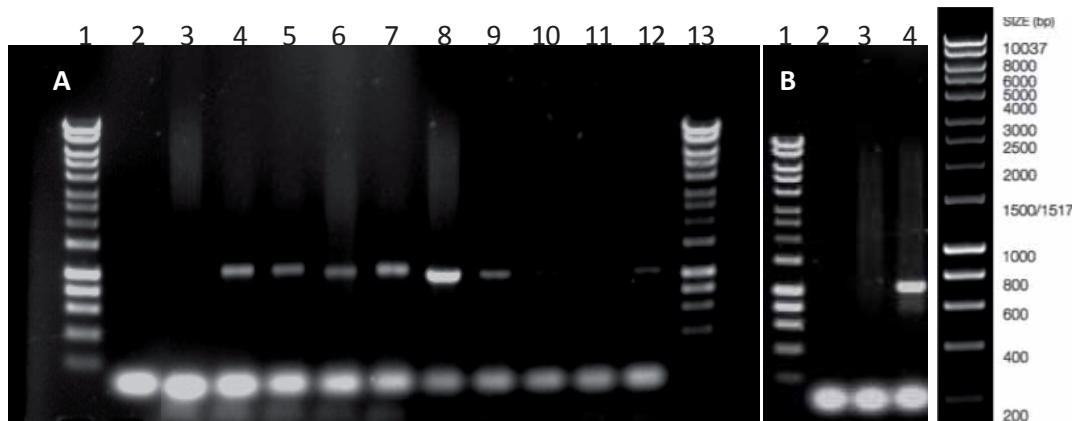


**Figure 5.18.** MZ3 derived clones characterisation by PCR. DNA Ladder used: HyperLadder™ 1kb (Bioline).

**Table 5.11.** Identification of the samples loaded on the agarose gels presented in Figure 5.18

GEL A				GEL B	
Lane	ID sample	Lane	ID sample	Lane	ID Sample
1,13	DNA Ladder	7	Clone 4b	1	DNA Ladder
2	H <sub>2</sub> O (Neg Ctrl)	8	Clone 5	2	H <sub>2</sub> O (Neg Ctrl)
3	293MZ3 (Neg Ctrl)	9	Clone 6	3	293MZ3 (Neg Ctrl)
4	Clone 1	10	Clone 7	4	Clone 9
5	Clone 2	11	Clone 7b		
6	Clone 3	12	Clone 8		

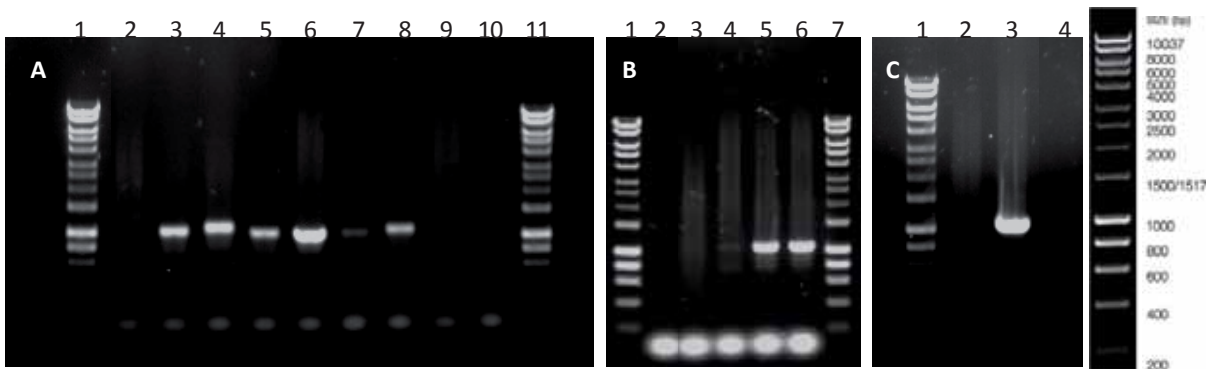


**Figure 5.19.** MZ9 derived clones characterization by PCR. DNA Ladder used: HyperLadder™ 1kb (Bioline).

**Table 5.12.** Identification of the samples loaded on the agarose gels presented in Figure 5.19

GEL A				GEL B			GEL C	
Lane	ID sample	Lane	ID sample	Lane	ID Sample	Lane	ID Sample	
1	DNA Ladder	7	Clone 19	1,7	DNA Ladder	1	DNA Ladder	
2	293MZ3(Neg Ctrl)	8	Clone 20	2	H <sub>2</sub> O (Neg Ctrl)	2	293MZ9 (Neg Ctrl)	
3	Clone 13b	9	Clone 21	3	293MZ9 (Neg Ctrl)	3	Clone 23b	
4	Clone 14	10	Clone 24	4	Clone 17	4	H <sub>2</sub> O (Neg Ctrl)	
5	Clone 15	11	DNA Ladder	5	Clone 17b			
6	Clone 18			6	Clone 22b			

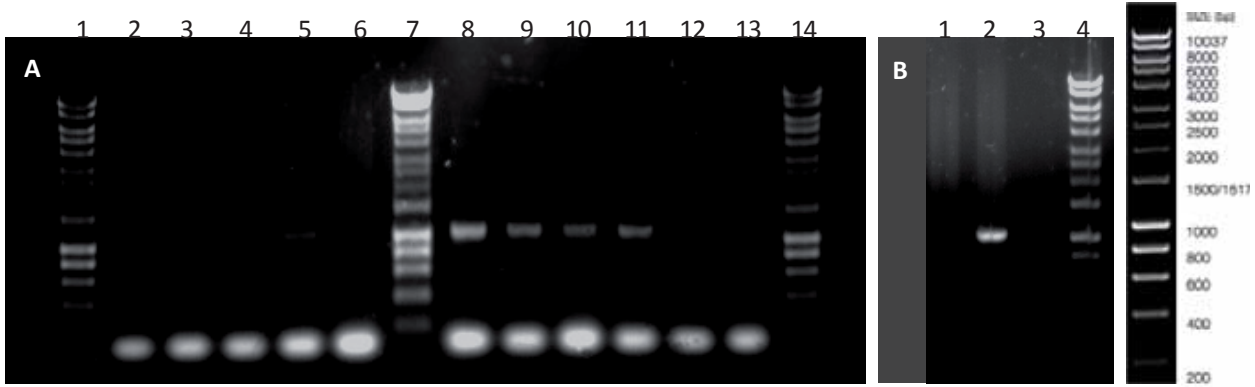


**Figure 5.20.** MZ10 derived clones characterization by PCR. DNA Ladder used: HyperLadder™ 1kb (Bioline).

**Table 5.13.** Identification of the samples loaded on the agarose gels presented in Figure 5.20.

GEL A				GEL B	
Lane	ID sample	Lane	ID sample	Lane	ID Sample
1,7,14	DNA Ladder	8	Clone 29	1	293MZ10 (Neg Ctrl)
2	H <sub>2</sub> O (Neg Ctrl)	9	Clone 30	2	Clone 26
3	293MZ10 (Neg Ctrl)	10	Clone 31	3	H <sub>2</sub> O (Neg Ctrl)
4	293MZ10 (Neg Ctrl)	11	Clone 32	4	DNA Ladder
5	Clone 25	12	Clone 33		
6	Clone 27	13	Clone 34		

#### 5.3.1.4. SCREENING OF CLONES FOR SELECTION OF THE BEST CapPCV2 PRODUCER.

293 clones characterised as positive for RMCE were selected to evaluate the production and secretion of the protein of interest (CapPCV2). Cells were plated at  $0.2 \times 10^6$  cell/cm<sup>2</sup> and cultured under selective pressure (i.e. geneticin and ganciclovir) for four days. Extracellular protein was quantified 24h and 96h post-seeding in order to evaluate protein secretion. Intracellular protein was quantified 96h post seeding. The results of this initial screening are presented in Figure 5.21. First of all, it must be mentioned that the problems on protein secretion previously detected in the clones obtained by illegitimate DNA integration were also encountered for the clones obtained after RMCE. Protein could not be detected in the supernatant samples of any of the clones evaluated, regardless the time of harvest (24h or 96h post seeding). Concerning intracellular production, the clone 22b was selected as the best producer among the 23 clones tested. This clone presented a specific production of 0.178 pg/cell which was around 10 times higher in comparison to the rest of the clones.



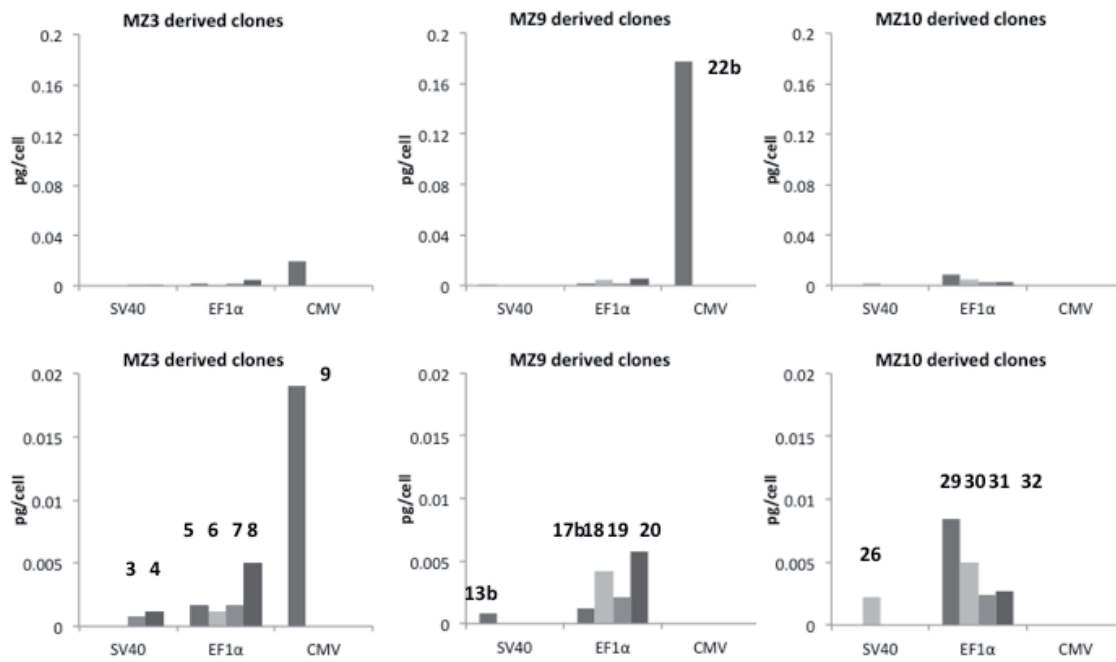


**Figure 5.21.** CapPCV2 specific production (intracellular fraction). The number on the top of each bar refers to the number of the clone. Upper chart: all clones included. Lower chart: All clones except 22b are depicted in order to easily compare specific production depending on promoter and cell line.

The results also indicate that CMV promoter performed better than SV40 and EF1 $\alpha$  promoters. Nevertheless, this cannot be undoubtedly stated because (1) any clone in which GOI expression was driven by CMV promoter could be analyzed for 293MZ10 and (2) only one clone for the other two master cell lines could be analyzed. Hence, the heterogeneity of protein expression that was found for the SV40 and EF1 $\alpha$  cannot be determined for CMV promoter. Concerning the site of GOI integration, it could not be established any relation between the master cell line and a higher level of protein production. This fact indicates that in our case, the expression of the gene was equally affected by the transcription signals emanating from its surrounding genetic environment.

### 5.3.1.5.CHARACTERISATION OF CapPCV2-293MZ9 CELL LINE

The clone 22b was selected for cell expansion due to its higher protein specific production. The cell line established from this clone will be referred to as CapPCV2op-293MZ9 cell line. After the preliminary results prior presented, a more accurate characterisation of cell growth and protein productivity was assessed. In order to do so, triplicates of cell growth in presence and absence of the selective pressure (i.e. geneticin and ganciclovir) were carried out and the titration of six independent cell cultures was performed. In Figure 5.22 cell growth and viability profiles are presented. It can be noticed that cells grew equally under antibiotic selection pressure and without the selective pressure, indicating a good homogeneity of the cell line concerning the correct substitution of the cassette expression after RMCE and subsequent restoration of neomycin resistance. Maximal specific growth rates ( $\mu_{max}$ ) were within the same range and all cell cultures reached confluence 96h post seeding. It should be mentioned that cells cultures in absence of antibiotic reached overconfluence 120h post seeding, whereas cells cultured in the presence of antibiotic detached from cell plate after reaching confluence.

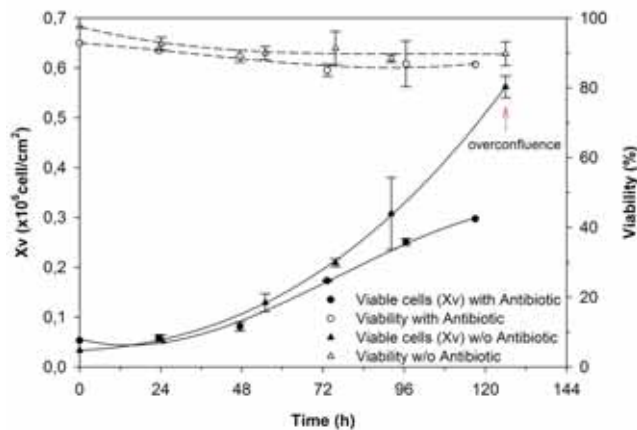


**Table 5.14.** Maximal specific cell growth rates of cultures presented in Figure 3.22

	$\mu_{max}$ ( $\times 10^{-2} h^{-1}$ )
Antibiotic presence	$2.23 \pm 0.3$
Antibiotic absence	$2.45 \pm 0.1$

**Figure 5.22.** Cell growth and viability profiles of CapPCV2op-293MZ9 cell line in presence and absence of antibiotic selective pressure. The antibiotics used were geneticin and ganciclovir.

After the titration of intracellular protein, the specific production ( $Y_{p/X}$ ) was determined to be of  $0.190 \pm 0.077$  pg/cell, which is in good concordance with the calculated value on the clone screening evaluation. Specific production was calculated as described in Eq. 5.1.

### 5.3.2. OBTENTION OF 293T CELL LINE-DERIVED CapPCV2 PRODUCERS.

#### 5.3.2.1. PARENTAL CELL LINE DESCRIPTION

Fifty putative 293T master cell lines were kindly provided by Dr S. Spencer (Helmholtz Zentrum für Infektionforschung –HZI– Braunschweig, Germany). All them were tagged by lentiviral infection encoding pLV sspwv vector (Figure 5.23). The infection was performed at very low MOI in order to increase the probability of obtaining single integration site cells. These putative master cells showed a higher intensity GFP-profile than 293 cell lines previously tested (i.e. MZ3, MZ9 and MZ10). Also, the GFP profile was more homogeneous in 293T cells than in 293 master cell lines. These two observations indicated that the sites of integration in 293T cell lines could be better hot-spots for protein expression than the ones in 293 cell lines already explored. Hence, it became interesting to obtain a CapPCV2 stable cell line from a 293T master cell line, as a higher protein production would be expected. In this direction, the characterisation of the cells for single site integration assessment was performed by Southern Blot (the protocol is detailed in Materials and Methods section 8.10.2.8). From the obtained results, one cell line (onwards 293T-17+) was selected to undergo RMCE in order to establish a new CapPCV2 producer cell line.

As in the case of the tagging vector used for 293 cell line (section 5.3.1, Figure 5.8), the exchanged sequence after RMCE of the pLV sspwv vector encodes for the green fluorescence protein reporter gene. Hence, after correct RMCE the lost of fluorescence should be observed.

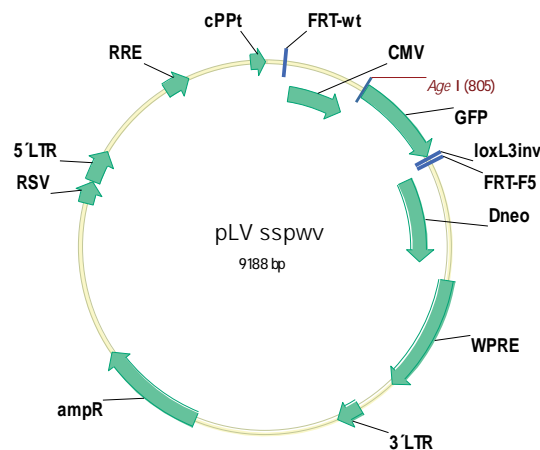


**Figure 5.23.** Tagging vectors used for the generation 293T cell lines.

Differently from the 293 cell lines, the tagging vector pLV sspwv vector did not encode for HTG gene, so the negative selection of positive clones by the addition of ganciclovir to cell media could not be applied. Besides, although  $\Delta neo$  is present in the tagging vector (*Dneo* in Figure 5.23), the addition of geneticin for positive selection of clones after RMCE could neither be used, as 293T are intrinsically

resistant to this antibiotic. Although the loss of GFP expression would indicate the replacement of the reporter gene by the gene of interest after RMCE, it is always recommended to have a reporter/selection gene linked to the GOI in order to avoid loss of the expression of gene of interest without noticing. Therefore, a new strategy for selection of positive clones had to be implemented and is described in the following sections.

### 5.3.2.2. OBTENTION AND CHARACTERISATION OF THE TARGETING VECTOR

According to the study of the effect of the promoter on the expression of *CapPCV2op* (results presented in section 5.3.1.4), only the original vector encoding for CMV promoter (i.e. pTAR-CMV-GCGRnew1, Figure 5.10) was selected for the obtention of the final targeting vector encoding for the *SSIL2-CapPCV2op*. In this case, the sequence finally cloned into the targeting vector was slightly different from the one considered for the construction of the targeting vectors for 293-MZs derived cell lines. Specifically, the cassette exchanged after RMCE will not only encode for the signal secretion peptide of IL-2 and the optimised sequence of *CapPCV2* (i.e. *SSIL2-CapPCV2op*) but also for the puromycin resistance gene. This modification will allow selecting positive clones that have undergone RMCE by the addition of puromycin to cell media.

The cassette *SS(IL2)-CapPCV2op-IRES-Puro<sup>R</sup>* (onwards GOI) was obtained from the pIRESpuro3-*SSIL2-CapPCV2op* vector (Figure 5.24) after EcoRV+XbaI digestion of the vector. These sites were selected because they were the closest to 5'-*SSIL2* and 3'-*Puro<sup>R</sup>* respectively.

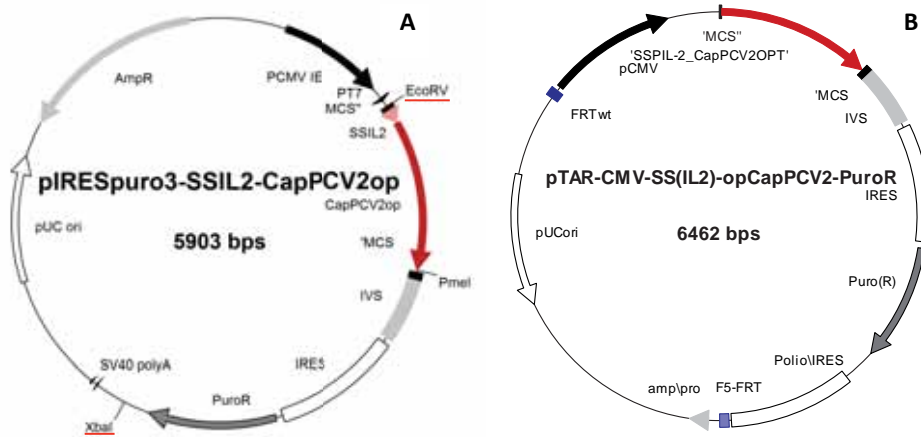


**Figure 5.24. (A)** pIRESpuro3-SSIL2-CapPCV2op vector. The enzymes used for the excision of the construct of interest (SSIL-2-CapPCV2op-IRES-Puro<sup>R</sup>) are red underlined (B) vector obtained after cloning the genetic construct SSIL2-CapPCV2op-IRES-puro<sup>R</sup> into pTAR-CMV EcoRI linearised. This vector was named as pTAR-4.

The cloning strategy was as similar as possible to the one followed for the generation of previous targeting vectors. Hence, after vector digestion GOI was isolated from agarose gel and the XbaI cohesive ends were filled in with Klenow fragment in order to get a 5' and 3' blunt end genetic construct. The targeting vector was restricted with EcoRI, filled-in with Klenow fragment and dephosphorylated with Calf Intestine Phosphorylase (CIP) to obtain blunt end-vectors ready to ligate with blunt-end GOI. The vector obtained was referred to pTAR-4 and it is depicted on Figure 5.24B. The characterisation by enzymatic restriction pattern of the selected *E. coli* clones is presented in the Figure 3.25. After PmeI digestion, three bands were expected. The size of the bands depending on the correct or incorrect direction of the GOI after cloning is depicted in Figure 5.25b. Also, the absence of mutations within the GOI due to the cloning process was assessed by sequentiation.

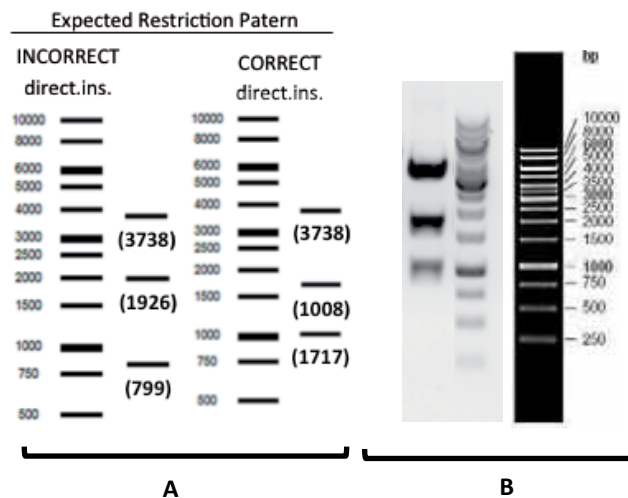


**Figure 5.25.** pTAR-4 characterisation (A) Expected restriction pattern. (B) Enzymatic restriction pattern results. First Lane: *E. coli* selected clone; Second Lane: DNA Ladder, 1kb DNA Ladder (Fermentas).

### 5.3.2.3. 293T PUROMYCIN KILL CURVE DETERMINATION.

As it was performed for HEK293-3F6 cell line, the puromycin kill curve was assessed for 293T cell line after the adaptation of the protocol to adherence-dependent cells. Based on the results obtained for the former cell line, a range from [puro]=0 $\mu$ g/mL to [puro]=3 $\mu$ g/mL was studied, but narrowing concentration stepwise for puromycin concentrations below 1.5  $\mu$ g/mL. Cells were seeded approximately 12h prior to the experiment onset in order to allow them to attach to the culture plate. At t=0h of the experiment, complete media replacement was carried out in order to change media and the addition of media with the desired puromycin concentration was performed.

The detrimental effect of puromycin on cell growth was already noticed at 48h post antibiotic addition (left chart of Figure 5.26) even at the minimum concentration tested (i.e. [puromycin]=0.5  $\mu$ g/mL). As the concentration of puromycin increased, an exponential decay on cell growth was observed and a higher percentage of cells were detached from cell plates. At the highest concentration tested (i.e. [puromycin]=3  $\mu$ g/mL), cell growth was not completely inhibited as it shown by the fact that 48h post addition total viable cell density (i.e. adhered and deadhered living cells) was higher than the inoculum cell density.

96h post antibiotic addition, a clear toxic effect was detected for [puromycin]  $\geq$ 1.25 $\mu$ g/mL. At these conditions, almost 100% of cells were detached from cell plate and those that were still adhered to cell plate showed very low viability (<15%). Cell cultures under a selective pressure of [puromycin]=0.5 $\mu$ g/mL and [puromycin]=0.75 $\mu$ g/mL did not significantly change from 48h post addition to 96h post addition. Cell growth was completely inhibited but cells continued attached to cell plate. Also, the drop on viability observed at [puromycin]<0.5 $\mu$ g/mL was more related to acidification of media due to cell growth.

The evaluation of these results led us to set puromycin concentration for positive clone selection at 1.25  $\mu$ g/mL, performing the first media replacement 96h post antibiotic addition.

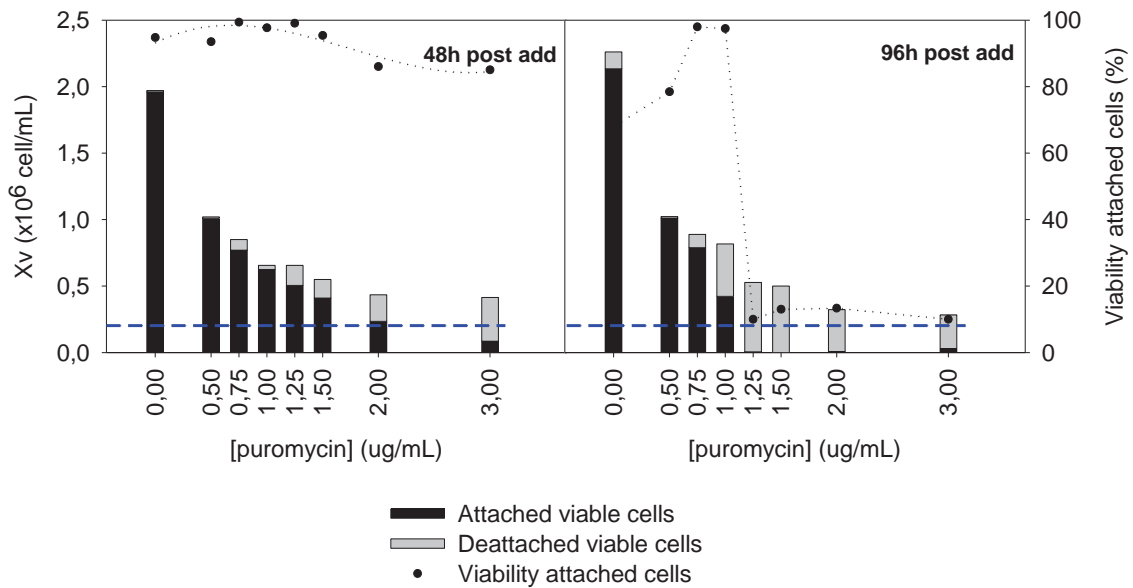


**Figure 5.26.** Puromycin kill curve of 293T cell line. Attached and detached viable cells are depicted as stacked bars. Hence, the total height of the curve represents total viable cell density. The dashed blue line indicates the viable cell density at seeding.

#### 5.3.2.4. GENERATION AND CHARACTERISATION CapPCV2-293T(17+).

##### 5.3.2.4.1. Generation

In Figure 5.27 a scheme of the procedure for the obtention of CapPCV2 producers derived from 293T-17+ master cell line is depicted. The main differences between this procedure and the protocol applied for the obtention of CapPCV2 producers derived from 293MZs (Figure 5.17) are underlined. In first place, electroporation transfection was changed by  $\text{Ca}_2\text{PO}_4$  transfection as the latter was recommended for 293T cell line. The complete  $\text{Ca}_2\text{PO}_4$  transfection protocol is detailed in Materials and Methods section 8.9.3. Secondly, it has already been mentioned that the selective pressure applied to 293T derived clones had to be done by the addition of puromycin at 2dpt. Finally, the selection of clones was carried out under fluorescence microscope instead of optical microscope in order to select colonies that have completely lost GFP expression. This way, the selection step and the lost of fluorescence characterisation step were combined in the same step, reducing the time for clone obtention. Doing it so, we would increase the probability of selecting pure clones which have correctly undergo RMCE before scaling them up

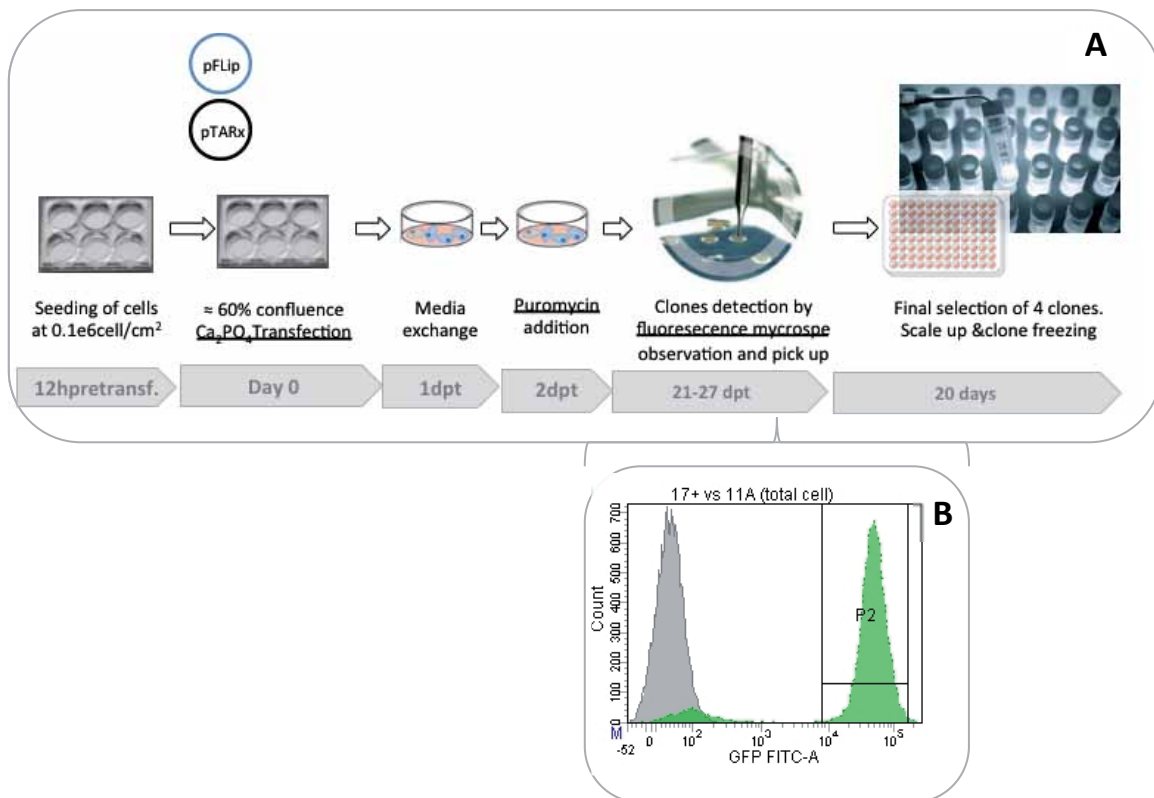


**Figure 5.27.** (A) Scheme of the process for the obtention of stable cell lines CapPCV2 producers derived from 293T-17+ master cell line after RMCE. (B) Example of selection of clones under fluorescence microscope: Overlapped fluorescence histograms obtained by flow cytometry of clone 11A (grey histogram) and 293T-17+ master cell line (green histogram).

### 3.3.2.4.2. Characterisation

The characterization of the clones was directly focused on the obtention of the protein of interest. Therefore, duplicates of the four clones selected were scaled up and r-CapPCV2 expression quantification was evaluated. 96h post seeding, cell confluence of approximately 75-80% was assessed for all cell cultures. The confluence was assessed in order to avoid slowing down of cell growth caused by “contact inhibition” mechanism<sup>9</sup> that would result in a possible underestimation of specific productivity. Then, cells were harvested and intracellular protein was quantified. Volumetric production ( $Q_p$ ) and specific production ( $Y_{p/x}$ ) values are compiled in Table 5.15. Except for clone 11B, which present a slightly lower  $Y_{p/x}$ , no significant differences were detected on this parameter among the other three clones evaluated. Besides, clone 11A and clone 11D grew slightly faster than the other clones, resulting in a higher [CapPCV2] due to higher cell density at time of harvest.

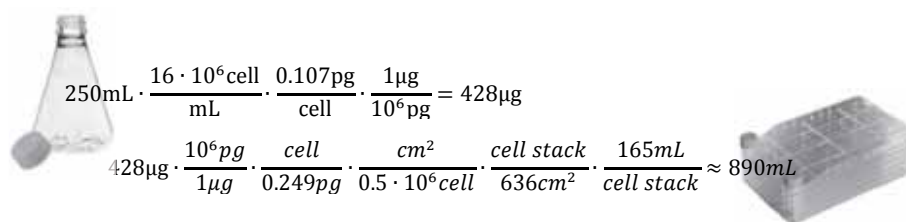


**Table 5.15.** Volumetric and specific productions of selected clones

Id clone	[CapPCV2] ( $\mu\text{g}/\text{mL}$ )	$Y_{p/x}$ (pg/cell)
1F	$5.20 \pm 0.49$	$0.273 \pm 0.026$
11A	$6.66 \pm 0.49$	$0.249 \pm 0.018$
11B	$2.94 \pm 0.33$	$0.188 \pm 0.021$
11D	$6.43 \pm 0.81$	$0.248 \pm 0.031$

In comparison with the clone 22b derived from 293MZs (characterised in section 5.3.1.4),  $Y_{p/x}$  was slightly higher in the new clones obtained, derived from 293T-17+ master cell line. As it has been stated, an increment on protein production was already expected, as the mean of fluorescence intensity of the parental cell line 293T-17+ was 2-log units higher than the mean of fluorescence intensity of the 293MZs. Nevertheless, the great difference on GFP expression was not proportional to the small increase on CapPCV2 production. This is in good correlation with the results obtained in Chapter 4, where it was noticed and commented that a sharp drop on protein productivity occurred when changing from the infection with rAdV-GFP to the infection with rAdV-CapPCV2 (i.e. recombinant adenovirus encoding for GFP or CapPCV2, respectively). The drop on protein production was not related to low efficient viral infection nor to virus replication, as the adenovirus titres obtained were similar after infection of cells with the two adenoviral vectors at the same conditions. All these results may indicate that the protein of interest selected in this work (CapPCV2) might be more difficult to express than other proteins such as GFP.

Regarding the stable cell line obtained after illegitimate integration (i.e. HEK293-F5), the specific production of clone 11A (onwards 293T-17+\_11Aad) doubled  $Y_{p/x}$  of the former one ( $0.107 \pm 0.088$  pg/cell). However, HEK293-F5 presented a huge advantage over 293T-17+\_11Aad. While the latter is an adherent cell line, HEK293-F5 is grown in suspension and cell densities over  $16 \times 10^6$  cell/mL can be reached. Taking into account that 293T-17+\_11Aad cells reach confluence at  $\approx 0.5 \times 10^6$  cell/cm<sup>2</sup>, it is possible to compare the two bioprocesses based on both cell lines (Figure 5.28).



$$250\text{mL} \cdot \frac{16 \cdot 10^6 \text{ cell}}{\text{mL}} \cdot \frac{0.107 \text{ pg}}{\text{cell}} \cdot \frac{1 \mu\text{g}}{10^6 \text{ pg}} = 428 \mu\text{g}$$

$$428 \mu\text{g} \cdot \frac{10^6 \text{ pg}}{1 \mu\text{g}} \cdot \frac{\text{cell}}{0.249 \text{ pg}} \cdot \frac{\text{cm}^2}{0.5 \cdot 10^6 \text{ cell}} \cdot \frac{\text{cell stack}}{636 \text{ cm}^2} \cdot \frac{165 \text{ mL}}{\text{cell stack}} \approx 890 \text{ mL}$$

**Figure 5.28.** Comparison of media volumes of two bioprocesses for r-CapPCV2 production based either in HEK293-F5 expression or in 293T-17+\_11Aad expression.

In order to obtain the same quantity of protein, five-fold increment on cell media volume would be necessary if cultivating the adherent cell line (293T-17+\_11Aad) in comparison to the cultivation of suspension cell line (HEK293-F5). In others words, although 293T-17+\_11Aad specific production is higher, volumetric production of the process would be more advantageous in a CapPCV2 production using HEK293-F5 cell line. For that reason, it was decided to adapt 293T-17+\_11ad to grow in suspension and evaluate the effect of the adaptation to protein production and productivity.

#### **5.3.2.5. 293T-17+\_11AAD CLONE ADAPTATION TO SUSPENSION. CELL GROWTH AND CapPCV2 PRODUCTION CHARACTERISATION OF 293T-17+\_11AAD AND 293T-17+\_11AS CLONES.**

293T-17+ cell line and the derivate clones were cultured in DMEM cell media FBS supplemented (10% v/v). However, preliminary studies already mentioned in Chapter1 showed how, in our hands, cells cultured in suspension using DMEM supplemented with FBS aggregated to a high extend, resulting into poor cell growth and drop on cell culture viability. Consequently, it was decided to adapt 293T-17+\_11Aad to suspension cell culture in a different cell culture media.

293T-17+ cell line and HEK293-3F6 cell line differ in some specific features but they both derive from the same parental cell line. Therefore, it was initially hypothesized that the best cell media encountered for HEK293-3F6 would also be suitable for the culture of 293T-17+. Consequently, we firstly cultured 293T-17+\_11ad cell line in HyQ SFMTransFx-293 4mM GlutaMAX, FBS and CB5 supplemented. The percentage of supplementation was initially set at 10% for both supplements, but concentration of FBS was gradually lowered until reaching a final concentration of 5% (v/v). By lowering the concentration on FBS, cells showed less aggregation but after some passages, a continuous drop on specific growth rate was detected, although viability remained over 85%. Then, It was decided to evaluate different concentrations of CB5 in order to assess if this supplement could be causing the cell growth impairment. After some passages for adaption to media, cell growth curves were assessed and the main kinetic parameters were evaluated, which are summarised in Table 5.16. Cell line referred to as 293T-17+\_11As, is the suspension cell line obtained after adaptation of 293T-17+\_11Aad.

**Table 5.16.** Main kinetic parameters of suspension cell cultures of 293T-17+\_11As growing in cell media with different CB5 percentage.

	[CB5] (v/v)		
	0%	3.3%	10%
$X_{v_{max}}$ ( $\times 10^6$ cell/mL)	7.54 $\pm$ 0.94	7.32 $\pm$ 1.25	3.70 $\pm$ 0.47
T $X_{v_{max}}$ (h)	168	180	180
$\mu_{max}$ ( $\times 10^{-2} h^{-1}$ )	2.44 $\pm$ 0.22	2.14 $\pm$ 0.07	1.80 $\pm$ 0.32
T $\mu_{max}$ (h)	90	90	90
Viab to $\mu_{max}$ (%)	89.54 $\pm$ 0.72	93.48 $\pm$ 0.91	95.39 $\pm$ 0.39

The results showed that CB5 supplementation affected negatively to cell growth, as  $\mu_{max}$  was reduced when increasing CB5 concentration. Moreover,  $X_{v_{max}}$  at the higher CB5 concentration was about the half than the one achieved on cell cultures without this supplement. Besides, although there were no significant differences on  $X_{v_{max}}$  between the lower CB5 addition and the absence of this supplement, the time needed to achieve this cell density was higher when CB5 was present in cell media, due to the reduction on specific growth rate. Accordingly to these results, it was decided to establish HyQ SFMTransFx 4mM glutaMAX 5%FBS but without CB5 supplementation as the cell culture media for 293T-17+\_11As cell line.

Once the cell media was selected, triplicates of cell culture with 293T-17+\_11As were performed in order to evaluate protein production. Also, to avoid possible inter-assay variability, triplicates of cell cultures with the parental adherent cell line (293T-17+\_11Aad) were carried out in parallel. Time of harvest (TOH) for protein evaluation was selected on basis to previous characterisation of the cell lines cell growth and inocula's cell density. Hence, for both cell lines TOH was set at approximately 100h, when adherent cells where 80% confluence and suspension cells still had 48h to reach maximal viable cell. (Figure 5.29).

Significative drop on  $Y_{p/x}$  of the cell line adapted to suspension was assessed after protein quantification. For the adherent cell line, the calculated specific production was 0.221 $\pm$ 0.036 pg/cell, which is in the range with the previous presented values for this parameter. In the case of the cell line adapted to suspension, specific production was 0.075 $\pm$ 0.035 pg/cell, which represents a three-fold reduction of this value in comparison to the adherent cell line.

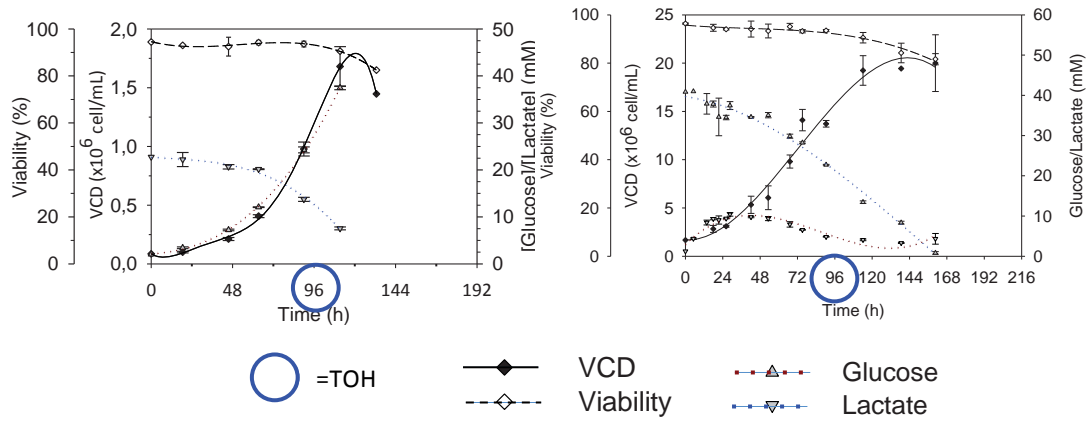


**Figure 5.29.** Cell growth, viability, glucose and lactate profiles of (A) 293T-17+\_11Aad and (B) 293T-17+\_11As. Cell density of adherent cell cultures was calculated as cell density ( $\text{cell}/\text{cm}^2$ ) at TOH  $\times$  cell plate area( $\text{cm}^2$ )/cell media per plate (mL)

## 5.5. CONCLUSIONS

The generation of stable cell lines enabled to overcome the low specific production of CapPCV2 encountered with the bioprocess based on adenovirus infection (Chapter 2). Specifically, a 5-fold increment on  $Y_{p/x}$  was achieved if we compare the most productive stable cell line with the bioprocess based on AdV\_CapPCV2 infection. Between the two cell strategies explored for stable cell generation (illegitimate DNA integration and site-directed integration by RMCE), the latter was the one that performed better. With RMCE a stable cell line was generated (293T-17+\_11Aad), which doubled the specific production of the one calculated for the cell line obtained after illegitimate DNA integration (HEK293-F5) (Table 3.20). This could be initially unexpected. As site directed integration events occur in much lower rates than randomly integration, and also because with the second strategy more than one copy of GOI can be inserted into the genome of the host, illegitimate integration normally results in higher protein productivities. Nevertheless, this statement strongly depends on the protein to be expressed and the final sites of integration, so the results cannot be predicted in advance. Our results indicate that the identified “hot-spot” in 293T\_17+ parental cell line is transcriptionally active enough to overcome the production obtained with HEK293F6.

**Table 5.20.** Summary of the main parameters of each clone obtained for stable cell line generation.

Clone	Gene integration	$Y_{p/x}$ (pg/cell)	$\mu_{max}$ ( $\times 10^{-2}$ h $^{-1}$ )	$X_{Vmax}$ ( $\times 10^6$ cell/mL)
HEK293-F5	Random	0.107±0.018	2.84±0.09	18.73±0.36
CapPCV2op-293MZ9	Site-directed	0.190±0.077	2.13±0.16	1.88±0.04
293T-17+_11Aad	Site-directed	0.221±0.036	2.38±0.02	1.63±0.30
293T-17+_11As	Site-directed	0.075±0.035	2.44±0.21	7.54±0.94

Finally, despite the higher specific production of 293T-17+\_11Aad in comparison to HEK293-F5, the fact that the latter could be grown in suspension resulted in higher volumetric production and more feasible bioprocess. Therefore, the adaptation of 293T-17+\_11Aad to grow in suspension was performed. This adaptation resulted in a significant drop on r-CapPCV2 specific production. Precisely,  $Y_{p/x}$  of the cell line adapted to suspension culture (293T-17+\_11As) was 0.075±0.035 pg/cell, which is almost three times lower than  $Y_{p/x}$  of the adherent cell line. Besides, the specific production of 293T-17+\_11As was in the range of the one calculated for the other stable suspension cell line generated in this work (HEK293-F5). However, higher cell densities were achieved with the latter clone and consequently, higher volumetric productivities would be achieved. Therefore, in terms of the production of this specific protein, HEK293-F5 would be the clone selected for bioprocess

development. An attractive alternative could be obtaining a stable cell line by site-directed integration of the gene into hot-spots of the genome of a cell line which already grows in suspension. These alternatives will also be discussed in the final conclusions of this thesis.

Finally, it must be mentioned the impossibility of secreting rCapPCV2 regardless the secretion signal peptide used. Regarding the use of SS-IL2, it must be mentioned that although interleukin-derived signal sequence are in common use both in commercial protein and production and in gene therapy<sup>23</sup>, recent studies demonstrate that the performance of IL-2 signal peptide can be improved substantially<sup>24</sup>, suggesting that the native sequence does not operate optimally. In the final conclusions of the thesis, further discussion will be addressed to this topic and alternatives for signal peptide selection will be discussed.

## 5.6. REFERENCES

1. Jostock, T. & Knopf, H.-P. in *Therapeutic Proteins SE - 15* (eds. Voynov, V. & Caravella, J. A.) **899**, 227–238 (Humana Press, 2012).
2. Zhang, J. in *Manual of Industrial Microbiology and Biotechnology* (ed. H, B. R.) 57–178 (2010).
3. Würtele, H., Little, K. & Chartrand, P. Illegitimate DNA integration in mammalian cells. *Gene Ther.* **10**, 1791–1799 (2003).
4. Ho, S. C. L., Tong, Y. W. & Yang, Y. Generation of monoclonal antibody-producing mammalian cell lines. *Pharm. Bioprocess.* **1**, 71–87 (2013).
5. Gaj, T. Genetic engineering with customizable recombinases and nucleases. (The Scripps Research Institute, 2013).
6. Akopian, A. & Marshall Stark, W. Site-Specific DNA Recombinases as Instruments for Genomic Surgery. *Adv. Genet.* **55**, 1–23 (2005).
7. Gaj, T., Sirk, S. J. & Barbas, C. F. Expanding the scope of site-specific recombinases for genetic and metabolic engineering. *Biotechnol. Bioeng.* **111**, 1–15 (2014).
8. Hirano, N., Muroi, T., Takahashi, H. & Haruki, M. Site-specific recombinases as tools for heterologous gene integration. *Appl. Microbiol. Biotechnol.* **92**, 227–239 (2011).
9. Ain, Q. U., Chung, J. Y. & Kim, Y.-H. Current and future delivery systems for engineered nucleases: ZFN, TALEN and RGEN. *J. Control. Release* **205**, 120–127 (2014).
10. Carroll, D. Genome engineering with targetable nucleases. *Annu. Rev. Biochem.* **83**, 409–39 (2014).
11. Cai, M. & Yang, Y. Targeted genome editing tools for disease modeling and gene therapy. *Curr. Gene Ther.* **14**, 2–9 (2014).
12. Schucht, R. *et al.* Rapid Establishment of G-protein-coupled receptor-expressing cell lines by site-specific integration. *J. Biomol. Screen.* **16**, 323–331 (2011).
13. Palomares, L. A., Estrada-mondaca, S. & Ramírez, O. T. in *Methods in Molecular Biology. Recombinant Gene Expression Reviews and Protocols* (eds. Balbás, P. & Lorence, A.) **267**, (Springer, 2004).
14. Angov, E. Codon usage: Nature's roadmap to expression and folding of proteins. *Biotechnol. J.* **6**, 650–659 (2011).
15. Fath, S. *et al.* Multiparameter RNA and codon optimization: A standardized tool to assess and enhance autologous mammalian gene expression. *PLoS One* **6**, (2011).
16. Niwa, H., Yamamura, K. & Miyazaki, K. Efficient selection for high-expression transfectants with a novel eukaryotic vector. *Gene* **2**, 193–199 (1991).

17. Lupton, S. D., Brunton, L. L., Kalberg, V. A. & Overell, R. W. Dominant Positive and Negative Selection Using a Hygromycin Phosphotransferase-Thymidine Kinase Fusion Gene. *Mol. Cel. Biol.* **11**, 3374–3378 (1991).
18. Ardiani, A., Sanchez-Bonilla, M. & Black, M. E. Fusion enzymes containing HSV-1 thymidine kinase mutants and guanylate kinase enhance prodrug sensitivity in vitro and in vivo. *Cancer Gene Ther.* **17**, 86–96 (2010).
19. Bradford, H., Advait, L. & Ashock, B. K. Overview : Generation of Gene Knockout Mice. *Curr Protoc. Biol.* 1–23 (2009). doi:10.1002/0471143030.cb1912s44.Overview
20. Gogos, J. a, Lowry, W. & Karayiorgou, M. Selection for retroviral insertions into regulated genes. *J. Virol.* **71**, 1644–1650 (1997).
21. Lanza, A. M., Kim, D. S. & Alper, H. S. Evaluating the influence of selection markers on obtaining selected pools and stable cell lines in human cells. *Biotechnol. J.* **8**, 811–821 (2013).
22. Yu, Y. *et al.* A Site-Specific Recombinase-Based Method to Produce Antibiotic Selectable Marker Free Transgenic Cattle. *PLoS One* **8**, (2013).
23. Stern, B., Olsen, L. C., Tröße, C., Ravneberg, H. & Pryme, I. F. Improving mammalian cell factories : The selection of signal peptide has a major impact on recombinant protein synthesis and secretion in mammalian cells. *Trends Cell Mol. Biol.* **2**, 1–17 (2007).
24. Zhang, L., Leng, Q. & Mixson, a. J. Alteration in the IL-2 signal peptide affects secretion of proteins in vitro and in vivo. *J. Gene Med.* **7**, 354–365 (2005).



## CHAPTER 6: HEK293 CELLS PHYSIOLOGY STUDY AND METABOLISM UNRAVELLING BY pFBA APPLICATION

### 6.1. INTRODUCTION

Physiology can be defined as the branch of science that studies the interaction between cells and their environment. It must be distinguished from metabolism in the sense that while the basic metabolic currencies remain the same across cells (e.g., ATP, acetyl coenzyme A [AcCoA], NADH, NADPH), the metabolic requirements of each cell type are determined by their tissue function and environment, and consequently, metabolic resources will be differently used<sup>1</sup>. For example, immune cells remain quiescent for extended periods but then rapidly proliferate upon stimulation. To accomplish this, cells shift from a state of low nutrient uptake to a state of increased nutrient uptake by the activation of anabolic pathways that facilitates rapid growth and division<sup>2</sup>. Differently, cardiac myocytes do not proliferate but have a high demand for ATP, so these cells strongly rely on oxidative phosphorylation to efficiently generate ATP<sup>3</sup>. Another interesting example are the hepatocytes, which are in charge of controlling blood chemistry and thus need flexibility to perform energy-intensive processes (i.e. synthesis of glucose, amino acids, and macromolecules), to recycle by-

products of metabolism from other tissues into useful metabolites while also excreting unneeded or toxic material as waste<sup>4</sup>. Each of these tissue physiologies requires different ratios of the metabolic currencies and employs unique regulatory circuits.

As stated in the introduction, metabolic engineering is one of the main branches in bioprocess optimisation, and particularly, flux balance analysis (FBA) is an important tool in order to better understand the physiology of cells and identify critical components in metabolic pathways. The advantage of FBA in comparison to other methodologies of flux analysis is that they are based on *in silico* genome-scale metabolic models which have been completed with databases, literature and experiments<sup>5</sup>, and they follow optimisation-based simulation techniques to analyse cellular metabolism. Hence, they usually don't need labelled isotopomers (which are quite expensive and the detection techniques are not easy to implement) and they can explore different cell physiological behaviours *in silico* or also predict metabolic capability when changing the pre-defined conditions. Nevertheless, it must be stated that FBA can result in mathematically feasible but biologically unfeasible solutions, so the study of the predictions must be performed and the outputs of metabolic and physiologic studies must be included in the models as an iterative optimization.

This chapter is focused on the study of the metabolic and physiologic behaviour of mammalian cells in batch culture has extensively been reported as the consumption of large amounts of glucose during exponential cell growth resulting in the secretion of lactate. The extracellular accumulation of lactate is one of the most important limitations of mammalian cell based bioprocesses. Some effects on the physiology of mammalian cell due to lactate accumulation are the inhibition of cell growth and protein expression<sup>6,7</sup> and alteration of protein glycosylation patterns<sup>8,9</sup>. In the following sections, the physiology of the HEK293 cells under certain environmental conditions is presented and studied. Moreover, flux balance analyses are presented in order to support the hypothesis proposed for unravelling the observed physiology.

## **6.2. STUDY OF DIFFERENTIAL LACTATE METABOLISM DEPENDING ON pH CONTROL**

As it has been pointed out in Chapter 3 of this work, substantial differences on lactate metabolism of HEK293 cells depending on the culture platform have been observed. One platform was a fully controlled stirred bioreactor while the other was a shake flask platform without pH and pO<sub>2</sub> control or monitoring.

When cells grew in bioreactor lactate was produced and secreted to media until the complete depletion of glucose (Figure 6.1). Thereafter, lactate consumption was observed together with a

decrease on the specific growth rate, concurrently with the end of the exponential growth phase. This cell metabolism has been extensively studied and accepted for animal cells by the scientific community. However, this metabolic behavior differed from the one routinely observed in shake flask cultures. When cultured in this platform, an initial phase of glucose consumption and lactate production was observed, followed by a shift towards lactate and glucose concomitant consumption. At the shift point, lactate concentration was always around of 11mM (which is far lower the lactate concentration reached in bioreactor) and glucose was not at limiting concentrations (approx.  $[gluc]=30mM$ ) (Figure 6.2).

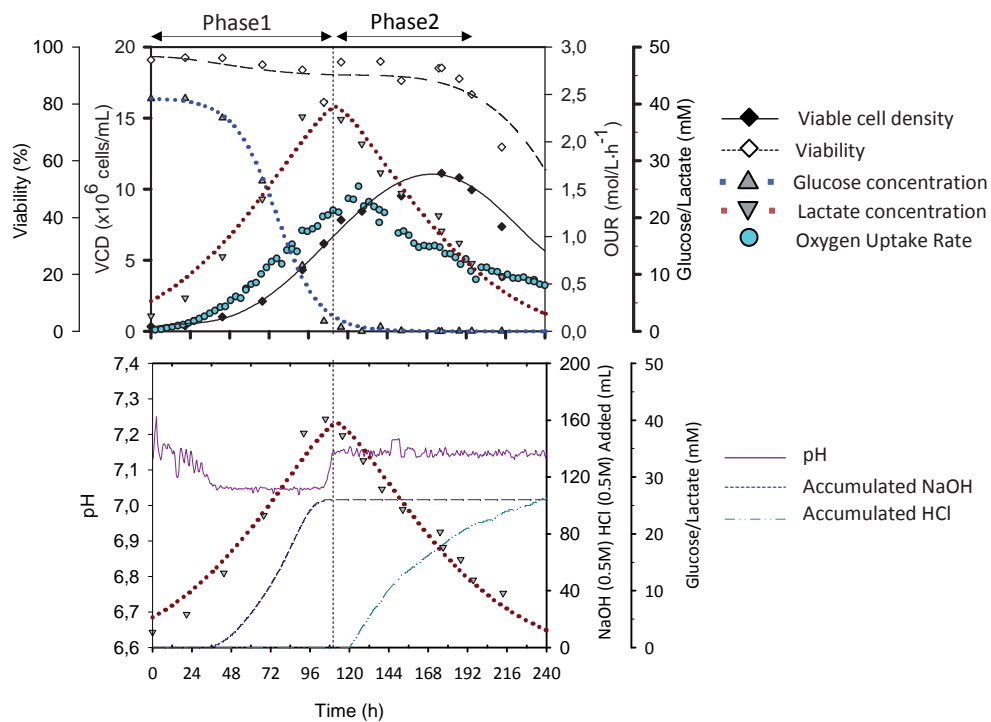


**Figure 6.1.** Batch cell culture of HEK293 suspension cells in a 2L bioreactor under controlled temperature, dissolved oxygen and pH conditions. Upper panel: cell growth, viability, glucose concentration, lactate concentration and OUR. Lower panel: pH evolution, accumulated NaOH and HCl and lactate concentration.

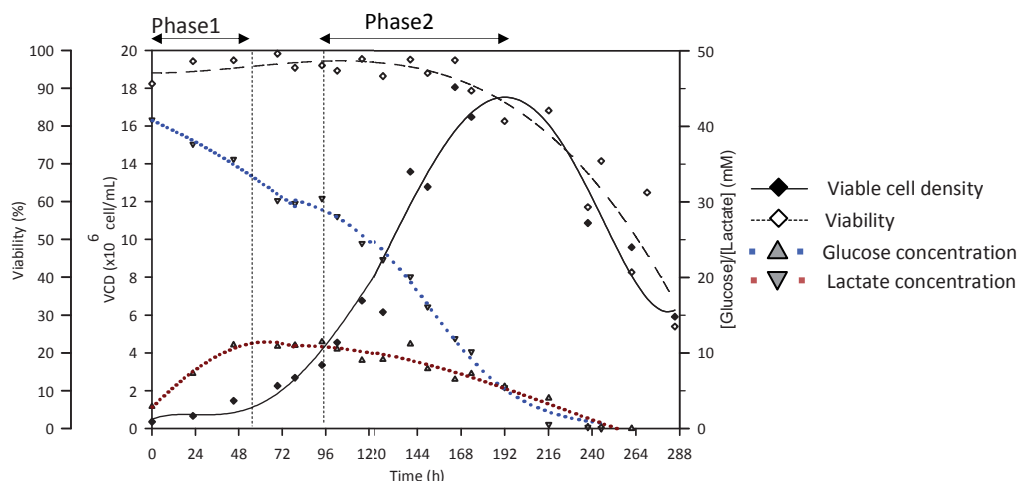


**Figure 6.2.** Batch cell culture in 1L-shake flask. Viable cell density, viability, glucose concentration and lactate concentration profiles are depicted.

The differences from one culture platform to the other were only  $pO_2$  and pH evolution (i.e. free in shake flask and controlled in bioreactor) as cell media, inoculum, and temperature were the same. Since cell density increased 9-fold in shake flasks after the metabolic shift from glucose consumption and lactate production to concomitant glucose and lactate consumption, we hypothesized that the triggering factor of the metabolic shift was more related to pH control than to  $O_2$  limitation. To evaluate this hypothesis, HEK293 cells were cultured and monitored in 2 litres bioreactor reproducing the conditions of shake flask regarding pH control: alkali buffer addition was avoided and pH was only controlled by means of  $CO_2$  addition to keep its value below 7.2. As depicted in Figure 6.3, under these conditions the metabolic behaviour observed in shake flasks was reproduced: in the initial stages of the cell culture glucose consumption and lactate production was also observed, but this stage was followed by a shift towards lactate and glucose concomitant consumption in the middle of the growth phase. At the metabolic shift point ( $t \approx 96h$ ), lactate concentration was around of 11-13mM and the remaining glucose was not at limiting concentrations (approximately 30mM).

As shown in Figure 6.1 (lower chart), the pH value was maintained around 7.1 (set point) by the addition of NaOH or HCl. When buffer addition was suppressed (Figure 6.3, lower chart), acidification of media was observed and pH dropped to values around 6.75. At that point (around 96h after inoculation), lactate secretion was stopped and net consumption of extracellular lactate was observed from  $t=120h$  onwards (Figure 6.3).

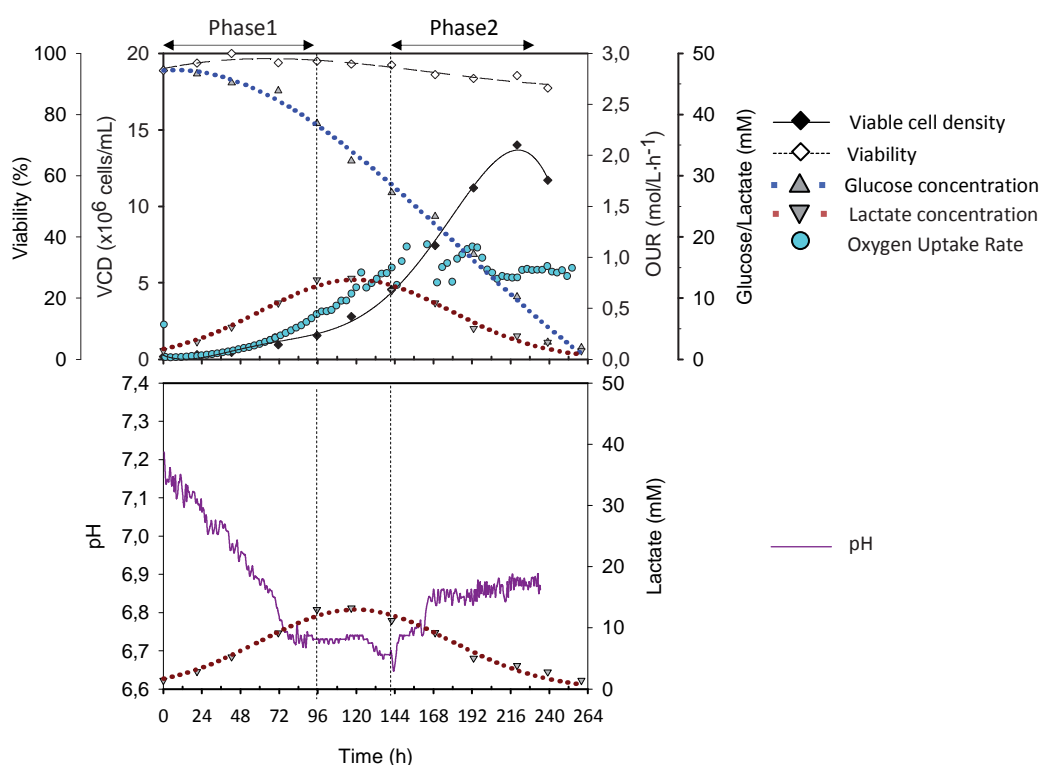


**Figure 4.3.** Batch cell culture of HEK293 suspension cells in a 2L bioreactor under controlled temperature and dissolved oxygen conditions. pH was kept controlled for basification of media by CO<sub>2</sub> addition (set point:6.95) Upper panel: cell growth, viability, glucose concentration, lactate concentration and OUR. Lower panel: pH evolution and lactate concentration.

Consumption and production rates for both culture strategies with different metabolic behaviour were assessed and are summarized in Table 6.1. Specific glucose uptake rate ( $q_{\text{gluc}}$ ) and lactate production rate ( $q_{\text{lac}}$ ) were similar for both cultures during Phase 1 (i.e. lactate production; onwards P1). On the contrary, significant differences were observed on those parameters when lactate was consumed (i.e. Phase 2 or P2). Whereas in pH-controlled batch the drop in  $q_{\text{gluc}}$  is related to the depletion of glucose in media, in pH-free batch the reduction of this parameter occurred despite the presence of this metabolite in non-limiting concentration. Finally, lactate uptake rate during P2 ( $q_{\text{lacP2}}$ ) was increased more than twice in cultures with controlled pH compared to cultures without pH control (36.45 and 14.01 nmol/(10<sup>6</sup>cell·h), respectively). This is probably due to the fact that, whereas in pH-controlled batch lactate was the sole substrate consumed during P2, in the cultures without pH control lactate was co-consumed together with glucose (although glucose was consumed at lower rates). The specific consumption and production rates of batch without pH control were in the range of those calculated for shake flask cultures (data not shown).

Interestingly, the cell density reached when pH was not controlled was slightly higher (Table 6.1), indicating that the different metabolic behaviour could be, somehow, beneficial for cell culture expansion. This is related to the dramatic drop on specific growth rate after the metabolic shift observed in pH-controlled bioreactor (three-fold decrement, Table 6.1) whereas only a slight reduction of this parameter was observed for cells in pH-free bioreactor. These results were in good agreement with those obtained in shake flask cultures. Additionally, cell viability was kept about 90% during the growth phase in both bioreactor fermentations, and Oxygen Uptake Rate (OUR) profile, which is an accurate on-line measurement of metabolic cell activity, also supported the idea of a more sustained cell growth when pH was not controlled.

**Table 4.1.** Cell growth, glucose and lactate related parameters of pH-controlled batch cell culture (NaOH/HCl control; depicted in Figure 4.1) and pH-free batch cell culture (CO<sub>2</sub> control; depicted in Figure 4.3).

	pH-controlled	pH-free
$X_{v_{max}}$ ( $\times 10^6$ cell/mL)	11.1	14.0
$\mu_{max}$ ( $\times 10^{-2}$ /h)	2.94	2.35
$t_{\mu_{max}}$ (h)	115	117
$M_{post-shift}$ ( $\times 10^{-2}$ /h)	1.09	1.82
$[lactate]_{max}$ (mM)	40.21	13.2
$[glucose]_{lactate_{max}}$ (mM)	1.78	32.4
$t_{lac_{swicht}}$ (h)	92	68
$q_{glucP1}$ (nmol/( $10^6$ cell·h))	220.02	193.64
$q_{lacP1}$ (nmol/( $10^6$ cell·h))	245.64	221.65
$q_{glucP2}$ (nmol/( $10^6$ cell·h))	n.a.*	32.03
$q_{lacP2}$ (nmol/( $10^6$ cell·h))	-36.45	-14.01

\* n.a.: (not applicable): glucose was depleted so no rate consumption could be calculated

Taking into account all those previous results, we hypothesized that the acidification of media due to lactate secretion might be the triggering factor of the HEK293 cells metabolism shift.

### 6.3. MODIFICATIONS OF CELL MEDIA FOR TRIGGERING THE METABOLIC SHIFT AT WILL

With the aim of evaluating the proposed hypothesis together with studying the possibility of triggering the concomitant glucose and lactate consumption when desired, we modified the initial conditions of the media reproducing the conditions in which the metabolic shift took place in previous experiments. We also aimed to find out whether cells are capable of switching metabolism due to environmental conditions or if the metabolism change was related to cell state after some hours of culture under certain conditions.

Three different conditions were tested in shake flask and are described below. Triplicates of cell culture in unmodified fresh media were included as controls.

**Partially consumed media (PCM):** A culture with the same characteristics of the one presented in Figure 6.2 was set. At the time that metabolic shift was detected ( $t \approx 100\text{h}$ ), cells were harvested and media was recovered and kept at  $4^\circ\text{C}$  until the experiment onset. Besides, cells were scaled up in order to obtain an inoculum of  $2.5 \times 10^6$  cell /mL of fresh cells and maintaining cell culture within a concentration of  $1-1.5 \times 10^6$  cell/mL (as described for cell passaging in Materials and Methods (section 8.3.1.3.1)).

**Sodium lactate-modified media:** The necessary volume of a 1M-sterile stock solution of sodium lactate ( $\text{NaC}_3\text{H}_5\text{O}_3$ ) was added to cell culture at the experiment onset. The initial lactate concentration was set at 12mM, which corresponds to the average lactic acid concentration at the time when the metabolic shift was observed in prior cultures without pH control.

**Lactic acid/pH-modified media:** A 1M-sterile stock solution of lactic acid ( $\text{C}_3\text{H}_6\text{O}_3$ ) was prepared and the necessary volume was added to cell media at the beginning of the experiment. As in the case of sodium lactate, the initial lactate concentration was set at 12mM.

As a consequence of the different lactate form used (i.e. endogenous lactate, exogenous sodium lactate or exogenous lactic acid) the initial pH was different for each condition tested. Experimental conditions and results are shown in Figure 6.4 and Table 6.2.

First of all, no significant differences in terms of specific growth rate among all the conditions tested were detected, being  $\mu_{\text{max}}$  within the range reported for HEK293 cells<sup>10</sup>. As shown in Figure 6.4A and compiled in Table 6.2, cells in fresh media performed identically as it was previously observed: cells grew to a final concentration of  $21.4 \pm 2.7 \times 10^6$  cell/mL. Also, there was an initial phase of lactate production until a concentration of  $10.41 \pm 0.44$  mM was reached (P1). At that point, lactate started to be consumed simultaneously to glucose assimilation resulting in a 4-fold drop on glucose consumption rate ( $q_{\text{gluc}}$  P2).

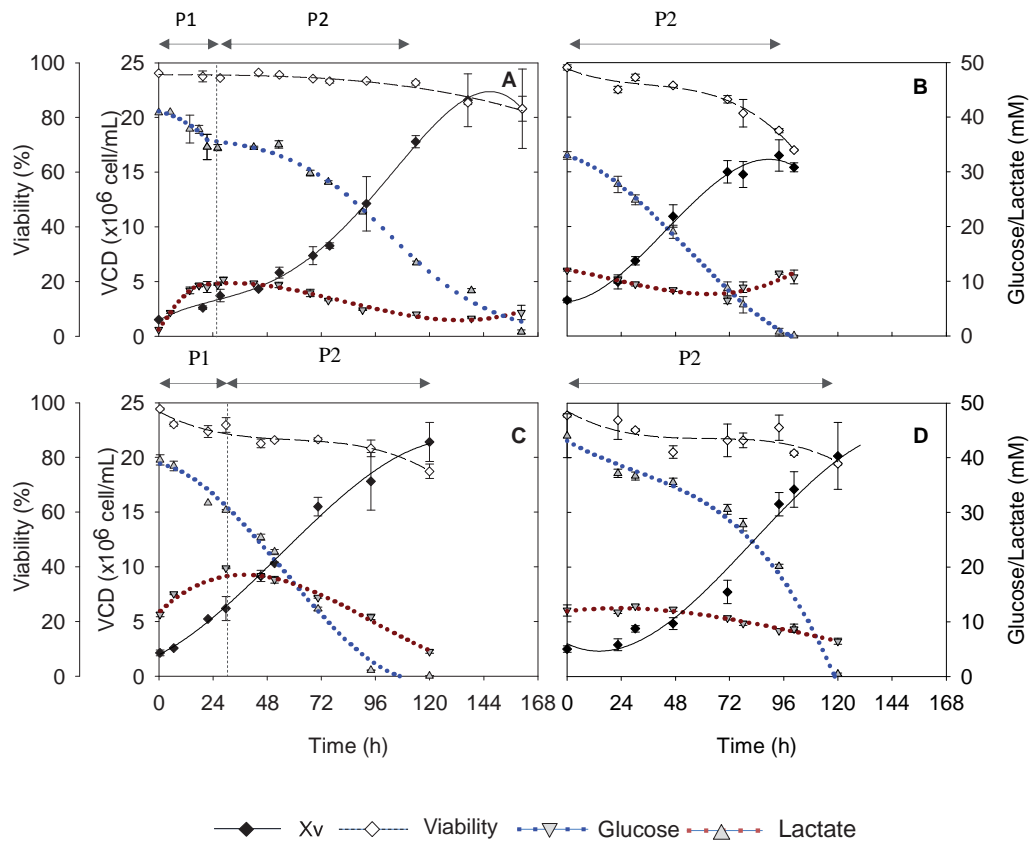


**Figure 6.4.** HEK293 suspension cell cultures in 125mL shake flask in different media conditions (A) When unmodified cell culture media (control cell culture) (B) partially-consumed cell culture media (C)  $\text{NaC}_3\text{H}_5\text{O}_3$ -modified media (D)  $\text{C}_3\text{H}_6\text{O}_3$ -modified media. cells were cultured in PCM (Figure 6.4B)  $X_{v_{\max}}$  was 1.3 fold lower with respect to unmodified media, which was already expected since initial nutrients concentrations were lower. Interestingly, consumption of lactate was detected from the very beginning of the culture, indicating that the metabolic shift was more related to environmental conditions rather to the internal cell's conditions. Moreover, cells were able to perform a fast adaptation to these environmental circumstances, resulting in a single growth phase with a metabolism identical to the one previously described in Phase 2 when glucose and lactate were simultaneously consumed. Regarding cells cultured in presence of sodium lactate (Figure 6.4C) both metabolic profile and cell growth evolution were quite similar to the fresh media cultures (control). Although the lactate concentration accumulated along the culture was higher, the increment in lactate concentration was almost the same than in control cultures (approximately 9mM) (Table 6.2). Therefore, the pH drop before the metabolic shift due to the lactate accumulation should be the same in both cases. Glucose and lactate uptake/production rates ( $q_{\text{glucP1}}$  and  $q_{\text{lacP1}}$ ) were similar to those calculated for control cell cultures. Altogether, confirmed that the addition of sodium lactate to the media had no influence on the metabolic behavior of cells.



Finally, when lactic acid was added to cell media (Figure 6.4D), pH dropped to 6.82, which was similar to the initial pH of PCM. Cell growth when lactic acid was added was like to the growth observed in fresh media, reaching  $X_{v_{max}}$  values as high as  $20.2 \pm 3.1 \times 10^6$  cell/mL. Remarkably, lactate metabolism was comparable to the one observed in the PCM condition: lactate consumption was triggered from the very beginning of the culture, therefore again only Phase 2 (P2) was observed. This fact indicates that the metabolic pattern of concomitant consumption of glucose and lactate had no negative effect on cell growth, confirming that the decrement on cell density in PCM was related to nutrient depletion rather than to the altered metabolic behaviour.

Besides the significant differences observed in the metabolic behaviour, it is worth to mention that glucose and lactate uptake rate were similar during P2 in all conditions tested (around 40 and 11 nmol/( $10^6$  cell·h) respectively).

**Table 6.2.** Summary of the different initial media conditions and values of main cell growth and metabolic culture parameters obtained from the profiles shown in Figure 6.4. P1 and P2 are defined on basis of the switch from lactate consumption to lactate production. Metabolite rates of both phases P1 and P2 were calculated taking only into account the measurements within the exponential cell growth phase.

	A	B	C	D
Culture condition	Unmodified media	PCM	NaC <sub>3</sub> H <sub>5</sub> O <sub>3</sub> added	C <sub>3</sub> H <sub>6</sub> O <sub>3</sub> added
[Lac] <sub>0</sub> (mM)	1.3	13.2	12.0	12.0
pH <sub>0</sub>	7.19	6.77	7.18	6.82
$X_{v_{max}}$ ( $\times 10^6$ cell/mL)	21.4 ± 2.7	16.5 ± 1.4	21.4 ± 1.8	20.2 ± 3.1
t $X_{v_{max}}$ (h)	139	94	120	120
$\mu_{max}$ ( $\times 10^{-2}$ /h)	2.17 ± 0.06	2.26 ± 0.01	2.67 ± 0.13	2.54 ± 0.15
t $\mu_{max}$ (h)	70	71	70	70
$q_{glucP1}$ (nmol/( $10^6$ cell·h))	117.09 ± 20.46	n.a.	92.76 ± 10.05	n.a.
$q_{lacP1}$ (nmol/( $10^6$ cell·h))	130.42 ± 13.27	n.a.	110.05 ± 15.23	n.a.
$q_{glucP2}$ (nmol/( $10^6$ cell·h))	30.18 ± 0.24	39.45 ± 1.22	42.48 ± 2.26	41.02 ± 2.18
$q_{lacP2}$ (nmol/( $10^6$ cell·h))	-12.14 ± 0.44	-8.50 ± 2.00	-12.63 ± 1.26	-10.99 ± 0.49
$\Delta$ Lac (mM)	8.51 ± 0.17	No accumulation	8.61 ± 0.41	1.24 ± 0.16

\* n.a.: (not applicable): lactate production (i.e. P1) was not observed. Hence, metabolite rates could not be calculated.

Comparing the lactate evolution of all the conditions, it can be concluded that pH plays a more important role on metabolic shift rather than the presence of lactate itself. When pH value was dropped around 6.8 co-consumption of glucose and lactate was noticed from the very beginning of the experiment, while for higher pH experiments (sodium lactate; pH<sub>0</sub>=7.18) the metabolic shift was delayed until 24-36h of cell culture. This delay might correspond to the time needed to decrease the pH until values close to 6.8 by means of lactic acid secretion as a result of the glucose metabolism during P1.

#### 6.4. INFLUENCE OF pH ON TIME TO TRIGGERING THE METABOLIC SHIFT

In order to confirm previous observations of how pH influenced the triggering of lactate shift (i.e. the lowest the pH, the prompter the shift would occur), cell cultures at different initial pH were performed. All the cultures were performed in presence of sodium lactate in media at a concentration of 12mM. It became interesting to follow pH evolution in order to correlate it with metabolism of lactate. In order to do so, cell cultures were performed in the SFR-RAMOS (Kühner AG) cell culture system (Materials and Methods, section 8.4.1.2.). This system enables to follow online important parameters such as pH and OTR of cell cultures performed in shake flask. Three initial values for pH were selected: 7.4, 7.0 and 6.6 and the results were evaluated in terms of influence of initial pH on triggering the lactate shift and on growth rate.

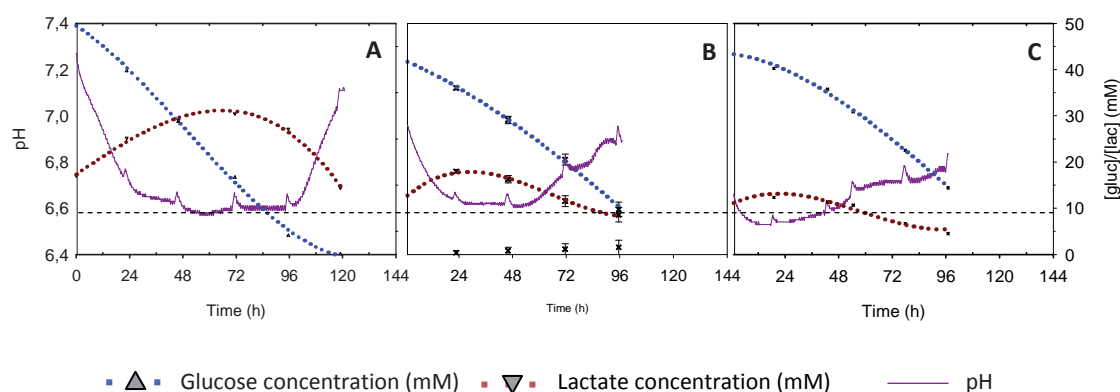


**Figure 8.5.** Evolution of glucose concentration, lactate concentration and pH of HEK293 cell cultures at different initial pH ( $pH_0$ ): (A)  $pH_0=7.4$ ; (B)  $pH_0=7$ ; (C)  $pH_0=6.7$

**Table 6.3.** Values of the main important parameters for cell growth and metabolite evolution of cell cultures depicted in Figure 6.5.

Id	$pH_0$	$\mu_{max}$ ( $\times 10^{-2} h^{-1}$ )	$q_{gluc} P1$ ( $(nmol/(10^6 cell \cdot h))$ )	$q_{lac} P1$ ( $(nmol/(10^6 cell \cdot h))$ )	$q_{gluc} P2$ ( $(nmol/(10^6 cell \cdot h))$ )	$q_{lac} P2$ ( $(nmol/10^6 cell \cdot h)$ )	$\Delta lac$ (mM)
A	7.4	$1.94 \pm 0.17$	$99 \pm 20.3$	$54.74 \pm 17.6$	$37.13 \pm 2.7$	$-37.04 \pm 2.0$	$13.37 \pm 1.3$
B	7	$2.21 \pm 0.35$	$103.80 \pm 8.6$	$106.5 \pm 27.96$	$45.51 \pm 2.9$	$-20.42 \pm 2.8$	$6.80 \pm 2.4$
C	6.6	$1.97 \pm 0.07$	*n.a.	*n.a.	$37.92 \pm 2.27$	$-10.02 \pm 0.95$	$0.53 \pm 0.2$

\*n.a.: (not applicable): lactate production (i.e. P1) was not observed. Hence, metabolite rates could not be calculated.

The first remarkable observation was that for all cell cultures, pH tended to drop until a value around 6.6 (Figure 6.5). After this soft acidification of media, the change from lactate production to lactate consumption occurred and consequently, pH of media increased. Therefore, it seemed that

there is a critical pH at which the metabolic shift is triggered. The higher the value of initial pH, the longer time that was required to achieve this critical point and to detect the lactate shift. The acidification of media would be related to the secreted lactate, as it indicates the values for the accumulated lactate ( $\Delta\text{lac}$ , Table 4.3): at initial pH of 6.6, almost no accumulation of lactate was detected, whereas this value increased with the increment of initial pH. It was also interesting that after the metabolic shift (Phase 2 or P2), a significant drop on glucose consumption rate was detected, and that the value was similar for all the conditions tested. On the contrary, lactate consumption rate during P2 was different depending on the initial pH. As the initial pH was higher, lactate consumption rate during P2 was also higher. This observation led us to hypothesize that aside from pH, there was also some relation between the concentration of lactate in media and the consumption of this metabolite. Specifically, we thought that cells could somehow detect the extracellular concentration of protons (i.e. the pH) and when this concentration could be detrimental for cell growth, cells would start to transport protons to the intracellular space as a strategy of pH detoxification. This import of protons would be made as a co-transport of lactate and protons. As initial pH increased, it also did the concentration of extracellular lactate reached in cell culture. Hence, there would be more available lactate to perform this co-transport and this might be related to the higher lactate consumption rates. Finally, it is worth to mention that the initial pH did not affect the specific growth rate of the cells. Although some detrimental effect could be expected due to the acidification of media, it was not noticed and cells grew equally regardless the initial pH.

#### **6.5. CO-METABOLISM OF GLUCOSE AND LACTATE IN HEK293 AS A pH DETOXIFICATION MECHANISM.**

In order to evaluate the effect of lowering pH on the lactate metabolism and cell growth, cell cultures at pH=6.62 in presence or absence of sodium lactate along with cell cultures in unmodified media were performed in parallel. Also, it became interesting to study the influence of the modification of pH on protein production. Therefore, cell cultures presented in this sections were carried out with a HEK293 cell line expressing GFP (HEK293-*eGFP*). This cell line is described in Material and Methods (section 8.1.1.1.2) and its growth and physiological characteristics were comparable to HEK293 cell line (data not shown). The results obtained after the modification of initial pH and lactate concentration, were completely different in terms of cell growth profiles and metabolic behaviour (Figure 6.6).

When sodium lactate was not added to media at low pH (Figure 6.6B), cell growth inhibition was detected resulting in a decrement of  $\mu_{\text{max}}$  in comparison to cell cultures in which sodium lactate was

added (Figure 6.6C) and also to control cultures (Figure 6.6A). Therefore, a significant decrease on cell expansion was observed reaching values about  $9 \cdot 10^6$  cell/mL, or in other words, a 50% drop on  $X_{v,max}$ . Moreover, aberrant cell morphology and high cell aggregation was noticed from the very beginning of cell culture, as well as a significant drop on viability beyond 120h. Interestingly, with the simple addition of sodium lactate the expected cell growth inhibition due to low pH was completely avoided. Exponential growth was extended for 114h, which was 24h longer than control cell cultures reaching similar final cell densities although the slight differences in  $\mu_{max}$  (Table 6.4).

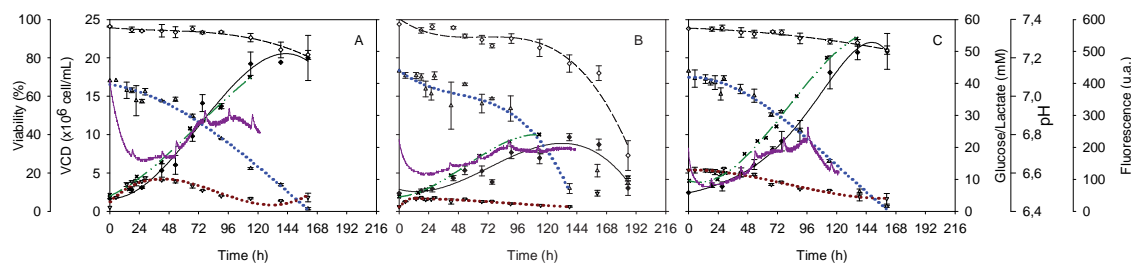


**Figure 6.6.** Cell growth, viability, glucose concentration and lactate concentration profiles of HEK293 suspension cell cultures in three different scenarios: (A)  $[lac]_0 = 0$  mM  $pH_0 = 7.02$  (B)  $[lac]_0 = 0$  mM  $pH_0 = 6.62$  (C)  $[lac]_0 = 12$  mM  $pH_0 = 6.62$ . Cultures were performed by triplicate in shake flask .

Focusing on the impact of low pH on GFP production, no negative effect was detected at low pH culture conditions. Intracellular fluorescence increased according to cell growth as expected for a constitutive expression of a recombinant protein, resulting in comparable protein production rates ( $q_{fluo}$ ) for all conditions.

Concerning the metabolic behaviour, not only lactate secretion was completely suppressed when lactate was added to cell media at pH 6.62, but also lactic uptake started from the very beginning, supporting the results presented in the previous section. As a result of the extracellular lactic acid uptake, media pH might increase and consequently, the culture conditions changed from inhibitory to a suitable environment for cell growth. In contrast, when lactate was not added at low pH media an initial secretion of lactate was detected during the lag phase ( $\Delta Lac \approx 4$  mM). Then, co-metabolism of lactate and glucose was triggered but at lower rates than for cultures where lactate was present from  $t=0$ h. The faster and prompt consumption of extracellular lactate when lactate was present from the very beginning could be related to a more effective  $H^+$  uptake to the intracellular space and consequently, a faster pH increment of media changing the conditions from inhibitory to a suitable environment for cell growth. The ultimate consequence of the faster lactate consumption would be a better environment for cell growth, which is reflected on the longer exponential phase and on the higher cell density reached (more than doubled when lactate was present in media). These results are also in good agreement with the results presented in prior section, in which a direct relation

between a higher lactate consumption rate and extracellular lactate concentration was noticed. Regarding to unmodified media, glucose and lactate consumption rates were clearly in the same range of those measured in cell cultures at low pH and initial lactate concentration about 12mM.

**Table 6.4.** Summary of the different initial media conditions and values of main cell growth and metabolic culture parameters obtained from the profiles shown in Figure 7.6. P1 and P2 are defined on basis of the switch from lactate consumption to lactate production. Cultures were performed in triplicates and the standard deviation is indicated.

	A	B	C
Culture condition	Control	Low pH	Low pH + NaC <sub>3</sub> H <sub>5</sub> O <sub>3</sub>
[Lac] <sub>0</sub> (mM)	0	0	12
pH <sub>0</sub>	7	6.6	6.6
Xv <sub>max</sub> (x10 <sup>6</sup> cell/mL)	20.00 ± 2.94	9.68 ± 0.46	20.85 ± 2.34
μ <sub>max</sub> (x10 <sup>-2</sup> /h)	2.20 ± 0.38	1.40 ± 0.16	1.77 ± 0.09
Tμ <sub>max</sub> (h)	90	67	114
q <sub>glucP1</sub> (nmol/(10 <sup>6</sup> cell·h))	123.56 ± 18.30	99.66 ± 20.36	n.d
q <sub>lacP1</sub> (nmol/(10 <sup>6</sup> cell·h))	128.30 ± 10.01	33.07 ± 4.25	n.d
q <sub>glucP2</sub> (nmol/(10 <sup>6</sup> cell·h))	32.76 ± 4.47	44.52 ± 2.86	32.29 ± 1.01
q <sub>lacP2</sub> (nmol/(10 <sup>6</sup> cell·h))	-12.60 ± 0.78	-3.78 ± 0.08	-11.33 ± 0.73
q <sub>fluo</sub> (FAU/(10 <sup>6</sup> cell·h))	487.97 ± 26.42	483.29 ± 10.05	475.61 ± 1.31

It must be pointed out that lactate consumption has been previously reported in literature. However, the metabolic behaviour presented in so far, differs from other published studies, which can be grouped in 4 different scenarios:

1) Reduction of lactate production rate or complete lacking of lactate secretion. A significant number of investigations have been directed to reduce the accumulation of lactate in extracellular media by means of limiting the carbon source in fed-batch strategies<sup>11-14</sup>. On these studies, the reduction or even the lack of lactate secretion to media has been effectively accomplished, but no net uptake lactate from cell media was observed.

2) Lactate consumption after complete glucose depletion was reported recently in an unmodified HEK293 cell line<sup>15</sup>. This metabolic profile coincides with the results of the batch with pH control at 6.1 presented before. In other previous studies with CHO cells, lactate was clearly uptaken from media when glucose was also depleted<sup>16</sup>. This behaviour allowed to develop a successful fed-batch control loop in which glucose concentration was maintained at values close to zero<sup>17</sup>. In the latter case, cell growth continued after the metabolic shift from lactate secretion to consumption, but

glucose was always in limiting conditions. The outcomes concerning P2 of our cell cultures when pH was not controlled completely differ from this behaviour since lactic and glucose co-consumption is clearly observed when glucose was far from its limiting concentration.

3) Lactate consumption in presence of glucose after glutamine depletion from medium has also been described in CHO cells<sup>18</sup>. In order to assess if this was the factor behind the lactate metabolic shift in *HEK293* cultures here reported, the concentration of amino acids was analyzed for the batch cultures with and without pH control at initial growth stages and also at the time of the metabolic shift (Figure 6.7). When co-metabolism of lactic acid and glucose was triggered, no limitation in any amino acid was detected. Glutamic acid and L-alanyl-L-glutamine dipeptide (glutaMAX®) concentration were around 2 mM and glutamine around 0.75 mM at the moment of the metabolic shift. Interestingly, when pH was set at 7.1 amino acids consumption were higher compared to the ones measured in cultures without pH control, which might indicate a more efficient metabolism in the latter conditions when concomitant glucose and lactate consumption was observed.

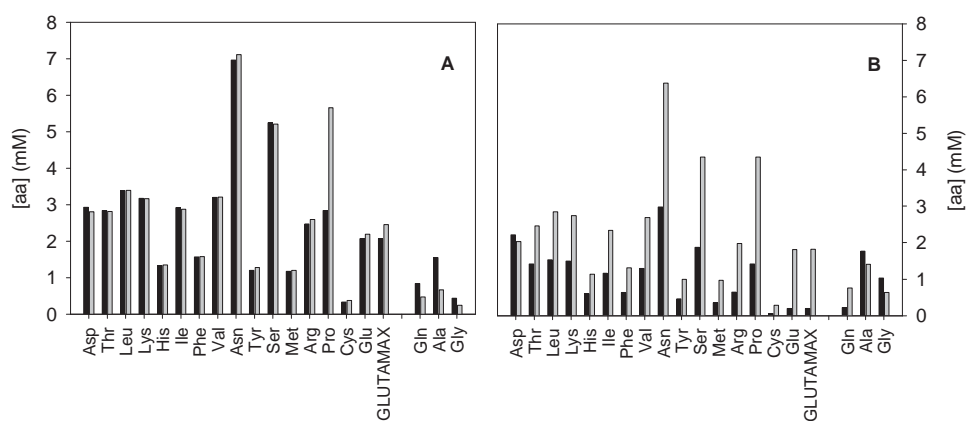


**Figure 6.7.** Concentration of principal amino acids in cell media at early stages of cell culture (Panel A) and at time of lactate metabolism switch (Panel B). Black bars correspond to batch cell culture of Figure 6.1 and grey bars refer to batch cell culture of Figure 6.3.

4) Concomitant glucose and lactate uptake at late culture stages or at the stationary phase. The simultaneous consumption of glucose and lactate has also been reported but mainly in CHO cell cultures<sup>16,19,20</sup> or in NS0 cell cultures<sup>21-23</sup>. Nevertheless, this shift occurred at late stages of cell culture, when cell growth was halted or only residual growth was observed. Recently, extracellular lactate uptake in the presence of glucose by means of media acidification has been reported in NS0 cell cultures<sup>24</sup>. However, the lactate consumption was quite low and was accompanied with a dramatic reduction on glucose uptake and cell growth, resulting in a drop of about 30% of the cell growth rate after the pH shift in comparison to the control cell cultures. In the results presented above, glucose and lactate were significantly consumed from media without any detrimental effect on cell growth when cells were cultured at the same pH as used in the mentioned paper.

In a nutshell, the flexibility of lactate metabolism of animal cells to adapt to different environmental conditions has been well reported in the literature. Nonetheless, from the different culture conditions, none of them fits with the results reported in this work, where co-metabolism of lactate and glucose was observed during exponential growth phase. Furthermore, the co-consumption of both metabolites has been triggered at will from the beginning of the cultures when initial pH (pH<sub>0</sub>) was set therein the range about 6.6–6.8 and the addition of exogenous lactate was performed. Interestingly, no negative effect on cell growth was detected under this culture conditions. Contrarily, at low pH values, cell growth was drastically inhibited when lactate was not added in the media.

The hypothesis arisen after the analysis of the results and the reviewed literature consists in that HEK293 cells metabolize extracellular lactate as a strategy for pH (H<sup>+</sup>) detoxification. Our hypothesis is in concordance with other studies reported in the literature, where authors show how the lactate is actively co-transported with H<sup>+</sup> into the cytosolic space and this is governed by MCT transporters<sup>25,26</sup>, which have also been found in HEK293 cells<sup>27</sup>.

Interestingly, glucose and lactate co-metabolization switch resulted in a better-balanced cell metabolism (reduction of glucose and amino acids uptake rate without affecting cell growth).

## 6.6. STUDY OF THE OPTIMAL INITIAL pH AND LACTATE CONCENTRATION FOR TRIGGERING LACTATE AND GLUCOSE CONCOMITANT CONSUMPTION FROM EARLY STAGES OF CELL CULTURE.

### 6.6.1. Experimental design

The data presented in prior section indicated that the co-consumption of glucose and lactate results in a more efficient metabolism based on the observation of a lower glucose consumption without affecting cell growth or protein production. In this direction, it was desired to further study the combined effect of initial lactate concentration and initial pH value in order to trigger the co-metabolism at will and obtain specific outcomes concerning cell growth, glucose consumption rate and lactate production rate. For this study, design of experiments was applied. Design of experiments (DoE) can be defined as “an approach that involves systematic and efficient examination of multiple variables simultaneously to create an empirical model that correlates the process responses to the various factors” (process variables and material attributes)<sup>28</sup>. In its basic outline, the DoE methodology investigates defined input factors to a converting biosystem from which mostly common and well-defined output factors or responses are generated (e.g. product yield and productivity). The strength of DoE is that, differently from mass balancing, it also reveals how interactions between the input factors influence the output responses<sup>29</sup>. The choice of an experimental design depends on the objectives of the experiments and the number of factors to be investigated. In Table 6.5, a summary table for choosing an experimental design is presented.

**Table 6.5.** Summary table for the selection of the most appropriate experimental design depending on the objective and the number of factors of the study. Adapted from<sup>30</sup>.

		Objective		
		Comparative	Screening	Response Surface
Number of factors	1	1-factor completely randomized design	--	--
	2-4	Randomized block design	Full or fractional factorial	Central composite or Box-Behnken
	5 or more	Randomized block design	Fractional factorial or Plackett-Burman	Screen first to reduce number of factors



In our case, a Box-Wilson (or Central composite) design of experiment was selected as we wanted to study the interaction between 2 factors ( $\text{pH}_0$  and  $[\text{lactate}]_0$ ) and we wanted to improve the settings of these to factors in order to fulfill the following objectives (i.e. outputs):

1. The minimization of accumulated lactate in media ( $\Delta\text{lac}$ ).
2. The maximization of specific growth rate ( $\mu_{\text{max}}$ ).
3. The minimization of lactate production rate ( $q_{\text{lac}}$ ) and glucose consumption rate ( $q_{\text{gluc}}$ ).

A central composite design (CCD) supports the building of a polynomial equation as follows:

$$y = \beta_0 + \sum_{j=1}^n \beta_j \cdot x_j + \sum_{j=1}^n \sum_{k=j+1}^n \beta_{jk} \cdot x_j \cdot x_k + \sum_{j=1}^n \beta_{jj} \cdot x_j^2 \quad (\text{Eq. 6.1})$$

Where:

$\sum_{j=1}^n \beta_j \cdot x_j$  is the individual effect of each studied factor

$\sum_{j=1}^n \sum_{k=j+1}^n \beta_{jk} \cdot x_j \cdot x_k$  indicate the interaction among the variables

$\sum_{j=1}^n \beta_{jj} \cdot x_j^2$  takes into account a possible non-linear/quadratic effect of some factors.

The studied factors are explored at five levels, which are defined by the “central point”, the “factorial points” and the “star points” (Figure 6.8). The factorial point is  $\pm 1$  from central point for each factor. Star point is  $\pm\alpha$  from central point for each factor and  $\alpha$  is calculated as indicated in Eq. 4.2.

$$\alpha = [2^k]^{1/4} \quad \text{Eq. 6.2.}$$

Where  $k$  is the number of studied factors.

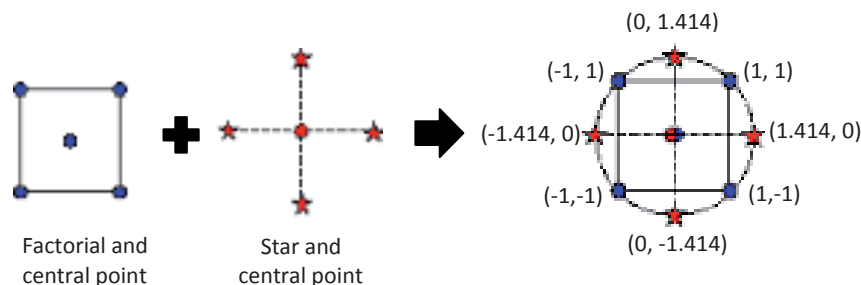


**Figure 6.8.** Design scheme of central composite design (CCD) with two variables

Then, it is possible to design an experimental matrix where the conditions for studying the selected experimental space are defined. The experimental matrix applied to this study is shown in Table 6.6.

**Table 6.6.** Experimental matrix for the determination of initial lactate concentration and initial pH depending on the evaluated response.

Pattern	Code levels		Real values	
	Variable 1	Variable 2	[lactate] <sub>0</sub>	pH <sub>0</sub>
--	-1	-1	3.51	6.72
-+	-1	-1	3.51	7.28
+-	+1	-1	20.48	6.72
++	+1	+1	20.48	7.28
00	0	0	12	7
00	0	0	12	7
00	0	0	12	7
00	0	0	12	7
-0	-1.414	0	0	7
+0	+1.414	0	24	7
0-	0	-1.414	12	6.6
0+	0	+1.414	12	7.4

### 6.6.2. Results analysis and discussion

The first point to mention from the results obtained, is that regardless [lactate]<sub>0</sub> and pH<sub>0</sub>, all cultures tend to reach the same pH (around 6.6) (Figure 6.9). pH never got lower than this value for any culture and the time to reach this pH was never longer than 72h of cell culture. Once this pH was reached, lactate stopped to be secreted, regardless the remaining glucose concentration in the media or cell density. Consequently, the lower the initial pH was, the prompter pH=6.6 was reached and lactate shift occurred. On those cultures where pH<sub>0</sub> was set at 6.6, lactate consumption was noticed from the very beginning of cell culture.

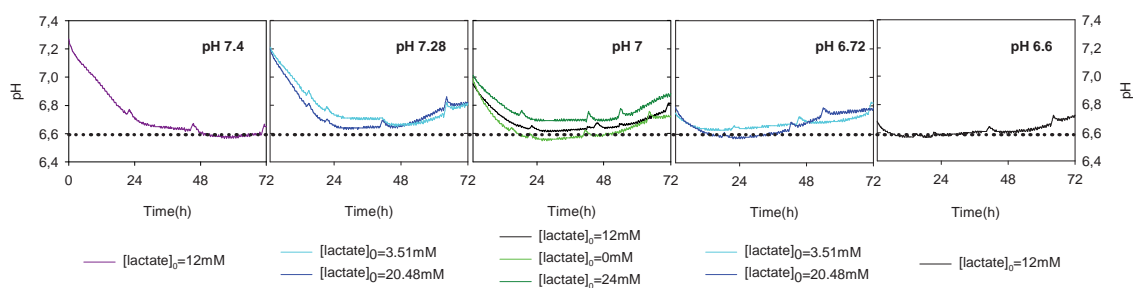


**Figure 6.9.** pH evolution during the first 72h of cell culture. The initial conditions for pH and [lactate] are indicated.

When pH<sub>0</sub> was set at 6.6, lactate secretion and consequently, accumulation in media was not observed (Figure 6.10a). Hence, although this value is one of the limits of the selected experimental

data, further minimization of the output variable (accumulated lactate) cannot be achieved. Besides, when incrementing the value of  $\text{pH}_0$ , the accumulation of lactate to media increases until a maximum of 17-18mM. The increment on the accumulated lactate due to the initial pH of the media is a little softer as the initial lactate in media increases. This might be related to a slight toxic effect on cells due to the total extracellular lactate concentration ( $[\text{lactate}]_{\text{total}} = [\text{lactate}]_0 + \Delta\text{lactate}$ ). This is in good correlation with the slight decrement on  $\mu_{\text{max}}$  at high  $\text{pH}_0$  and  $[\text{lactate}]_0$  predicted by the model (Figure 6.10b). Regarding this parameter, different combination of the factors reached the maximum value encountered for this cell line. This result must be interpreted as that different combinations of  $\text{pH}_0$  and  $[\text{lactate}]_0$  have no detrimental effect on cell growth. Nevertheless, when  $\text{pH}_0$  is low together with low  $[\text{lactate}]_0$ , the predicted specific growth rate is lower than the generally reported for this cell line<sup>10</sup>, hence, those conditions have a negative effect on cell growth. This is in good correlation with the results previously presented, where lowering pH to 6.6 without the addition of extracellular lactate resulted in an initial impairment of cell growth and a 50% drop on  $X_{v_{\text{max}}}$  (Section 6.5).

Concerning glucose specific consumption rate (Figure 6.10c), the minimum is achieved at the lowest  $\text{pH}_0$  level tested ( $\text{pH}_0=6.6$ ). The results show that glucose consumption rate is on function of pH and it does not generally depend on  $[\text{lactate}]_0$  within the studied range. Nevertheless, it is interesting to mention that when lactate is totally lacking from media ( $[\text{lactate}]_0=0$ ) a slight increment on glucose uptake rate is predicted. This is in good concordance with the hypothesis that when cells uptake lactate from media they use the metabolite as carbon source, hence, reducing glucose consumption. If there is no availability of this alternative carbon source, cells will consume glucose faster than in presence of lactate. Finally, negative lactate production rate (i.e. lactate consumption) is triggered from the very beginning of the cell culture at  $\text{pH}_0=6.6$  and  $[\text{lactate}]_0$  at concentrations higher than 4mM. On Figure 6.10d, a plane at  $q_{\text{lac}}=0 \text{ nmol}/(\times 10^6 \text{ cell} \cdot \text{h})$  has been overlapped to the surface response curve in order to easily notice at which conditions lactate starts to be consumed. Interestingly, at  $\text{pH}_0=6.6$  lactate consumption rate increases at higher initial lactate concentration in the media. This is also in good concordance with results previous presented (section 6.4) where it was hypothesized that the highest availability of extracellular lactate when pH was low (i.e. more protons in the extracellular media), the greatest the consumption of this metabolite will be. This resulted in a faster “detoxification” of the media and, eventually, in a consumption of lactate as carbon source, enabling cell to grow without consuming other metabolites such as glucose.

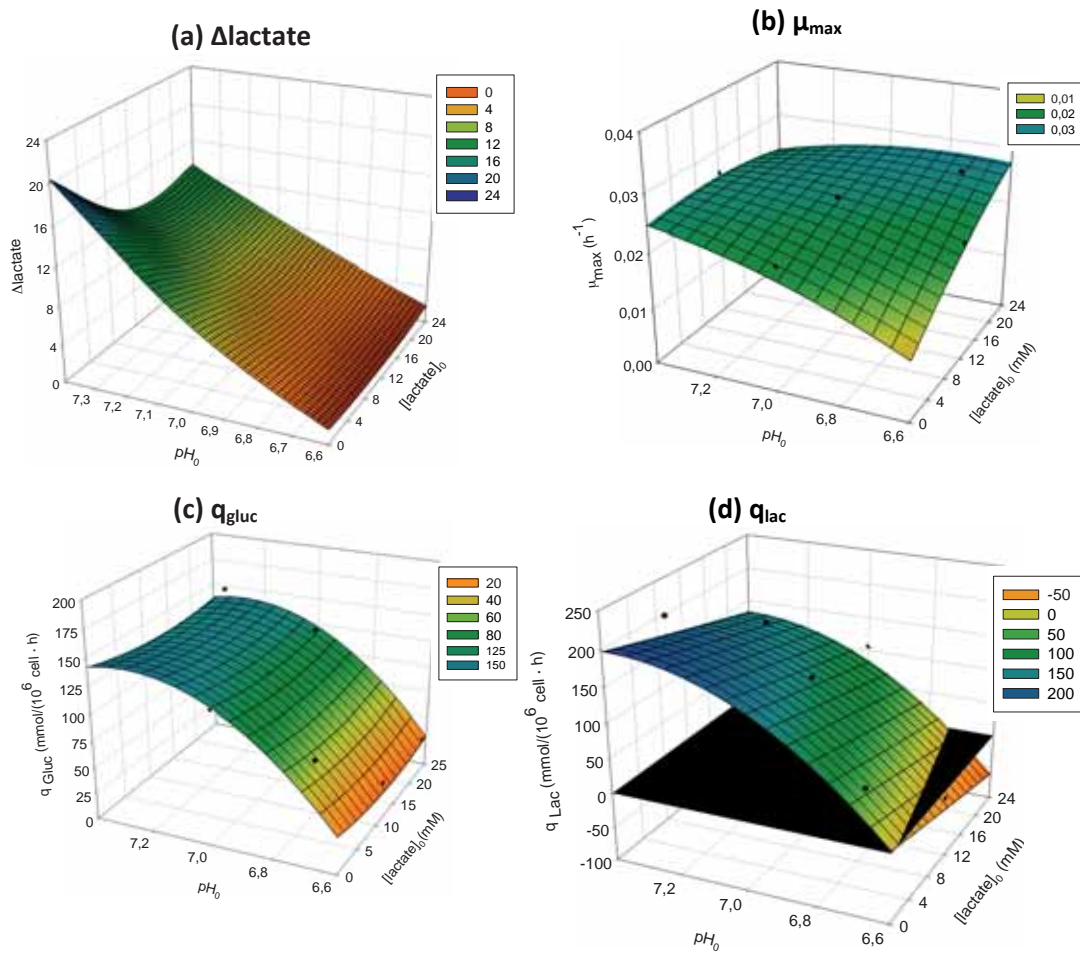


**Figure 6.10.** Surface respond curves obtained after the fitting of experimental data to central composite design equation for each studied parameter.

From the experimental space studied, the selected conditions would be  $pH_0=6.6$  and  $[lactate]_0$  in between 4 and 12mM. At these conditions, lactate consumption (and hence, avoidance of its accumulation in media) is achieved from the very beginning of cell culture and glucose uptake rate is at the minimum value encountered. Also, the maintenance of the expected  $\mu_{max}$  for this cell line is accomplished at the selected conditions. Further studies towards the optimization of these conditions might be addressed in future research.

### 6.7. FLUX BALANCE ANALYSIS APPLIED TO HEK293 CELLS.

The metabolic changes observed under different conditions were studied so far only from a physiological extracellular perspective. Changing this perspective towards a metabolic intracellular one would provide highly valuable information in order to better understand the differential physiologic behaviours. In this line of thinking, it was decided to perform flux balance analysis (FBA)

to HEK293 cells. As stated in the introduction of the present chapter, FBA is a mathematical method for simulating metabolism in genome-scale reconstructions of metabolic networks. With the increasing number of available genome-scale metabolic network reconstruction, FBA is a powerful tool to further comprehend the different phenotypes of cultured cells to optimize current bioprocesses or develop new ones. In our particular case, FBA was used for the study of the differential behaviours encountered in batch fermentations with and without pH control presented in section 2 of this chapter. Three different phases were defined and separately analysed by FBA (Figure 6.11). The methodology applied for the calculation of metabolic fluxes here presented is detailed in Materials and Methods (section 8.11) and in Appendix 10.5. Briefly, the HEK293 metabolic model was adapted from a previous HEK293 model<sup>31</sup> derived from the *Homo sapiens* community driven genome-scale reconstruction RECON-2<sup>32</sup>. Calculations for each phase were done using exometabolite experimental data from each culture phase as constrains. Metabolic flux distribution was obtained by pFBA (Parsimonious Flux Balance or Parsimonious Enzyme Usage<sup>33</sup> using maximization of consumed ATP objective function. Flux calculations were performed with OptFlux software<sup>34</sup>.

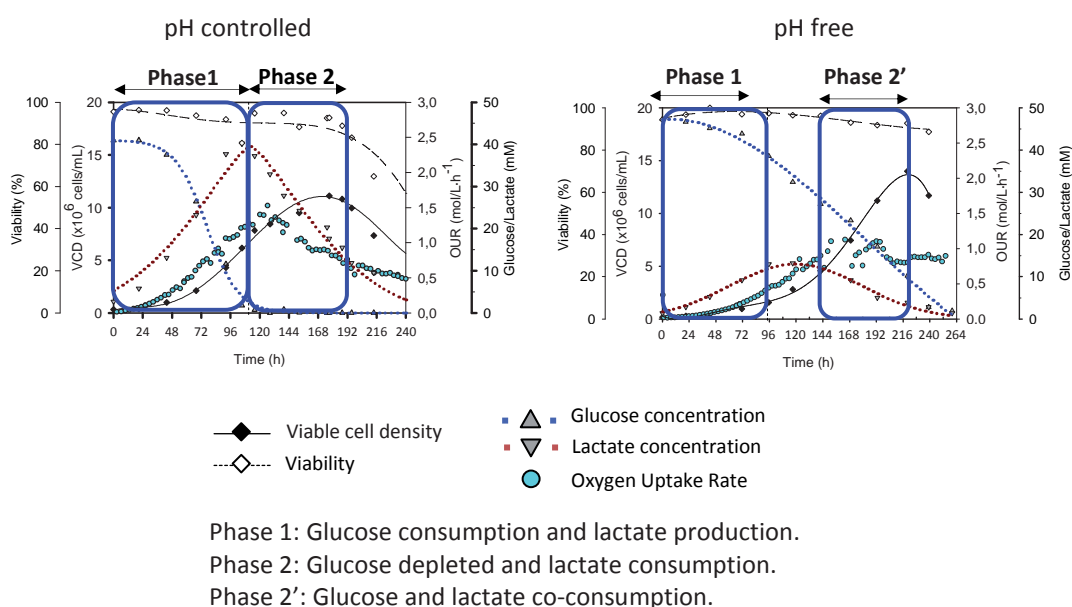


**Figure 6.11.** Batch cell culture under pH controlled condition and pH free condition. The different phases analyzed by FBA are indicated.

### 6.7.1. PFBA APPLIED TO pH CONTROLLED CELL CULTURES.

During Phase 1 of pH controlled condition, glucose was rapidly consumed and the flux through glycolysis was around 1350 nmol/(mgDW·h) (Figure 6.12). Nevertheless, only 20% of this glucose finally entered to the mitochondria via pyruvate and was completely metabolized in the tricarboxylic acid cycle (TCA), hence, obtaining the maximal energy (NADH+H<sup>+</sup>) from the carbon source.

In animal cell lines, pyruvate obtained from glucose is predominantly converted into acetyl CoA; however, in continuous mammalian cell lines, pyruvate is primarily converted into lactate (particularly in the case here studied, 80% of glucose is converted to lactate). It has already been reported that in HEK293, hybridoma and CHO cells, this conversion takes place at high rates regardless of the level of oxygen in the culture<sup>35</sup> and for the HEK293 cells here studied, O<sub>2</sub> is not limiting at any phase of the cell culture (Figure 6.11). The conversion of pyruvate to lactate seems to be the only means in continuous mammalian cells of complete cytoplasmic NADH regeneration, which has been generated in the degradation of a glucose molecule to two pyruvate molecules (Glyceraldehyd 3-phosphate + NAD<sup>+</sup> + H<sup>+</sup> → 1,3-biphosphoglycerate + NADH). Since the mitochondrion is not permeable to NADH + H<sup>+</sup>, an indirect transport system, the malate-aspartate shuttle, is needed. As it is shown in Figure 6.12, the flux of redox equivalents inside the mitochondria via malate-aspartate shuttle is limited to 197, meaning that the hat the remaining 1104 should be regenerated in the cytoplasm via lactate deshidrogenase. Hence, it can be said that the cell metabolism in Phase 1 is highly unefficient as the majority of the carbon source is not used for the generation of energy and biomass. Also, this metabolism should be understood as an “unbalanced” metabolism which causes lactate formation and secretion.

The calculated TCA fluxes were around 230nmol/(mgDW·h). This could be the cause behind the limitation of pyruvate entrance to the mitochondria. Inside this organelle acetyl CoA is obtained from pyruvate (97,8%) or from the degradation of the amino acids (2,2%). The acetyl CoA is combined with oxalacetate to form citrate. The amount of citrate obtained is split between the formation of α-ketoglutarate and the lipids synthesis outside the mitochondrion. Finally, the intracellular flux in the tricarboxylic acid cycle is balanced by the incorporation of α-ketoglutarate produced from glutamate.

When glucose is depleted from media (Phase 2), lactate is used as carbon source: 10% of the influx is directed to gluconeogenesis and the remaining 90% enters the mitochondria (Figure 6.13). But the calculated influx to the cell (68 nmol/(gDW·h)) was much lower tan the influx calculated for glucose in the prior phase. Also, in Phase 2, the fluxes in malate-aspartate shunt are almost neglictible and as it is shown in Figure 6.13, the TCA fluxes in Phase 2 are 4-fold reduced in comparison to Phase 1.

Consequently, cell growth was drastically reduced and specific growth rate dropped more than 2.5-fold (Table embedded in Figure 6.12). At this lower growth rate, cells continued growing for 60 hours and thereafter cells entered to death phase of the culture.

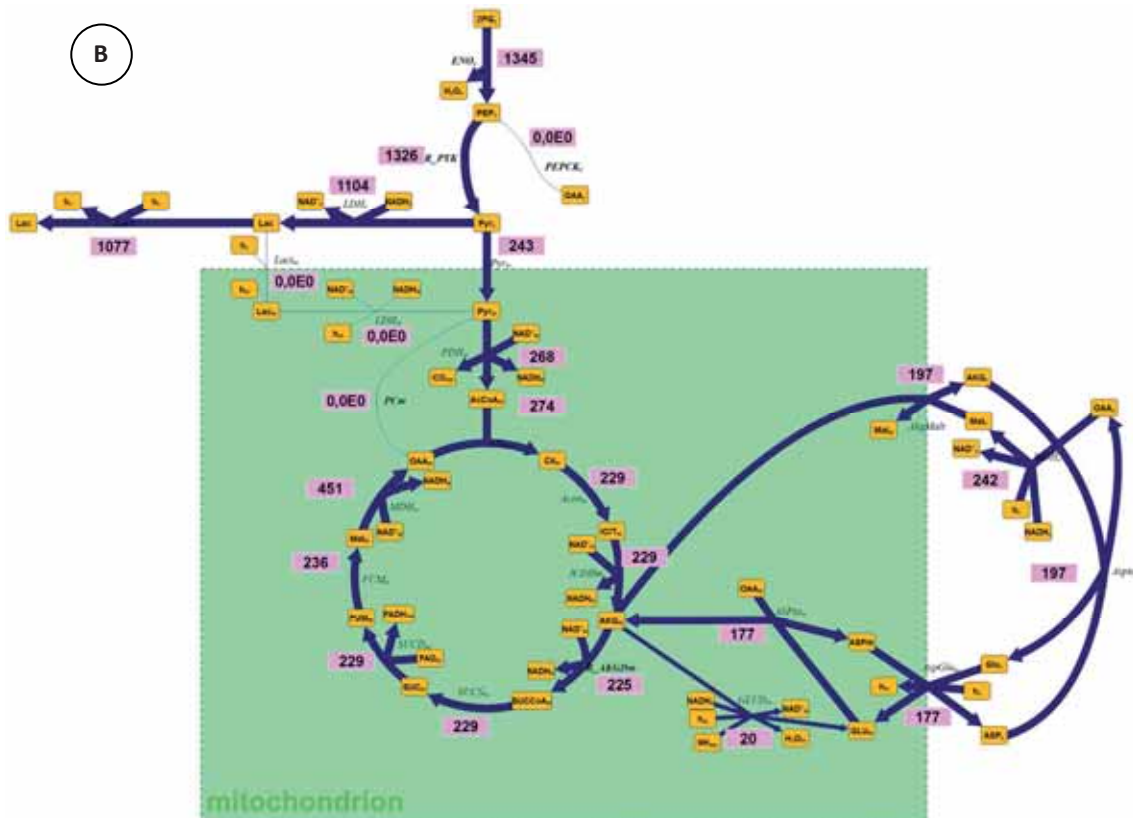
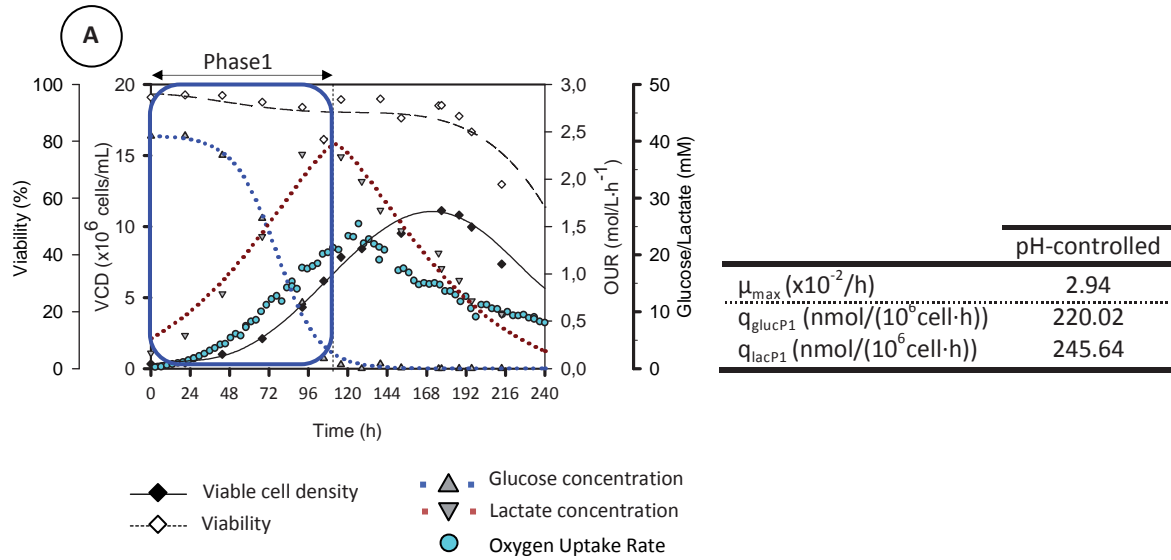


**Figure 6.12.** (A) cell growth, viability, glucose and lactate profiles of culture under pH controlled conditions. The table embedded in the Figure summarizes the main kinetic parameters. (B) Main fluxes around TCA during Phase 1 of cell culture



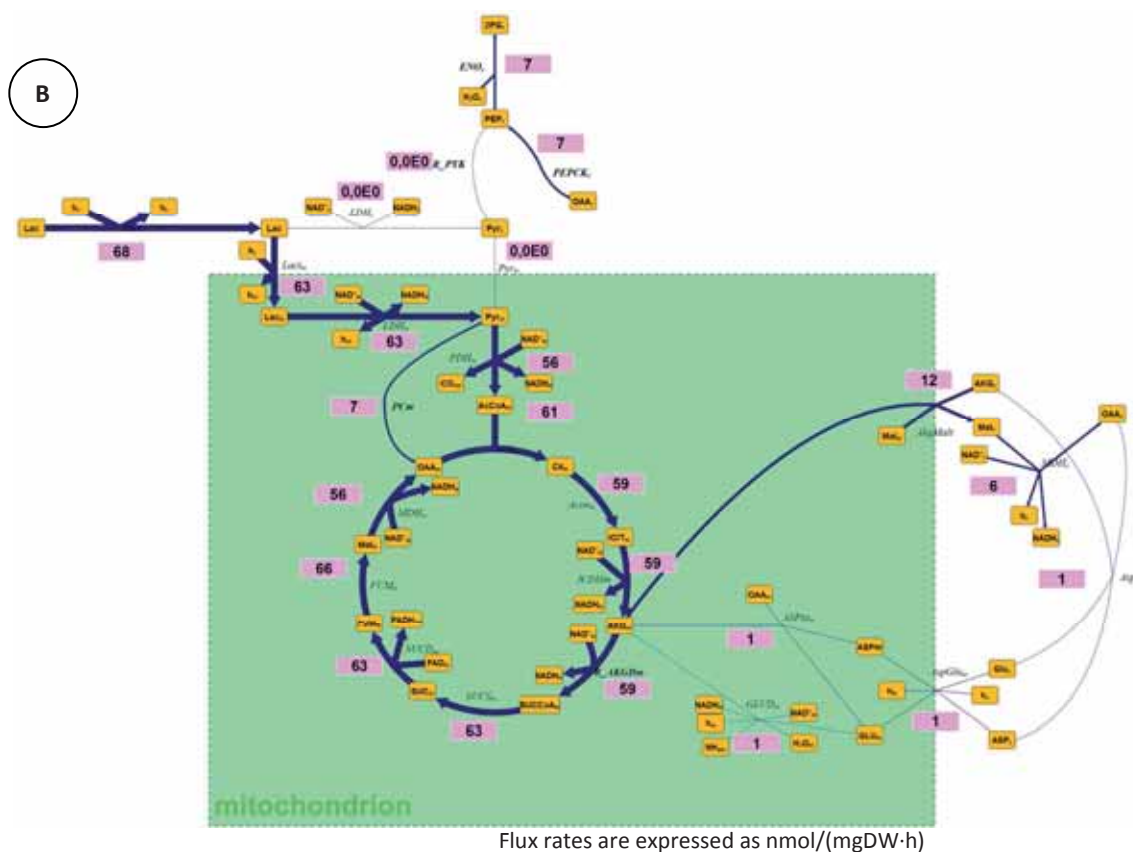
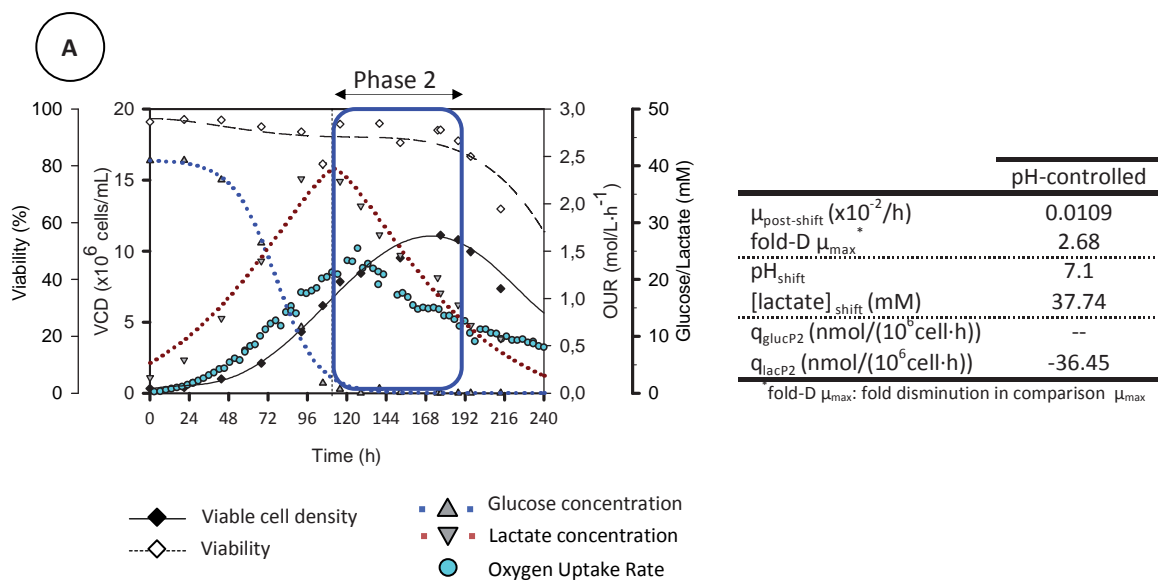


**Figure 6.13.** (A) cell growth, viability, glucose and lactate profiles of culture under pH controlled conditions. The table embedded in the Figure summarizes the main kinetic parameters. (B) Main fluxes around TCA during Phase 2 of cell culture.



### 6.7.2. PFBA APPLIED TO pH NON-CONTROLLED CELL CULTURES.

Similarly to what was observed for pH controlled cell cultures, during P1 the fluxes through glycolysis were higher than the fluxes entering the mitochondria, resulting in only approximately 20% of the initial glucose reaching TCA cycle (Figure 6.14). It must be pointed out that although the percentages of totally-oxidized glucose are similar for pH controlled and pH non-controlled cultures, the glycolytic fluxes were almost 2-fold reduced in the latter situation.

On the contrary, Phase 2 of the pH non-controlled cell cultures (onwards Phase 2') was completely different than Phase 2 previously described. In Phase 2', TCA fluxes could be maintained as in Phase 1 or in other words, at the maximal rate encountered ( $\approx 230 \text{ nmol}/(\text{mgDW}\cdot\text{h})$ ). Hence, the energy available for cells to grow was similar than to Phase 1 and specific cell growth was only slightly reduced (1.3-fold reduction, Table embedded in Figure 6.15) resulting in the achievement of higher cell densities in comparison to Phase 2. It must be said than differently from Phase 1, the influx to the TCA came from two different sources: 80% of the influx was from glycolysis and 20% came from lactate influx from the extracellular media to the mitochondria. Interestingly, lactate influx was in the same range regardless it was used as sole carbon source (Phase 2) or in combination with glucose (Phase 2'). However, the most interesting fact of the fluxes obtained for Phase 2', was the drastic reduction on glycolysis fluxes. As shown in Figure 6.12, when glucose was the unique carbon influx to the cell (Phase 1), fluxes through glycolysis pathway were around  $1350 \text{ nmol}/(\text{mgDW}\cdot\text{h})$  whereas when glucose and lactate were consumed concomitantly (Phase 2'), the fluxes through this pathway were of  $182 \text{ nmol}/(\text{mgDW}\cdot\text{h})$ , which represents approximately only a 13.5% of the initial rates. Besides, malate-aspartate shunt is working at 80% of the observed in Phase 1 and fluxes in TCA cycle are only 9% reduced. That means that the energy obtained is almost the same even when glucose uptake rate has diminished at 86,5 % of the original rate, and the growth rate in this phase of co-metabolism is similar to the obtained or observed in the phase 1.

The sum of the fluxes coming from glycolysis and from lactate influx results in the maximal flux at which TCA can operate. In other words, entering to Phase 2' results in a change from an unbalanced metabolism during Phase 1 (glycolysis  $\gg\gg$  TCA) to a balanced metabolism (glycolysis $\approx$ TCA) on Phase 2', avoiding lactate generation and secretion, which is the major drawback of the metabolism during Phase 1. This unbalanced/balanced metabolism should be understood under the perspective of that eukaryotic cells are the symbiosis of two organisms, one anaerobic (pre-eukaryotic cell) and the other aerobic (bacteria) (Endosymbiotic Theory<sup>36-39</sup>). The anaerobic organism must be able to uptake and process carbon source at a high rate, as only 2 ATPs (i.e. low energy amount) will be obtained from each glucose molecule. On the contrary, the aerobic bacteria would generate much more energy (34 ATPs) from each initial carbon source. Hence, the metabolism of the aerobic organism

can “work” slower than the anaerobic-organism metabolism, as it is far more efficient. When the aerobic bacteria entered to the anaerobic organism, these two metabolisms must be somehow coupled to each other. The logical solution would be reducing the glycolysis fluxes to the values capable to support by the mitochondria (i.e. the aerobic bacteria). Nevertheless, eukaryotic mammalian cells are naturally forming part of higher organisms, hence the carbon source influx is not controlled by the cell itself but by a “external” control system (i.e. nervous system). Consequently, cells might have not evolved to the reduction of glycolysis pathway as they naturally do not encounter an unbalanced carbon source condition. When cells are extracted from the higher organism and cultured as “individual” cells, they do not have the regulation of the external system, resulting in the unbalanced and unefficient metabolism. The study of the use of lactate as a pH-detoxification strategy, has lead to generate extracellular conditions that resulted in changes through the metabolic pathway around the TCA cycle. These metabolic changes can be the consequence of the upregulation or downregulation of different genes. The metabolic model generated in this work opens the possibility to study target genes in order to generate engineered cell lines that present a balanced metabolism throughout all cell culture, avoiding lactate secretion to media. This optimized metabolism would result in bioprocess optimization and development of new culture strategies towards higher cell densities and recombinant protein titers.

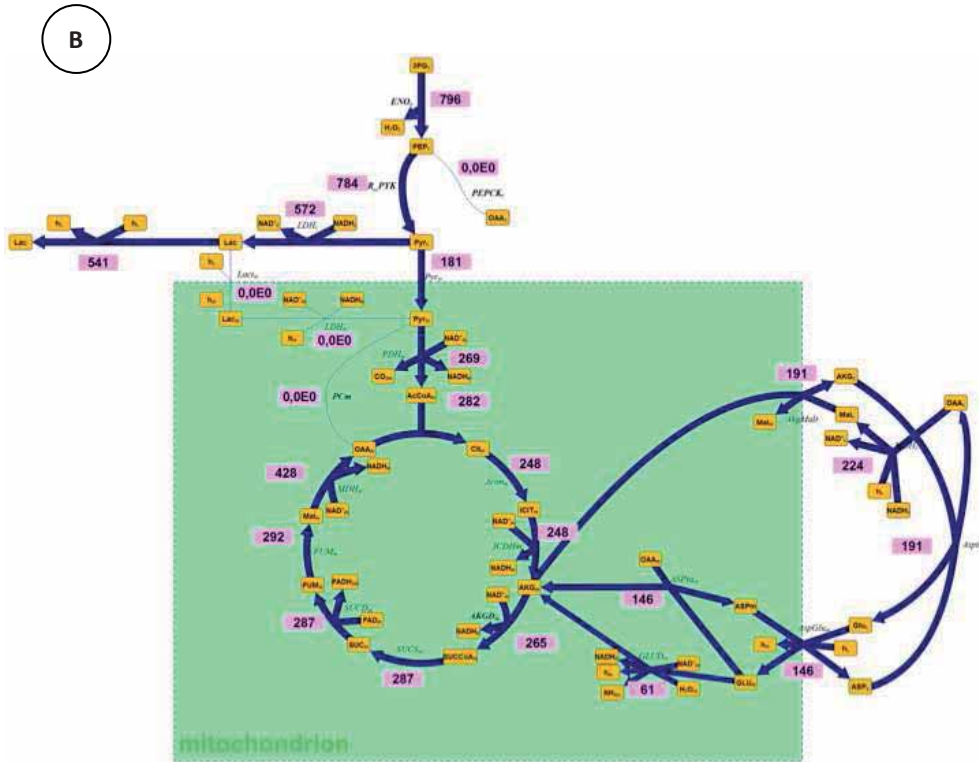
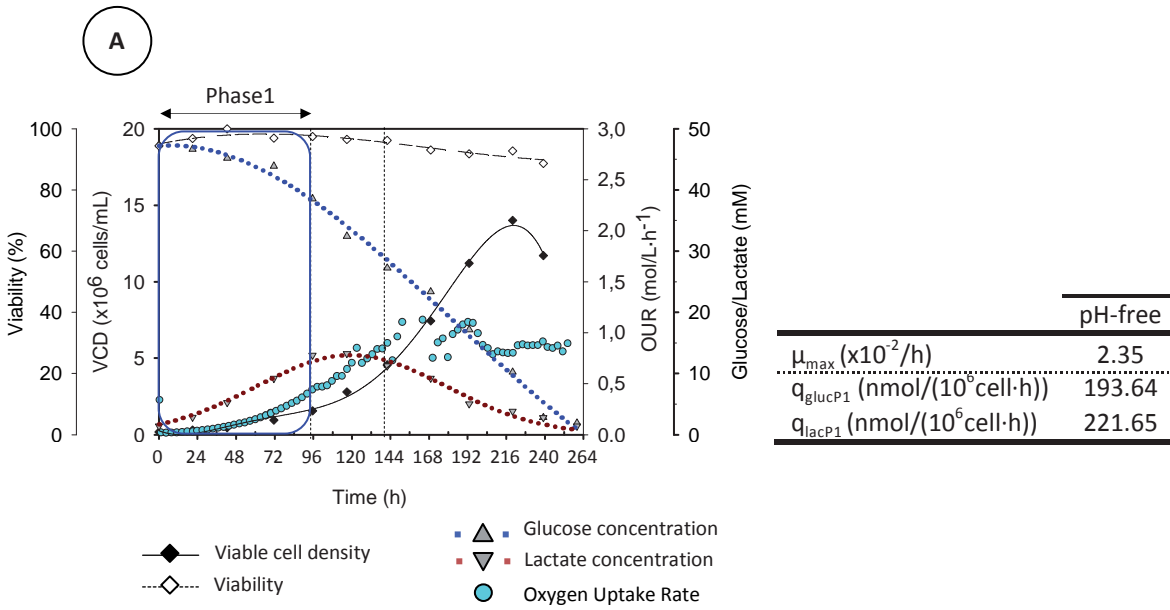


**Figure 6.14.** (A) cell growth, viability, glucose and lactate profiles of culture under pH free condition (only addition of CO<sub>2</sub> was performed). The table embedded in the Figure summarizes the main kinetic parameters. (B) Main fluxes around TCA during Phase 1 of cell culture.

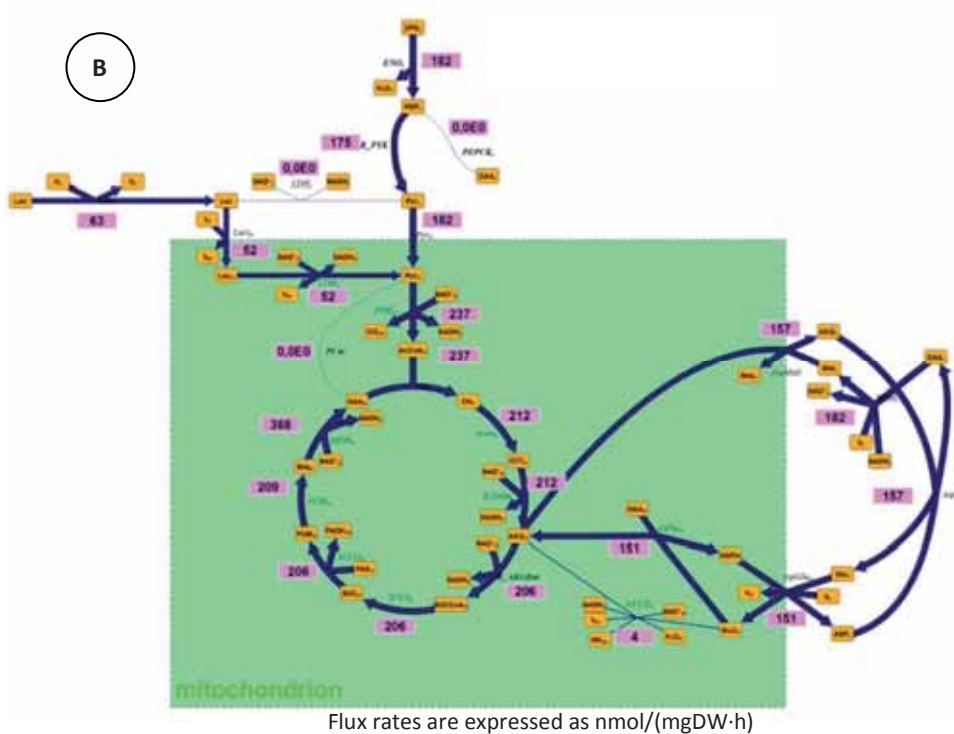
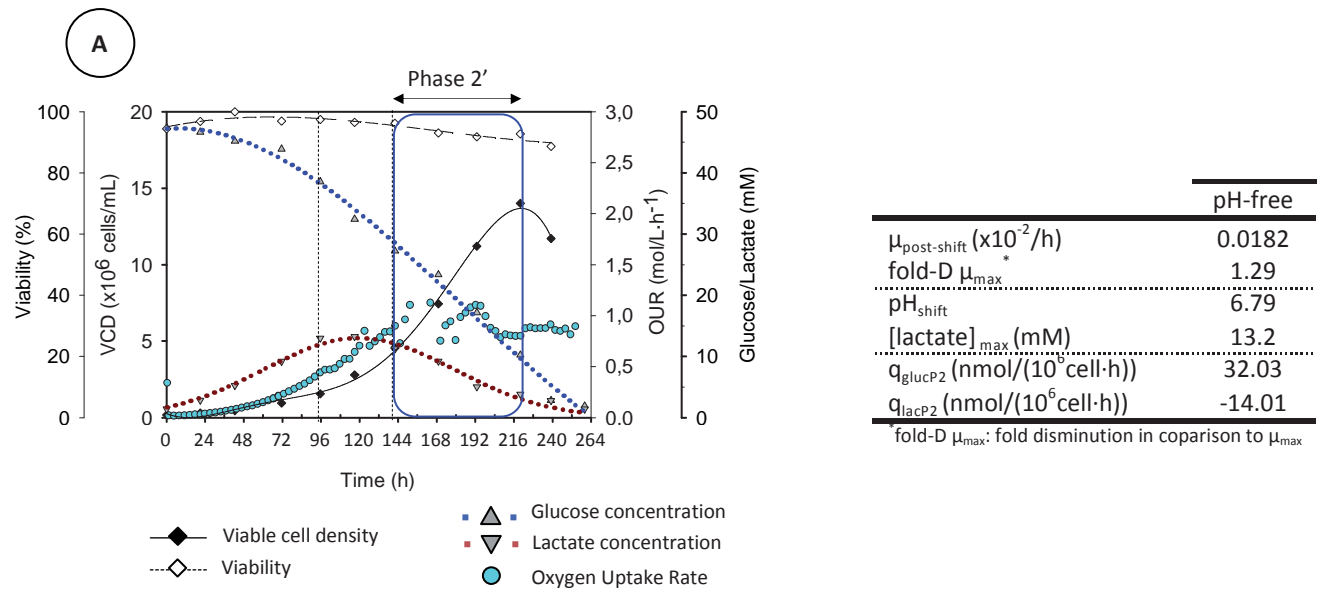


**Figure 6.15.** (A) cell growth, viability, glucose and lactate profiles of culture under pH free condition (only addition of CO<sub>2</sub> was performed). The table embedded in the Figure summarizes the main kinetic parameters. (B) Main fluxes around TCA during Phase 2' of cell culture.

### 6.8. EVALUATION OF THE MECHANISM FOR LACTATE ENTRANCE TO THE MITOCHONDRIA.

As stated in section 6.5, several authors have reported the consumption of lactate by mammalian cells. Among these studies, there is a considerable controversy about how lactate reaches the mitochondrial matrix. While some authors report the possibility of direct entrance of lactate through the mitochondrial transporters, much other state that lactate is converted to pyruvate at the cytosol and thereafter, pyruvate is transported inside the mitochondria. For the calculation of fluxes presented in previous section, the direct lactate entrance to the mitochondria was considered. Although entrance via pyruvate conversion cannot be ruled out, we obtained data (presented below) that supports the hypothesis that lactate can directly enter to mitochondria. These results represent quite valuable data towards unravelling the scientific community discussion about lactate entrance mechanisms.

For the study of lactate entrance to the mitochondria, respirometries with isolated mitochondria from HEK293 cell culture were performed. The main function of mitochondria is to produce ATP, hence, energy for the cell. For the production of ATP, mitochondria need the consumption of oxygen. Respirometry is a technique that enables to measure respiration activity of a living organism by measuring changes on O<sub>2</sub> and/or CO<sub>2</sub>. Hence, this methodology can be used for the assessment of mitochondrial activity, as the highest O<sub>2</sub> consumption is related to a higher mitochondrial activity. The protocol used for mitochondrial isolation and the methodology used for O<sub>2</sub> measurement is detailed in material and methods chapter (section 8.10.5). In preliminary studies, it was found out that when mitochondria were cultivated in the presence of lactate, the oxygen consumption was higher than when the organelles were cultured in presence of pyruvate (Figure 6.16). If the transformation of lactate to pyruvate in the cytosolic space were mandatory, then the activity of mitochondria would be the same regardless the metabolite (pyruvate or lactate) present in media. The fact that mitochondria were more active when cultured in lactate indicated that this metabolite could enter the mitochondria through an alternative route to pyruvate transformation. The alternative mechanism could be the direct entrance through mitochondrial lactate transporters (MCT).

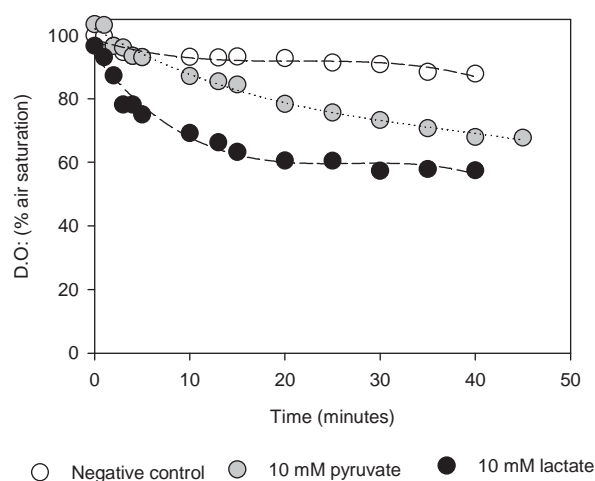


**Figure 6.16.** Oxygen consumption of mitochondria (185 $\mu$ g/mL) in respiration buffer (negative controls, open circles), respiration buffer + pyruvate (10mM) (green circles) or respiration buffer + lactate (10mM).

In order to further evaluate this hypothesis, mitochondria were cultivated under the presence of lactate in the buffer and in parallel with the addition of lactate and  $\alpha$ -cyano-4-hydroxycinnamic acid (CINN). CINN is an inhibitor of various subtypes of MCTs<sup>40,41</sup>. Hence, if lactate directly enters mitochondria through these transporters, the respiratory activity should be reduced when the addition of this molecule is performed.

In Figure 6.17, the results of the experiment are presented. When only lactate was present in the respiratory buffer, a oxygen consumption profile similar to the previously presented was obtained. Moreover, the measurement of extracellular lactate was carried out and it was confirmed that the respiratory activity detected was related to the consumption of this metabolite. When MCTs were blocked as a consequence of CINN addition, the respiratory activity of the mitochondria was completely stopped and the oxygen consumption profile was similar to the negative control. The reduction of mitochondrial activity after blocking MCTs has been previously reported in other cell type, but never for HEK293 cells. This data confirms that lactate can enter the mitochondria of HEK293 using mitochondrial lactate transporters instead than being transformed into pyruvate at the cytosolic space. Although this data is not sufficient to completely rule out the entrance of lactate to mitochondria via pyruvate, the thermodynamics of the LDH reaction might provide some additional data to this discussion. The thermodynamics of the conversion from pyruvate to lactate is energetically favourable, being the  $\Delta G$  of this reaction of -25.1. Hence, the reverse reaction (conversion of L-lactate to pyruvate in the cytosol) would be thermodynamically unfeasible. In fact, this has already been pointed out by other scientists<sup>42-44</sup>. Nevertheless, further research is currently

being addressed in order to experimentally demonstrate the mechanism of lactate entrance to the mitochondria.

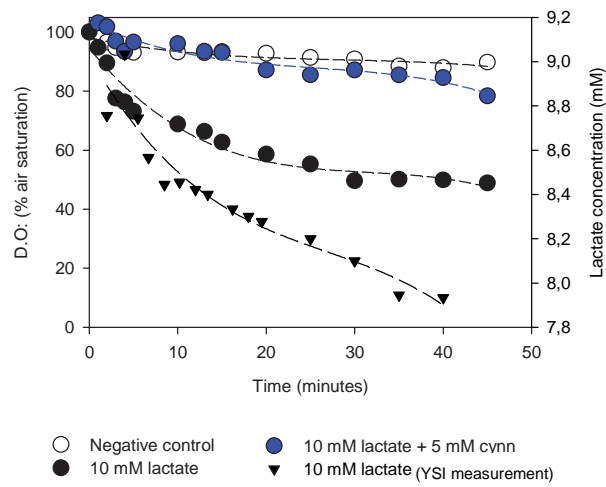


**Figure 6.17.** Oxygen consumption of mitochondria (205 $\mu$ g/mL) in respiration buffer (negative controls, open circles), respiration buffer + pyruvate (10mM)+CINN (blue circles) and respiration buffer + lactate (10mM) (black circles). The consumption of lactate for the condition of presence of lactate (without any blocking agent) is also depicted (black triangles).

## 6.9. CONCLUSIONS

The study of lactate and glucose co-consumption has been addressed along this chapter. Lactate consumption in presence of glucose has been reported previously but only on late stages of cell culture, at which stationary cell growth was noticed. Differently, the co-metabolisation of both metabolites here presented has been observed in exponentially growing cell cultures. It was found out that pH is the key factor to trigger the lactate shift from production to consumption and this shift could be triggered at will by means of lowering extracellular pH to pH=6.6 together with the addition of lactate to media. At this pH, the proper concentration of extracellular lactate would be in between 4-8mM, in order to trigger lactate consumption (hence, avoiding lactate accumulation), minimize glucose uptake rate and maximizing specific growth rate.

The co-metabolisation of glucose and lactate might be a mechanism for pH detoxification. HEK293 cells could somehow detect the acidification of extracellular environment and trigger the co-transport of lactate and  $H^+$  to the intracellular space, resulting in an increment of extracellular pH towards more physiological values. Lactate might be used as carbon source for the cell, resulting in a more balanced metabolism. Flux balance analysis supported this hypothesis and revealed that when lactate and glucose are consumed together, metabolic fluxes through the glycolysis pathway become equilibrated (this is, in the same range) with the TCA fluxes, avoiding pyruvate accumulation in the cytosol.

The novel hypothesis proposed of the ability of the cells to detoxify extracellular media, together with the implementation of a HEK293 metabolic network model, opens the study of target genes that can be modified in order to generate metabolic optimized HEK293 cell lines. These engineered cell lines would result in bioprocess optimization and development of new culture strategies towards higher cell densities and recombinant protein titres.



**6.10. REFERENCES**

1. Metallo, C. M. & Heiden, M. G. Vander. Understanding metabolic regulation and its influence on cell physiology. *Mol. Cell* **49**, 388–398 (2013).
2. Wang, R. *et al.* The transcription factor Myc controls metabolic reprogramming upon T lymphocyte activation. *Immunity* **35**, 871–882 (2011).
3. Khairallah, M. *et al.* Profiling substrate fluxes in the isolated working mouse heart using <sup>13</sup>C-labeled substrates: focusing on the origin and fate of pyruvate and citrate carbons. *Am. J. Physiol. - Hear. Circ. Physiol.* **286**, H1461–H1470 (2004).
4. Merritt, M. E., Harrison, C., Sherry, A. D., Malloy, C. R. & Burgess, S. C. Flux through hepatic pyruvate carboxylase and phosphoenolpyruvate carboxykinase detected by hyperpolarized <sup>13</sup>C magnetic resonance. *Proc. Natl. Acad. Sci.* **108**, 19084–19089 (2011).
5. Lee, S. Y., Park, J. M. & Kim, T. Y. *Application of metabolic flux analysis in metabolic engineering. Methods in Enzymology* **498**, (Elsevier Inc., 2011).
6. Cruz, H. J., Moreira, L. & Carrondo, M. J. T. Effects of ammonia and lactate on growth, metabolism and productivity of BHK cells. *Enzyme Microb. Technol.* **66**, 43–52 (1999).
7. Ozturk, S. S., Riley, M. R. & Palsson, B. Effects of Ammonia and Lactate on Hybridoma Growth, Metabolism, and Antibody Production. *Biotechnol. Bioeng.* **39**, 418–431 (1991).
8. Yang, M. & Butler, M. Effects of ammonia on CHO cell growth, erythropoietin production, and glycosylation. *Biotechnol. Bioeng.* **68**, 370–380 (2000).
9. Andersen, D. & Goochee, C. The effect of ammonia on the O-linked glycosylation of granulocyte colony-stimulating factor produced by chinese hamster ovary cells. *Biotechnol. Bioeng.* **47**, 96–105 (1995).
10. Altaras, N. E. *et al.* Production and Formulation of Adenovirus Vectors. *Adv. Biochem. Engin. Biotechnol.* **99**, 193–260 (2005).
11. Gambhir, A., Europa, A. F. & Hu, W.-S. Alteration of cellular metabolism by consecutive fed-batch cultures of mammalian cells. *J. Biosci. Bioeng.* **87**, 805–810 (1999).
12. Kurokawa, H., Park, Y. S., Iijima, S. & Kobayashi, T. Growth characteristics in fed-batch culture of hybridoma cells with control of glucose and glutamine concentrations. *Biotechnol. Bioeng.* **44**, 95–103 (1994).
13. Siegwart, P. *et al.* Adaptive control at low glucose concentration of HEK-293 cell serum-free cultures. *Biotechnol Prog* **15**, 608–616 (1999).
14. Zhang, L., Shen, H. & Zhang, Y. Fed-batch culture of hybridoma cells in serum-free medium using an optimized feeding strategy. *J. Chem. Technol. Biotechnol.* **79**, 171–181 (2004).

15. Vallée, C., Durocher, Y. & Henry, O. Exploiting the metabolism of PYC expressing HEK293 cells in fed-batch cultures. *J. Biotechnol.* **169**, 63–70 (2014).
16. Altamirano, C., Paredes, C., Illanes, A., Cairó, J. J. & Gòdia, F. Strategies for fed-batch cultivation of t-PA producing CHO cells: substitution of glucose and glutamine and rational design of culture medium. *J. Biotechnol.* **110**, 171–179 (2004).
17. Gagnon, M. *et al.* High-end pH-controlled delivery of glucose effectively suppresses lactate accumulation in CHO fed-batch cultures. *Biotechnol. Bioeng.* **108**, 1328–1337 (2011).
18. Zagari, F., Jordan, M., Stettler, M., Broly, H. & Wurm, F. M. Lactate metabolism shift in CHO cell culture: the role of mitochondrial oxidative activity. *N. Biotechnol.* **30**, 238–245 (2013).
19. Kuwae, S., Ohda, T., Tamashima, H., Miki, H. & Kobayashi, K. Development of a fed-batch culture process for enhanced production of recombinant human antithrombin by Chinese hamster ovary cells. *J. Biosci. Bioeng.* **100**, 502–510 (2005).
20. Le, H. *et al.* Multivariate analysis of cell culture bioprocess data--lactate consumption as process indicator. *J. Biotechnol.* **162**, 210–223 (2012).
21. Mulukutla, B. C., Gramer, M. & Hu, W.-S. On metabolic shift to lactate consumption in fed-batch culture of mammalian cells. *Metab. Eng.* **14**, 138–149 (2012).
22. Khoo, S. H. G. & Al-Rubeai, M. Metabolic characterization of a hyper-productive state in an antibody producing NSO myeloma cell line. *Metab. Eng.* **11**, 199–211 (2009).
23. Zhou, W. & Hu, W.-S. On-line characterization of a hybridoma cell culture process. *Biotechnol. Bioeng.* **44**, 170–177 (1994).
24. Ivarsson, M., Noh, H., Morbidelli, M. & Soos, M. Insights into pH-induced metabolic switch by flux balance analysis. *Biotechnol. Prog.* **00**, n/a–n/a (2015).
25. Halestrap, A. P. & Price, N. T. The proton-linked monocarboxylate transporter (MCT) family: structure, function and regulation. *Biochem J* **343**, 281–299 (1999).
26. Halestrap, A. P. & Wilson, M. C. The monocarboxylate transporter family--role and regulation. *IUBMB Life* **64**, 109–119 (2012).
27. San Martín, A. *et al.* A genetically encoded FRET lactate sensor and its use to detect the Warburg effect in single cancer cells. *PLoS One* **8**, e57712 (2013).
28. Kumar, V., Bhalla, A. & Rathore, A. S. Design of experiments applications in bioprocessing: Concepts and approach. *Biotechnol. Prog.* **30**, 86–99 (2014).
29. Mandenius, C. & Brundin, a. REVIEW: BIOCATALYSTS AND BIOREACTOR DESIGN Optimization, Bioprocess Methodology, Using Design-of-experiments. *Biotechnol Progr* **24**, 1191–1203 (2008).
30. NIST & SEMATECH. e-Handbook of Statistical Methods. at <http://www.itl.nist.gov/div898/handbook/>

31. Quek, L. E. *et al.* Reducing Recon 2 for steady-state flux analysis of HEK cell culture. *J. Biotechnol.* **184**, 172–178 (2014).
32. Dennis, M. K. *et al.* A community-driven global reconstruction of human metabolism. *Nat Biotechnol* **5**, 358–366 (2013).
33. Lewis, N. E. *et al.* Omic data from evolved E. coli are consistent with computed optimal growth from genome-scale models. *Mol. Syst. Biol.* **6**, 390 (2010).
34. Rocha, I. *et al.* OptFlux: an open-source software platform for in silico metabolic engineering. *BMC Syst. Biol.* **4**, 45 (2010).
35. Paredes, C. *et al.* Modification of glucose and glutamine metabolism in hybridoma cell through metabolic engineering. *Cytotechnology* 85–93 (1999).
36. Mereschowsky, K. Theorie der zwei Plasmaarten als Grundlage der Symbiogenese, einer neuen Lehre von der Entstehung der Organismen. *Biol Cent.* 353–367 (1910).
37. Wallin, I. The mitochondrial problem. *Am. Nat.* **57**, 255–261 (1923).
38. Wallin, I. *Symbiogenesis and the origin of the species.* (Williams & Wilkins, 1927).
39. Sagan, L. On the origin of mitosing cells. *J Theor Biol* **3**, 255–274 (1967).
40. Kennedy, K. M. & Dewhirst, M. W. Tumor metabolism of lactate: the influence and therapeutic potential for MCT and CD147 regulation. *Futur. oncol* **6**, 1–32 (2010).
41. Manning Fox, J. E., Meredith, D. & Halestrap, a. P. Characterisation of human monocarboxylate transporter 4 substantiates its role in lactic acid efflux from skeletal muscle. *J. Physiol.* **529**, 285–293 (2000).
42. Rasmussen, H. N., van Hall, G. & Rasmussen, U. F. Lactate dehydrogenase is not a mitochondrial enzyme in human and mouse vastus lateralis muscle. *J. Physiol.* **541**, 575–580 (2002).
43. Sahlin, K., Fernström, M., Svensson, M. & Tonkonogi, M. No evidence of an intracellular lactate shuttle in rat skeletal muscle. *J. Physiol.* **541**, 569–574 (2002).
44. Passarella, S., Paventi, G. & Pizzuto, R. The mitochondrial L-lactate dehydrogenase affair. *Front. Neurosci.* **8**, 1–4 (2014).